UNIVERSITY OF CALIFORNIA SAN DIEGO

Physical mechanisms influencing hypoxia in Bahía Almirante, Panamá, a shallow, tropical estuary

A dissertation submitted in partial satisfaction of the
requirements for the degree Doctor of Philosophy

in

Oceanography

by

Anne Elizabeth Adelson

Committee in charge:

Professor Geno Pawlak, Chair
Professor Carlos F.M. Coimbra
Professor Kristen A. Davis
Professor Peter J. Franks
Professor Sarah N. Giddings
Professor Mark A. Merrifield

2024

The Dissertation of Anne Elizabeth Adelson is approved, and it is acceptable in quality and form for publication on microfilm and electronically.

University of California San Diego

2024

EPIGRAPH

You can swim all day in the Sea of Knowledge and still come out completely dry.

Norton Juster, The Phantom Tollbooth

TABLE OF CONTENTS

LIST OF FIGURES

LIST OF TABLES

ACKNOWLEDGEMENTS

First and foremost, I would like to express my gratitude for my advisor, Geno Pawlak. I'm lucky to have an advisor who is genuinely interested with my work (despite the numerous squirrels we chased). You were generous with your time, and I am grateful for everything that I learned from you – ranging from environmental fluid mechanics to the most useful tool in nearly any situation (channel locks).

For the past few years, I have felt like Kristen Davis and Sarah Giddings are my co-advisors. We spent countless hours on Zoom with the Bocas team and many hours in the field, and it is not lost on me that I was able to get the attention of such smart (and busy) people who were not formally my advisors to help me with the work presented in this dissertation. I especially appreciate your honesty and support as I've tried to understand what I want from my career.

I would like to thank my committee members Carlos Coimbra, Peter Franks, and Mark Merrifield for their valuable feedback on my dissertation and for making themselves available to talk about my science when I asked. My research is better because of your input, and I am filled with gratitude.

A very big thank you to Rachel Collin, my Smithsonian Advisor, for being so open and supportive throughout the years we've worked together. I'm so grateful for how much effort you put in to make sure that we had everything we needed when we were in the field and for your mentorship and perspective. I'd like to thank the final members of the Bocas physical oceanography and hydrology crew, Sam Kastner and Kasey Clark, and my additional co-authors, Andrew Altieri, Ximena Boza, Alan Gaul, and Victoria Reed. It was really fun talking science with you.

To the past and present members of the Pawlak and Giddings labs, thank you for your feedback during my lab meeting updates and especially the comraderie. I'm grateful I got to spend first year as the member of two cohorts. To my AOS cohort, Billy, Bofu, Eric, Kelley, and Narda and PO cohort, Alice, Bobby, Channing, Emma, Lauren, and

Noel, thank you for being great classmates and even better friends.

There are many people who mentored me along the way to get on this path. To name them all feels impossible, but I'd like to thank the people who led my field studies courses and those who taught me at Hopkins Marine Station and Stanford at Sea, when I was just starting to become interested in oceanography. I'd also like to thank the faculty and students in the Stanford Environmental Fluid Mechanics Lab who helped me understand the beauty of first principles and were so kind to a recent biology grad with a weak math background. Thank you to Barb, Rob, Rodolfo, Fio, Scott, Steve, and Stephen for giving me research opportunities. They helped me be sure that a Ph.D. was the path I wanted to take, which was an important reminder during the tough parts of graduate school. I came to SIO knowing that I loved field work — thank you to Cara, Pasha, Eva, Justin, Mike, Lena, Jessica, Mallory, Sam, and Emma for the time we spent in the field together and the opportunities to explore new places.

Thank you to all of the people who have helped me across the SIO and MAE departments, especially Gilbert Bretado, Shelley Weisel, Dana Jimenez, Tomomi Ushii, Emily Cunningham, Jimmy Lee, Taylor Nelson, and Jake Blair. Thank you to the SIO Cody fellowship, NSF, and the Smithsonian Institution for providing me support while I completed this work. I'd also like to thank the staff members at SIO who keep the campus functional and beautiful and allow those of us to come here to do research to focus on our science.

There are so many folks involved in making field work run smoothly (or run at all). I am incredibly grateful for the many folks at UCSD and STRI and everywhere in between. Thanks to the folks at UCSD Outbound Shipping and the shipping department at STRI for ensuring we had our instruments, tools, and batteries in the field when we needed them. Thank you to the folks at RDI, PME, and Sea-Bird who provided field support and troubleshooting advice. Thank you to the staff at STRI for making sure we had the permits we needed and our visits were good to go. A big thank you to the UCSD scientific

diving program, Christian, Rich, Ashleigh, Chad, and Jess, and Raul, the STRI DSO, for making sure that we were able to conduct our work safely and efficiently. A special thank you to Rich Walsh for his near-instant problem solving and thoughtful friendship.

I have so much gratitude for the staff at the STRI Bocas Research Station. Bocas has been an excellent place to conduct field work, and it is in large part due to the efforts of Plinio and the staff at STRI who worked hard to accommodate us and ensured we had everything we needed. Everyone at STRI truly went above and beyond. Thank you to Urania, Nitzia, Raul, Rohman, Xiomara, Noemi, Damian, Odinais, Cynthia, Deyvis, Murray, Kais, and everyone who worked at the gardita, especially David. You all helped with this work in different ways — scheduling field activities, making sure labs were clean, giving me peace of mind, maintaining boats, and so much more. Muchas, muchas gracias. Thank you to Sebastian Castillo for teaching me how to be a good oceanographic boat driver. Your insight into Bahía Almirante made this work better and our field work safer.

Thank you to Isabella Arzeno-Soltero, Max Rintoul, Duncan Wheeler, and Jennifer Yin for making the trip to Bocas to help with my field work. I am so appreciative that you took time from your own projects to work long days helping me with mine. And you're welcome for all the boat naps. Thank you to the folks working in Bocas who volunteered to spend some of their time in the field with me. I am immensely grateful to become part of a community of researchers at the Bocas Station when I was there — there are too many to name. It was fun eating meals with you, learning about your work, exploring the islands, and sharing that unique experience of field work in Bocas and everything that comes along with it. Thanks for bringing me beers when I was in the lab working late, and for taking a break to chat when I did the same.

There are three people without whom my field work experience would have been entirely different, Ximena Boza, Carolina Cesar, and Viviana Bravo. Thank you for spending so many hours transecting Bahía Almirante with me, for your support, for welcoming me with open arms. Your friendship has truly been one of the highlights of my

Ph.D. experience, and you made Bocas feel like home to me. Ustedes son las fichas.

I have the best friends in the world, and it would take another one hundred and thirty odd pages to name and thank them all for everything they've done for me since I started my Ph.D (not to mention the many years before). Thank you for your patient understanding, your uplifting encouragement, and for making me feel so loved. A few SIO friends deserve special thanks for their support in the final stretch. Thank you to Lauren and Bobby for making me laugh through the highs, lows, and office sewage floods. Margaret, vamos vamos vamos yeah.

Thank you to Max for being a source of buoyancy over the past few years. My Ph.D. experience has given me a lot that has nothing to do with physical oceanography — some Panamanian slang, a few stamps in my passport, chances to explore island jungles and kelp forests, a sense of pride in finishing something that I have found challenging for a very long time, among so many others. Of all those things, I feel most fortunate for the time getting to know you. I am very excited to explore estuaries (and lots of other landscapes) with you.

Thank you to my grandparents, Ellen and Steve, for setting an example of what it means to be a lifelong learner. I am so grateful for your support and encouragement to follow my interests, wherever they take me. I hope to be as generous and curious throughout my life as you have. To my aunts, uncles, and cousins, thank you for being a reliable source of joy. I am incredibly fortunate to have such a supportive, generous, loving, and fun extended family, which has only become more so as it gets bigger with more cousins-in-law and babies.

I am so grateful to my parents, Carol and David, for their steady support. Among so many other things, thank you to David for showing me what it is like to be guided by your passions throughout all stages of your career, and thank you to Carol for teaching me how to pay attention and follow through. Your support has been absolutely essential.

Thank you to my sisters-in-law, Sarah and Emma Rose. I am so lucky that my

brothers chose partners who I adore. Thank you to Emma Rose for modeling how much joy can come from a job well done and for being so caring and capable. Thank you to Sarah for rigorously engaging in conversations ranging from my research to yours, from academic workers' rights to whether Clueless is a faithful adaptation of Emma. You are both so bright in every way.

My brothers, Peter and Joe, are the two most brilliant people I know, and I've always admired how deeply they think. Joe, I am endlessly grateful to have a mind like yours so eager to think about my fluid mechanics problems, but I feel even more fortunate for your attentiveness and making sure I feel included in Sonia's and Felix's lives. Peter, thank you for being the even keel during my grad school squalls. I admire your ambition in all things, including getting the dance floor going. I am so, so lucky to have you as my brothers.

Finally, thank you to my niece, Sonia Louise and my brand new nephew, Felix. Sonia, I can say without hyperbole that throughout your entire life, you have delighted me. Once you have a niece or nephew, you might understand how happy you've made me during the final stretch of my Ph.D., by picking out a book and sitting in my lap or simply saying my name. Felix, you've only been around for few weeks, but you have my whole heart too.

"The UC San Diego community holds great respect for the land and the original people of the area where our campus is located. The university is built on the un-ceded territory of the Kumeyaay Nation. Today, the Kumeyaay people continue to maintain their political sovereignty and cultural traditions as vital members of the San Diego community. We acknowledge their tremendous contributions to our region and thank them for their stewardship." — the UC San Diego Intertribal Resource Center

The field work to support this research takes places on the land that belonged to the Dorasquez, Changuinas, Miskitos, Guaymies, Viceitas, Teribes, Terrabas, Borucas,

Urinamas, Changuenas and Chalibas peoples prior to colonization. I thank them for their stewardship.

Chapter 2, in full, is a reprint of the material as it appears in Limnology and Oceanography, 2022. Adelson, A.E., Altieri, A.H., Boza, X., Collin, R., Davis, K.A., Gaul, A., Giddings, S.N., Reed, V. and Pawlak, G., 2022. Seasonal hypoxia and temperature inversions in a tropical bay. *Limnology and Oceanography*, 67(10), pp.2174-2189. Used with permission. The dissertation author was the primary investigator and author of this paper.

Chapter 3, in part, is currently being prepared for submission for publication of the material. Adelson, A.E. Collin, R, Davis, K.A., Giddings, S.N., Kastner, S.E., and Pawlak, G., Barotropic and baroclinic influences on a multi-inlet tropical estuary. The dissertation author was the primary investigator and author of this paper.

Chapter 4, in part, is currently being prepared for submission for publication of the material. Adelson, A.E. Collin, R, Davis, K.A., Giddings, S.N., Kastner, S.E., and Pawlak, G., Deep water renewal episodes dictate hypoxic state of a shallow tropical estuary. The dissertation author was the primary investigator and author of this paper.

VITA

2015	B.S., Biology, with Honors, Stanford University
2015	M.S., Civil and Environmental Engineering, Stanford University
2024	Ph.D., Scripps Institution of Oceanography, University of California San Diego

ABSTRACT OF THE DISSERTATION

Physical mechanisms influencing hypoxia in Bahía Almirante, Panamá, a shallow, tropical estuary

by

Anne Elizabeth Adelson

Doctor of Philosophy in Oceanography

University of California San Diego, 2024

Professor Geno Pawlak, Chair

Tropical regions are understudied relative to their temperate counterparts, and there is inadequate data to elucidate the dynamics and function of tropical estuarine systems. Reducing the scientific bias in the understanding of estuarine dynamics is important because coastal processes in the tropics can differ from higher latitudes. Dissolved oxygen (DO) is a critically important ecological variable, and the prevalence of hypoxia is expected to increase due to the combined effects of ocean warming and eutrophication; however, there are still fundamental knowledge gaps in the role that low-DO levels and multiple stressors play in ecosystem health, and dead zones in the tropics are likely severely under-reported.

This dissertation examines the physical processes that are important in regulating hypoxia and temperature inversions in Bahía Almirante, a multi-inlet tropical estuary on Panamá's Caribbean coast, which has experienced documented hypoxia and warming events resulting in coral bleaching and die offs. We use a 10-year record of observations at seven locations in Bahía Almirante to identify seasonal temperature inversions and hypoxia at depth that often co-occur. DO reductions correspond to periods with high freshwater input, resulting in strong salinity stratification that isolates bottom waters, allowing biological oxygen demand to draw down DO.

We conducted a two-year intensive study from September 2019-2021 and find that an alongshore pressure gradient drives net flow through Bahía Almirante, and the depth-mean velocity measured in the channel correlates to an along-coast current on the shelf. Water properties indicate hydrographically distinct sub-basins, with a largely isolated inner bay, even during periods of high net flow conditions. In the inner bay, DO at depth drops to hypoxic levels seasonally. Reoxygenation occurs with inflow at depth and inflow density that exceeds the inner bay bottom layer density, sharing a mechanistic similarity to deep water renewal commonly observed in fjords. In Bahía Almirante, we show that warming of the isolated bottom water mass via radiative heating significantly contributes to density reduction, a novel mechanism for density reduction in deep water renewal dynamics. Hypoxia seasonality is attributed to variability in offshore density and stratification that is associated with annual variations in precipitation.

Chapter 1

Introduction

1.1 Background

The tropics host much of the earth's biodiversity, yet scientific research has predominantly focused on temperate systems (Kurien, 1996; Spalding et al., 2023; Vieillard et al., 2020). Furthermore, a disproportionate share of the global population lives along coastlines, and urban tropical estuaries are of particular significance due to the combination of environmental and societal factors (Oczkowski et al., 2020). Therefore, addressing the scientific investment bias is particularly important when it comes to tropical estuarine dynamics because coastal processes in the tropics can exhibit fundamental differences from higher latitudes. For example, there are important differences in nutrient cycling (Vieillard et al., 2020). Furthermore, solar radiation and precipitation are high and weakly vary over the annual cycle, as compared to temperate areas (Nittrouer et al., 1995). This can have important implications for vertical stratification and vertical mixing and thus a multitude of cascading physical and biogeochemical processes.

Efforts to understand the dynamics of tropical estuaries have been made in systems including the Upper Gulf of Thailand (Saramul and Ezer, 2014), and in Brazil, including the Amazon estuary (Menezes et al., 2009), the Caravelas estuarine system (Schettini et al., 2013), Itamaracá (Medeiros and Kjerfve, 2005), São Vicente, Santos and Bertioga estuarine channels (Moser et al., 2005), and Baía de Todos os Santos (Fonseca et al., 2024),

and the Magdalena River in Colombia (Restrepo et al., 2018), among other systems, but there remains considerable need and opportunity for identifying processes that are critical to tropical estuarine function.

Tropical coastal systems, including coral reefs, are at increasing risk of hypoxia and other potential concurrent stressors, including ocean acidification and warming. Hypoxia is commonly defined as dissolved oxygen (DO) < 2 mg L^{-1}, but there are adverse implications for many species above this threshold (Vaquer-Sunyer and Duarte, 2008). Low DO events are expected to become more prevalent due to the combined effects of ocean warming and eutrophication (Altieri and Gedan, 2015; Breitburg et al., 2018; Stramma et al., 2010). While deoxygenation is well studied in the open ocean and temperate regions (Diaz and Rosenberg, 2008; Howarth, 2008), there have been fewer studies in tropical areas (e.g., Altieri et al., 2017; Johnson et al., 2021; Hughes et al., 2020; Nelson and Altieri, 2019; Pezner et al., 2023). A meta-analysis by Altieri et al. (2017) suggests that dead zones in the tropics have been under-reported, perhaps by an order of magnitude, due to a lack of DO measurements.

In order to understand the potential implications of hypoxia and other ecosystem threats for tropical estuaries in a changing climate, we must understand the physical dynamics of these systems; however, this objective faces challenges associated with data scarcity. Collin and colleagues (in review) advocate for integrating the physics of tropical coastal areas with biological interactions and social dynamics to comprehensively study and address local and global drivers of change. The biogeochemical processes that modify water properties including DO and pH are modulated by physics, such as residence times and stratification, and are also modulated by water properties, including temperature and salinity. (Nelson and Altieri, 2019). Therefore, it is critical to understand the interplay of physical dynamics and DO concentrations in order to predict, and if possible, mitigate hypoxia.

1.2 Research objectives

Though progress has been made, there is considerable opportunity for better understanding tropical estuaries. The primary goals of this research are to:

1. identify mechanisms that govern water properties within a shallow tropical estuary,
2. determine the processes that contribute to initiation of hypoxic conditions, and
3. resolve the processes that lead to reoxygenation along with the associated timescales.

In the three main chapters, we seek to provide new insight into the dynamics of tropical estuaries and address how physical mechanisms influence hypoxia. We analyze unprecedented field observations collected in Bahía Almirante, long-term monitoring data, and global model outputs to shed light on this system specifically and further the scientific community's understanding of tropical estuaries generally.

1.3 Study site: Bahía Almirante, Panamá

Bahía Almirante is a multi-inlet estuary in the Bocas del Toro province of Panamá (Figure 1.1). The embayment is surrounded by Isla Colon, Isla Carenero, and Isla Bastimentos, with interior islands Isla Pastores and Isla San Cristobal. There are two primary channels that connect Bahía Almirante to the Caribbean Sea, Boca del Drago and Canal de Bastimentos, and a smaller channel, Cayo Coral, that connects to the Laguna de Chiriquí.

The watershed of Bahía Almirante is approximately equal in area to the surface area of the embayment (Kaufmann and Thompson, 2005). One boundary is the Cordillera de Talamanca, mountains approximately 60 km to the west which reach altitudes greater than 3400 m. The primary landcover includes secondary forests and agricultural land types (e.g., cacao farms and cattle pastures) and swamps, including the peat swamp

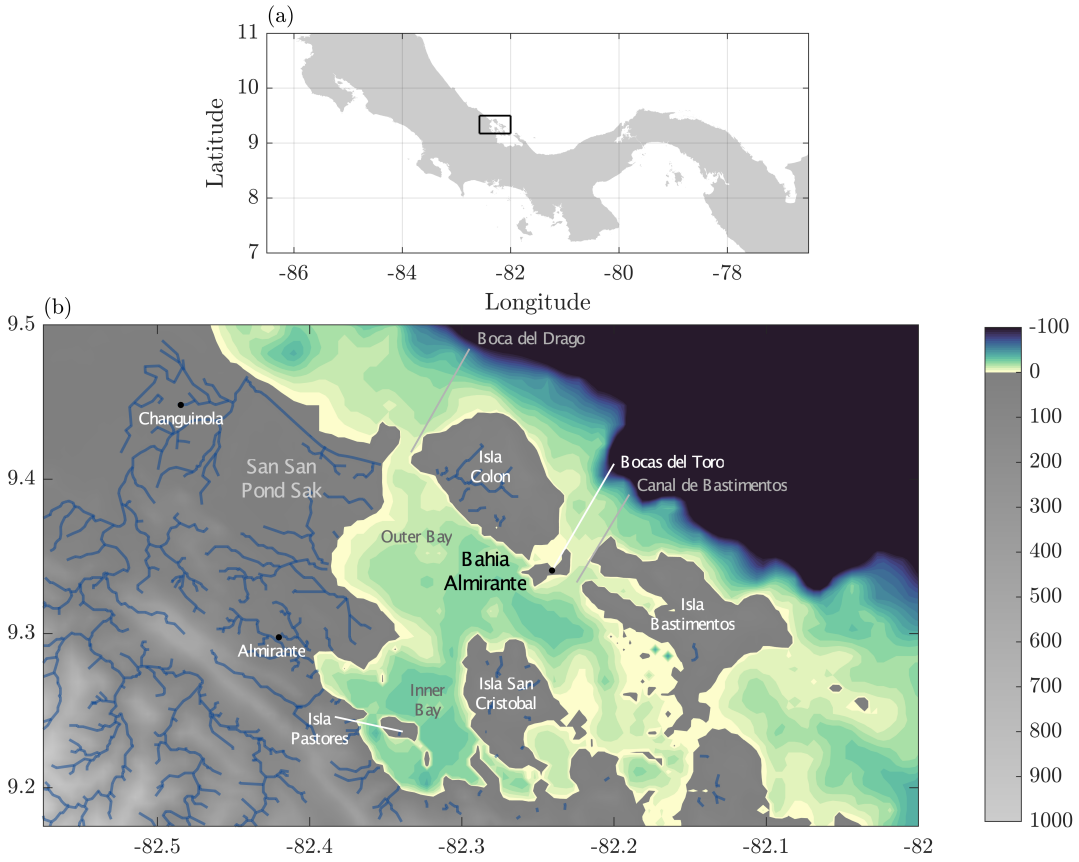

Figure 1.1. (a) Panamá Coast, with Bahía Almirante in black box. (b) Bahía Almirante region, with terrestrial elevation (grayscale) and bathymetery (color). Rivers in blue. Adapted from Collin et al., in review.

forest San San Pond Sak, in the low-lying coastal areas (Clark et al., 2022, Collin et al., in review). Urban developments in the Bahía Almirante catchment include Bocas del Toro (Isla Colon; population 10,042), Old Bank (Isla Bastimentos; population 2,679), and Almirante (mainland; population 19,646). (Estadístico, 2021; Clark et al., 2022, Collin et al., in review). There are many diffuse and flashy rivers along the mainland that drain into Bahía Almirante (Clark et al., 2022). The Changuinola River discharges into the Caribbean Sea, approximately 12 km north of the Boca del Drago inlet, and there is an man-made canal through the swamp forest connecting the Changuinola River to Bahía Almirante (Collin et al., in review).

Bahía Almirante's climate is classified as a tropical rainforest (Af Koppen-Geiger climate classification; Beck et al., 2018). The precipitation patterns in this region differ from other parts of the tropics (including other regions of Panamá), with two rainy seasons (April-August, November-December) and two dry seasons (January-April, September-October; Kaufmann and Thompson, 2005; Patton, 2023). Bahía Almirante has average annual precipitation of 3629 ± 549 mm yr^{-1}, and there is significant rainfall through the dry season, with a minimum monthly average of 172 mm (October) (Patton, 2023, Collin et al., in review). The seasonality in solar radiation, rainfall, wind speed, air temperature, and relative humidity are all generally weak (Kaufmann and Thompson, 2005).

The Caribbean Sea is strongly stratified, with a well-mixed surface layer extending to 50 m (Gallegos, 1996). Intertropical Convergence Zone (ITCZ) migration, propagation of atmospheric tropical waves through the Atlantic basin, and variations in weather patterns drive changes in offshore water temperature and salinity (Kaufmann and Thompson, 2005). There is a southeastward surface flow associated with the Panamá-Colombia Gyre (Andrade and Barton, 2000; Mooers and Maul, 1998), however this coastal circulation is modified by westward-propagating Caribbean Current eddies (Kastner et al., submitted).

Similar to other tropical estuaries, there has been little research focused on the hydrography and circulation of Bahía Almirante. The estuary has strong vertical stratification, driven by a pronounced halocline that results from the significant regional precipitation. The top layer is typically cooler as well, with a layer of warm, salty water below (Kaufmann and Thompson, 2005). Water temperatures range from 27-32 °C, with the highest temperatures observed in shallow regions of the bay (Li and Reidenbach, 2014; Collin and Chan, 2016; Lucey et al., 2020a, Collin et al., in review). A depth-uniform modeling study showed spatially-variable residence times that drove changes in sea surface temperatures (Li and Reidenbach, 2014). This spatial gradient, with higher values for both residence times and sea surface temperatures in the inner bay, is observed in other parameters, including chlorophyll and dissolved organic matter (Weinstock et al., 2022)

and biogeochemical parameters including DO, pH, and water temperature tend to covary within Bahía Almirante (Lucey et al., 2020a, Collin et al., in review).

Regional nutrient dynamics are poorly understood, but low nitrogen and phosphorus levels suggest that primary productivity in Bahía Almirante is nutrient-limited (D'Croz et al., 2005). A more recent study found that nutrient levels in rivers generally fall within government standards, although it is suggested that urban point source contributions are a more important nutrient source for Bahía Almirante than riverine discharge (Clark et al., 2022).

Bahía Almirante's ecosystems include mangroves, seagrass beds, and patch reefs (Collin, 2005; Guzman et al., 2005) Coral communities have most Caribbean species (Guzman and Guevara, 2001) and are relatively shallow (Collin et al., in review). There have been documented die-offs due to persistent temperature inversions (Neal et al., 2014) and hypoxia (Altieri et al., 2017; Johnson et al., 2021), as well as measurable sublethal effects in sea urchins that experience hypoxic conditions that are observed in the bay (Lucey et al., 2020b). Spatial patterns in hypoxia are reflected in the localized biodiversity (Lucey et al., 2021; Weinstock et al., 2022).

1.4 Outline of dissertation

As described above, there is substantial scientific research on the biology of Bahía Almirante and the effects of hypoxia. However, observations of the physical dynamics of the system are scarce. This thesis aims to provide a deeper understanding of the circulation and dominant physical mechanisms in Bahía Almirante and to identify how they regulate DO dynamics, thus addressing gaps in our knowledge of Bahía Almirante specifically and shedding light on how tropical estuaries may function.

This dissertation is divided into five chapters. Chapter 1 outlines the motivation for the research, the relevant background, and the key questions that will be answered in

the dissertation. A description of the work completed is included here.

In Chapter 2, we use a ten-year time series of weekly profiles of water properties at seven sites within in Bahía Almirante to examine the physical processes that are important in regulating hypoxia and temperature inversions. We show that seasonal hypoxia develops at depth and temperature inversions occur within Bahía Almirante. We demonstrate that these features are concurrent with seasonal increases in precipitation, which drives strong salinity stratification of the water column. A case study suggests that reoxygenation can occur due to lateral advection of oxygenated water. We show that hypoxia and temperature inversions are more severe and persistent in inner bay and that physical dynamics tend to lead to coincident stressors.

In Chapter 3, we investigate the relative influences of barotropic and baroclinic flow on Bahía Almirante. We use data from a two-year intensive field campaign to show that there is a residual barotropic flow between inlets in Bahía Almirante associated with alongshore pressure gradients that are modulated by larger scale processes. We find that baroclinic exchange is generally weaker than barotropic transport and is damped during periods of strong mean flow. Spatial variations in water property data (e.g., salinity, water temperature, DO) build on results from Chapter 2 and suggest hydrographically-distinct regions of the estuary, and we demonstrate that the inner bay is often isolated, particularly at depth, due to limited exchange, while the outer bay water properties approach offshore conditions for periods of strong net flow.

In Chapter 4, we attribute reoxygenation in Bahía Almirante to physical forcing, specifically lateral advection. We show that deep water renewal is the primary mechanism for hypoxia breakdown, and consequently that Bahía Almirante, a shallow tropical estuary, shares some dynamical similarities with fjords, which are typically deep and glacially-carved systems. We identify mechanisms for density reduction of the stagnant, hypoxic water mass. We demonstrate that diapycnal mixing, typical in fjords, cannot account for the change in bottom temperature during isolation events, and thus that radiative heating

plays an important role in density reduction of the bottom layer. We show that the DO drawdown timescale is shorter than the renewal timescale, and therefore this system tends towards hypoxia. The renewal timescale is linked to the offshore density, and consequently the seasonal hypoxia, described in Chapter 2, is driven by offshore influences.

These three main chapters combine long-term monitoring datasets, focused observational datasets, and a global reanalysis product to investigate the dynamics of tropical estuaries on different timescales. We consider the seasonal timescale via climatological means (Chapters 2 and 4), as well as through time series analysis (Chapters 2, 3, and 4), and the event timescale (Chapters 2 and 4). Chapter 5 summarizes the research presented in this dissertation and outlines areas of opportunity for future research. Ultimately, these chapters contribute to an improved understanding of tropical estuary physical dynamics and drivers of hypoxia in the tropics. Given the bias towards higher latitudes in oceanographic research, investigating these systems is crucial to equitably and effectively address ocean sustainability challenges.

Chapter 2

Seasonal hypoxia and temperature inversions in a tropical bay

2.1 Abstract

Dissolved oxygen (DO) is a critically important ecological variable, and the prevalence of marine hypoxia is expected to increase due to the combined effects of ocean warming and eutrophication. Thermal stress can co-occur with hypoxia, especially in tropical systems, and can exacerbate its effects. We examine the physical processes that are important in regulating hypoxia and temperature inversions in Bahía Almirante, a semi-enclosed tropical embayment on the Caribbean coast of Panamá. A 10-year record of observations at 7 locations within Bahía Almirante reveals seasonal temperature inversions and hypoxia at depth that often co-occur. These features are more severe and persistent in the back bay, though they occur throughout Bahía Almirante. DO reductions correspond to periods with high freshwater input, including direct precipitation, resulting in strong salinity stratification that isolates bottom waters, allowing biological oxygen demand to draw down DO. Evidence indicates that lateral advection can contribute to reoxygenation events, and the relationship between near bottom DO and bottom salinities in the mid bay and back bay is consistent with deep water renewal as the mechanism for bottom water ventilation. These hypoxia and temperature inversion events impact the biological communities of Bahía Almirante, and the physical dynamics that regulate these coincident

and persistent stressors for marine organisms are likely present in other shallow, tropical estuaries.

2.2 Introduction

Ocean deoxygenation is a prevalent phenomenon in many regions of the ocean (Diaz and Rosenberg, 2008). Dissolved oxygen (DO) affects ecosystem function, biodiversity, and biogeochemistry in the ocean (Breitburg et al., 2018), and the number, intensity, and duration of hypoxic episodes is expected to increase due to the combined effects of ocean warming and eutrophication (Levin and Breitburg, 2015). Hypoxia is commonly defined as DO <2 mg/L, but adverse effects for many species occur above this threshold (Vaquer-Sunyer and Duarte, 2008).

Hypoxia is particularly common in estuarine and coastal waters (Gilbert et al., 2010) where both biogeochemical processes including primary production and oxygen consumption (e.g. respiration and sediment uptake) and physical mechanisms (e.g. stratification, mixing, and advective transport) impact hypoxia development and breakdown. Eutrophication contributes to deoxygenation of coastal waters through organic material decomposition and associated microbial respiration and can lead to hypoxia (Breitburg et al., 2018). In estuaries and coastal waters, eutrophication is often linked to rivers laden with anthropogenic nutrients (Howarth, 2008), but there are also natural mechanisms that deliver nutrient-rich and/or oxygen-poor waters to continental shelves (Diaz and Rosenberg, 2008), including upwelling (Chan et al., 2008) and watersheds with naturally high nutrient and organic matter (Wetz et al., 2006). Furthermore, conducive physical conditions can lead to hypoxia with or without excess nutrient inputs, such as water column stratification, water retention, or a combination thereof. Estuaries are often highly stratified such that a pycnocline isolates incoming, oceanic water from the outgoing, surface layer (Fennel and Testa, 2019). When water column stratification inhibits bottom water ventilation

and there is no other mechanism for oxygen replenishment, hypoxia can develop, without nutrient additions.

Common mixing mechanisms that can contribute to coastal and estuarine bottom water ventilation, thus providing brief DO replenishment or full reoxygenation, include cooling convection (e.g., Boesch and Rabalais, 1991), wind-driven mixing (e.g., Stanley and Nixon, 1992), and tide-driven mixing (Kemp et al., 2009). Advection due to baroclinic longitudinal estuarine exchange and lateral circulation can also enhance vertical mixing and break down stratification (MacDonald and Geyer, 2004; Smith, 1976), thus impacting DO. Additional advective processes including variations in river inflows (Scully, 2013) and deep water renewal, commonly observed in fjords (Gade and Edwards, 1980), also contribute to DO dynamics.

Hypoxia has been primarily documented in temperate coastal waters and estuaries (Diaz and Rosenberg, 2008; Breitburg et al., 2018). Tropical estuaries are poorly studied relative to their temperate counterparts, and consequently there is inadequate data to elucidate the dynamics and function of tropical estuarine systems (Vieillard et al., 2020). While low DO in deep tropical waters has been given some attention (e.g., Scranton et al. (2014); Avendaño-Alvarez et al. (2017); Bates (2017); Kealoha et al. (2020)), few studies have focused on hypoxia in shallow tropical embayments. Ocean warming and acidification are frequently cited as threats to coral reefs, but there are still fundamental knowledge gaps in the role that low-DO levels and multiple stressors play in ecosystem health (Hughes et al., 2020), and a review of global literature by Altieri et al. (2017) suggests that dead zones in the tropics are likely severely under-reported, perhaps by an order of magnitude.

While similarities to temperate regions exist, fundamental differences in tropical climate, oceans, and ecology suggests that alternate mechanisms may affect hypoxic events. For example, there are salient differences in nutrient cycling (Vieillard et al., 2020). Additionally, solar radiation and rainfall are high and exhibit weak seasonal patterns relative to temperate regions (Nittrouer et al., 1995). These factors can contribute to stratification

patterns, and can thus affect mixing and DO dynamics. Additionally, warm temperatures increase microbial respiration associated with organic material decomposition (Pomeroy and Wiebe, 2001). Thus, while the mechanisms that regulate tropical DO dynamics are similar to temperate systems, there are tropics-specific contributors that can modify these factors.

Tropical coral reef environments typically have high water clarity, and consequently, incident shortwave radiation can penetrate deep into the water column. Wells et al. (2012) observe bottom waters that warm quickly, leading to temperature inversions that are maintained by salinity stratification. Thermal stress at depth has been observed in tropical systems (Neal et al., 2014) and can co-occur with, and exacerbate the effects of, hypoxia (Vaquer-Sunyer and Duarte, 2011). Tropical ecosystems are generally oligotrophic and may be more vulnerable to the detrimental effects of eutrophication (Corredor et al., 1999), in part due to ecological feedbacks and thresholds in ecosystem state (Altieri et al., 2021). The paucity of comprehensive DO observations in the tropics demonstrates a critical need for understanding hypoxic events dynamics in order to predict and, if possible, mitigate the effects on corals and other foundation species. This study aims to examine physical mechanisms that impact the evolution of hypoxia in a tropical estuary that differ from temperate systems, including precipitation patterns and a surface heat budget, and the role they play in the hypoxia evolution and breakdown.

In this paper, we examine over ten consecutive years of hydrographic data documenting recurring seasonal hypoxic events in a semi-enclosed tropical embayment in the Bocas del Toro Archipelago on the Caribbean coast of Panamá. This analysis highlights the physical processes that are important in regulating hypoxia and temperature inversions in Bahía Almirante (Figure 2.1). We aim to (1) document the patterns of seasonal variation in physical parameters, including temperature, salinity, and DO and (2) use these patterns to shed light on the likely physical mechanisms impacting the development and breakdown of hypoxia.

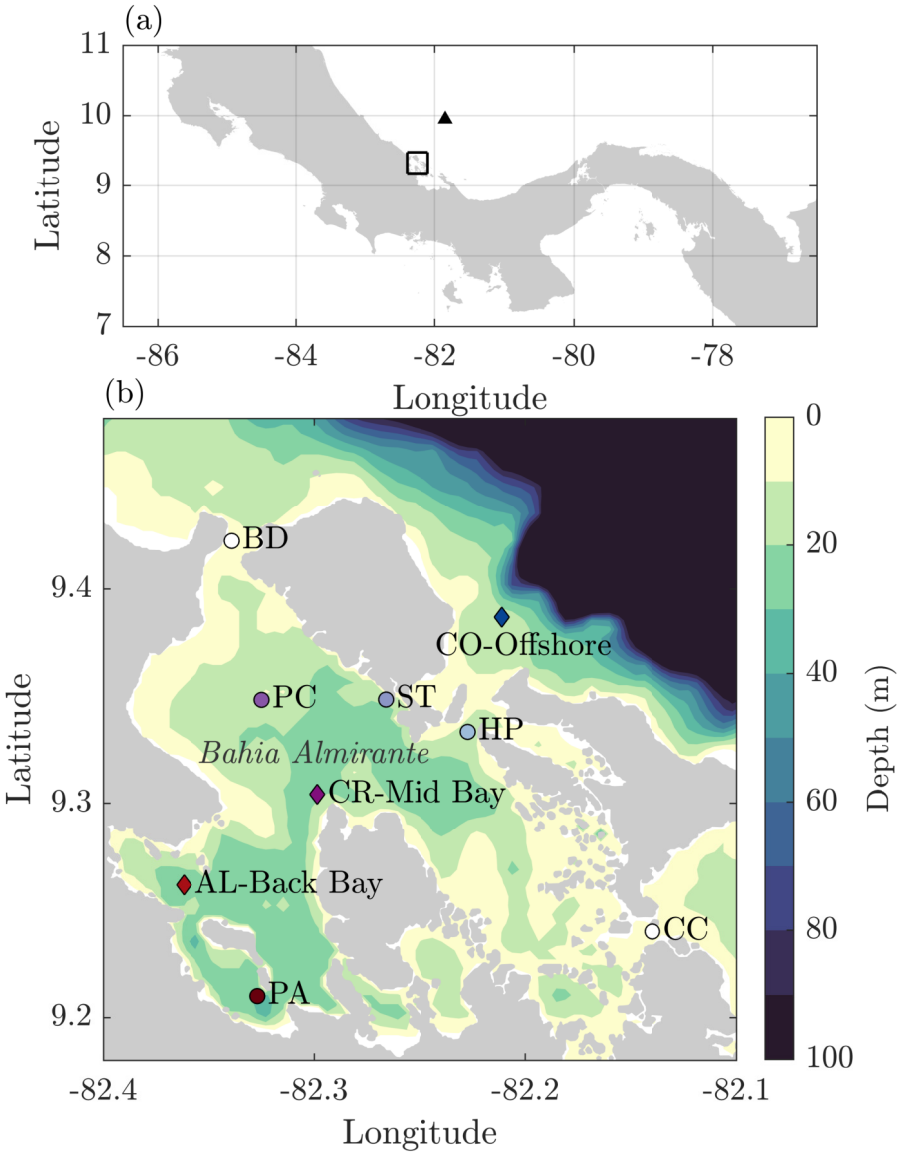

Figure 2.1. (a) Panamá Coast, with Bahía Almirante in black box. Triangle indicates location of ECMWF winds. (b) Weekly monitoring sites, colored by distance from offshore (blues) to the back bay (reds), used in subsequent figures. Diamonds indicate sites used to represent the bay regions in Figure 2.3. ST is also the location of the local meteorological station. Bathymetry in color (GEBCO 2014). Sampling sites not used in this analysis are shown in white.

2.3 Methods

2.3.1 Site description

Bahía Almirante's area is approximately 500 km^2, and the watershed is comprised of an equivalent area, although approximately half of it is coastal wetlands (Kaufmann and Thompson, 2005). The bay's ecosystems include mangroves, seagrass beds, and patch reefs (Collin, 2005). Previous work has noted pronounced haloclines in Bahía Almirante resulting from high rainfall (3 m/year) and river runoff, with a top layer of low-salinity, typically cooler water transitioning sharply to a bottom layer of warmer water with near oceanic salinity (Kaufmann and Thompson, 2005). A 2D (depth uniform) modeling study of Bahía Almirante linked horizontally spatially-variable flow patterns and residence times to sea surface temperatures within regions of the bay (Li and Reidenbach, 2014). Regional nutrient dynamics are poorly understood, but low nitrogen and phosphorus levels indicate that primary productivity in Bahía Almirante is nutrient limited (D'Croz et al., 2005), suggesting that eutrophication would meaningfully change the biological system. A recent study of river water quality in the Bahía Almirante watershed suggests that urban point source contributions are a more important nutrient source for the bay than riverine discharge (Clark et al., 2022).

Water properties in Bahía Almirante are affected by offshore ocean conditions through its multiple inlets. The bay has three major channels: Boca del Drago and Canal de Bastimentos connect Bahía Almirante to the open ocean and Cayo Coral opens into Laguna de Chiriqui (Figure 2.1). Offshore water temperature and salinity are affected by the migration of the Intertropical Convergence Zone (ITCZ), the propagation of atmospheric tropical waves through the Atlantic basin, and variations in weather patterns (Kaufmann and Thompson, 2005). The key circulation feature offshore is a southeastward surface flow associated with the cyclonic Panamá-Colombia gyre. There is debate on the persistence of this feature (Andrade and Barton, 2000), although Centurioni and

Niiler (2003) observed strong cyclonic flow based on five years of drifter observations. The Caribbean Sea has a well-mixed surface layer extending to 50 m, overlying a region (50-250 m) with strong stratification (Gallegos, 1996).

Bahía Almirante's ecosystems face common coastal threats, including thermal, photic, and physical stresses. Persistent temperature inversions have led to increased thermal stress at depth (Neal et al., 2014). Bahía Almirante has experienced low-oxygen events combined with warming, leading to widespread bleaching and mortality of corals and other marine invertebrates (Neal et al., 2014; Altieri et al., 2017). In addition to the lethal effects of hypoxia, a recent experiment shows that some organisms, including sea urchins, exhibit measurable sublethal changes in performance when subjected to oxygen levels that reflect hypoxic conditions in Bahía Almirante (Lucey et al., 2020a).

2.3.2 Data description

This analysis uses data from the Smithsonian Tropical Research Institute (STRI)'s Physical Monitoring Program at the Bocas del Toro Research Station in Panamá (Patton, 2023). STRI has collected air temperature, wind speed and direction, solar radiation, relative humidity, sea surface height, and water temperature data at a meteorological station (9.35°N, 82.26°W; Figure 2.1), from June 17, 2002 to present. Values from June 2002 to April 2005 were recorded hourly. Beginning in June 2005, variables were measured every 10 seconds with average values recorded every 15 minutes. The European Centre for Medium Range Weather Forecasts (ECMWF) reanalysis product winds and total precipitation approximately 90 km offshore in Mosquito Gulf (9.95°N, 81.85°W; Figure 2.1) provide regional meteorological context.

STRI has conducted a spatial sampling program from October 2010 to present. Nominally weekly vertical water column profiles of salinity, temperature, and DO were collected at sites around Bahía Almirante (Figure 2.1). Seven sites were regularly visited (Almirante, Cristobal, Hospital Point, Pastores, Punta Caracol, and STRI within the bay;

and Colon just offshore), and in 2019, a site near the channel at Boca del Drago was added. Measurements were taken in the same order at approximately the same time of day for each site, generally between 08:00 and 13:00 local time. Because the survey sites were sampled from offshore to onshore, there is some potential for diurnal aliasing. As a point of reference, data collected by a near-surface, moored YSI multiparameter sonde at STRI, located in shallow water near dense communities of seagrass, indicates that, on average, over the typical sampling period, water temperature increases by 0.5 °C due to solar heating, and DO increases by 0.7 mg/L due to photosynthesis. This provides an upper bound for near-surface bias, with smaller changes expected at depth.

Before May 2015, samples were collected at four discrete depths (0.5 m, 5 m, 10 m, 20 m) via bottle samples. Since May 2015, vertical profiles were measured using a YSI multiparameter sonde, including an optical DO sensor. Salinity accuracy is 1.0% of reading or 0.1 ppt (whichever is greater), temperature accuracy is 0.01°C, and DO accuracy is ± 0.1 mg/L or 1% of reading, (whichever is greater). Because profiles were not uniformly steady, profile data were averaged into 2 meter bins and weighted by the vertical distance between measurements. When possible, only the downcast was considered, unless there was only an upcast (1% of casts). Density was calculated from measured salinity, temperature, and depth using Gibbs Seawater toolbox of TEOS-10 (McDougall and Barker, 2011). Values with a negative stratification were excluded (1.6% of casts). Annual averages for all parameters were computed using semimonthly means (24 equally-spaced time bins per year).

2.3.3 Surface heat flux calculation

To assess bulk contributions due to advective heat fluxes, the net surface heat flux (Q_{SHF}) was calculated by estimating the shortwave (Q_{SW}), longwave (Q_{LW}), sensible

(Q_S), and latent (Q_L) heat fluxes, where

$$Q_{SHF} = Q_{SW} + Q_{LW} + Q_S + Q_L. \tag{2.1}$$

Shortwave heat flux was estimated using measured solar radiation, Q_{meas}, modulated by the sea surface albedo, α.

$$Q_{SW} = (1 - \alpha)Q_{\text{meas}}. \tag{2.2}$$

Albedo was estimated via atmospheric transmittance and sun altitude, following Payne (1972). Longwave heat flux was calculated following Talley (2011) and Johnson et al. (2018) using observed sea surface temperature, air temperature, and water vapor. The method incorporates fractional cloud cover, estimated from satellite observations of cloud data from NASA's Clouds and the Earth's Radiant Energy System (CERES) project (NASA/LARC/SD/ASDC, 2015). Latent and sensible heat fluxes were computed using sea surface temperature, surface air temperature, wind speed, and relative humidity using the package developed by Pawlowicz et al. (2001) (algorithm from Fairall et al. (1996)). Shortwave, latent, and sensible heat flux time series were calculated at 15 minute intervals, while the longwave heat flux was calculated hourly.

2.4 Results

2.4.1 Meteorological conditions

Regional winds in Mosquito Gulf, approximately 90 km offshore, reflect seasonal nominally-northeasterly trade winds that weaken during the northern phase of the ITCZ (Andrade and Barton, 2000), with seasonal average magnitudes up to 2.75 m s^{-1} (Figure 2.2f). The local seasonal average winds are similar in magnitude (Figure 2.2a) and are steered by the Cordillera de Talamanca, mountains approximately 60 km to the west

which reach altitudes greater than 3400 m. The regional and local winds are maximum in January through March, and minimum in August through October, with a second, smaller wind peak in July.

There is significant freshwater influx to the bay through year-round precipitation, with moderate seasonality exhibiting precipitation increases in June through August and November through January (Figure 2.2b). The phasing is similar to the wind peaks (Figure 2.2a). Because Bahía Almirante's watershed is similar in area to the bay, roughly half of the freshwater input is expected to occur through direct precipitation, with the relative amount determined by the size of the bay versus the watershed. Offshore precipitation (Figure 2.2g) has a dry season from January to April and a rainy season from June to December.

2.4.2 Hydrography for Bahía Almirante

Similar to most estuarine systems, salinity is the most important parameter setting density stratification in the bay. The thermal contribution to density is on average approximately 11% of the salinity contribution. All sites exhibit vertical salinity stratification, including the offshore site (Figure 2.2c,h and Figure 2.3a,b,c). The lowest surface salinities are typically observed in the back bay, increasing slightly towards the mid bay, with higher surface salinities offshore (Figure 2.3a-c). Back bay salinities at depth are similar to, and occasionally exceed, the salinity at the offshore location. At 20 m, on average, the salinity difference between the bay sites and offshore is within 0.3-0.4 ppt. There are seasonal cycles in both surface and bottom salinities within the bay and thus in the water column stratification (Figure 2.2c, 2.2i). Surface salinities reach minimums in July/August and December/January, corresponding to periods with high precipitation (Figure 2.2b). The seasonal signal in salinity at 20 m is much weaker, with slight reductions from October-April, following offshore salinity Figure 2.2c, 2.2i).

Water temperatures in Bahía Almirante have an average of 28.9 °C with slightly

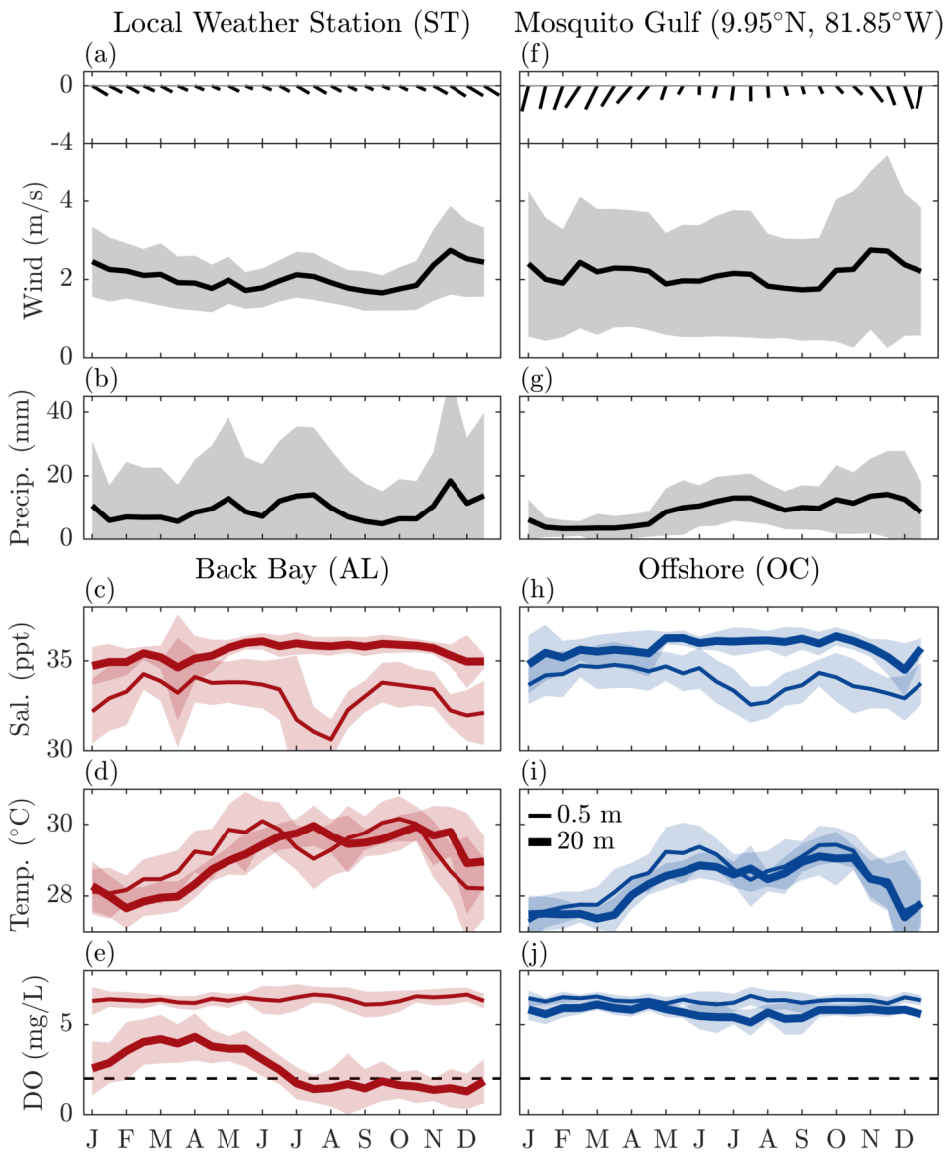

Figure 2.2. Climatologies for meteorological and hydrographical variables averaged in half month intervals. (a) local winds measured at STRI, and local root-mean-squared wind speed magnitude (black line); (b) precipitation at STRI (2002-2019); (c-e) show STRI sampling data for Almirante (a back bay site, Figure 2.1) with (c) salinity; (d) temperature; (e) DO; (f) offshore (9.95°N, 81.85°W) regional wind speed and direction and (g) total precipitation from ECMWF (ERA5, 2010-2020); (h-j) STRI sampling data for Colon (offshore site; Figure 2.1) for (h) salinity; (i) temperature; (j) DO. In (c-e) and (h-j), 0.5 m and 20 m are shown by light and heavy lines, respectively. Patches in all panels indicate ±1 standard deviation. 2 mg/L DO line (dashed) is shown for reference in (e,j).

cooler temperatures offshore (2.2d,i and 2.3d-f). The seasonal cycle dominates variability with the range and phasing consistent with values reported by Kaufmann and Thompson

(2005). Two seasonal peaks in the average surface temperatures (back bay; Figure 2.2d and g) coincide with each solar radiation maximum, while the 20 m temperature peaks lag the surface by approximately one month within the bay. The temperature maxima phasing is coincident with the formation of seasonal temperature inversions, with temperature at depth exceeding surface temperatures in July/August and November/December in the back bay (Figure 2.2d and Figure 2.3d-f). Seasonal temperature inversions are generally strongest in the back bay, decreasing in strength in the mid bay, and further weakened offshore (Figure 2.2d,i). Although increasing inversion strength weakens vertical stratification, the strongest temperature inversions are typically accompanied by strong bulk salinity gradients that maintain water column stability.

DO levels throughout Bahía Almirante vary and are typically normoxic. The critical exceptions are severe DO reductions that occur seasonally at depth ((Figure 2.2e and Figure 2.3g,h). On average, DO levels at depth begin to decline in May and reach hypoxic levels (<2 mg/L) in July (Figure 2.2e). Hypoxia can persist until bottom water ventilation occurs in December/January (Figure 2.2e). The time series at each of the three sites along the onshore-offshore line (Figure 2.3g-i) depict a pronounced spatial pattern of hypoxia in Bahía Almirante. Hypoxia occurs with the greatest regularity, intensity, and persistence in the back bay (Figure 2.3g), where DO reductions also occur at shallower depths. Corresponding seasonal DO declines are observed in the mid bay (Figure 2.3h), although these events rarely reach the 2 mg/L threshold and exhibit greater intermittency than the back bay. Offshore, hypoxia is never observed, and while weak DO declines occur at depth in June-September, values typically remain greater than 5 mg/L. There is no significant, long-term DO trend. While there is a strong seasonal pattern (Figure 2.2e), all sites demonstrate considerable interannual variability in the intensity, spatial extent, persistence, and depth of hypoxic waters in Bahía Almirante. For further exploration of the year-to-year variations in hypoxia (Figure S1, Figure S2) and temperature inversions (Table S1), see the Supporting Information.

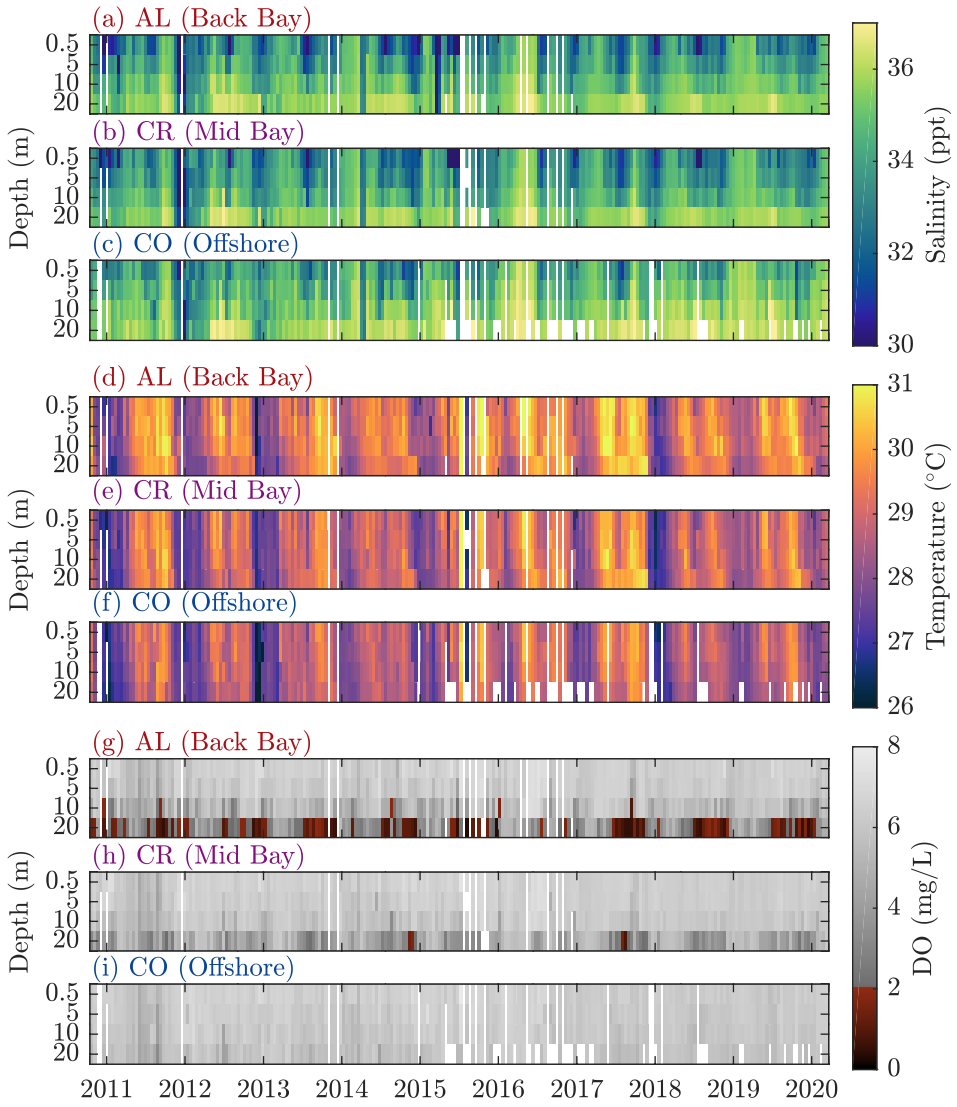

Figure 2.3. Salinity (ppt) (a-c), temperature (°C) (d-f), and DO (mg/L) (g-i) from water sample measurements (bi-weekly bins) at four discrete depths (0.5 m, 5 m, 10 m, and 20 m) at three of the survey sites, indicated with diamonds on Figure 2.1. Almirante (a,d,g) represents the back bay, Cristobal (b,e,h) represents the mid bay, and Colon (c,f,i) represents offshore conditions.

The spatial pattern evident in the data may be somewhat muted by the diurnal aliasing of the measurements, noted earlier. The offshore site is measured at an earlier point in the diel cycle than the back bay sites such that DO and water temperature will be relatively lower. This tends to counteract the spatial trend observed in the data. Tidal aliasing may also impact the measurements, but its effect is expected to be small because

of the small tidal range and phase shift between the diurnal cycle and the tides.

2.4.3 Seasonal and spatial patterns in hypoxia and temperature inversions

We examine the measurement period with higher vertical resolution (2015-2020) to provide a more comprehensive look at the variability and vertical structure of hypoxia and temperature inversions (Figure 2.4). The timing of the hypoxic season changes from year to year, with hypoxia onset typically occurring between May and July and bottom water ventilation between late December and February. Intermittent recoveries are common, particularly in the mid bay where few hypoxic episodes last more than a few consecutive weekly measurements (Supporting Information, Figure S1).

At all interior sites, average subsurface DO is reduced during hypoxic periods (Figure 2.4d); however, DO reductions are most extreme in the back bay (Almirante and Pastores; Figure 2.3g-i and 2.4a), where individual measurements are lower than 0.1 mg/L (the instrument accuracy limit) and individual hypoxic measurements reach depths as shallow as 7m. The average DO profiles for the hypoxic period in the mid bay (Cristobal, Hospital Point, Punta Caracol, STRI) exhibit minimum average levels as low as 3 mg/L (Figure 2.4d), a threshold known to have sub-lethal effects (Vaquer-Sunyer and Duarte, 2008). The offshore site remains normoxic and shows little variation between the hypoxic and normoxic periods. During the normoxic period, the mid bay sites exhibit DO profiles similar to offshore, while the back bay has reduced DO (Figure 2.4d,e).

Water temperatures tend to be warmer during the hypoxic periods relative to the normoxic periods (Figure 2.4b,f,g). Temperature inversions greater than 1°C commonly occur during the hypoxic period (Figure 2.4b, black dots) but are infrequent during the normoxic periods. Temperature inversions tend to occur in the mid water column, where hypoxic-period ensemble average temperatures can exceed 30°C (Figure 2.4e). The warmest temperatures occur in the back bay, with the mid-water column 1.1°C warmer

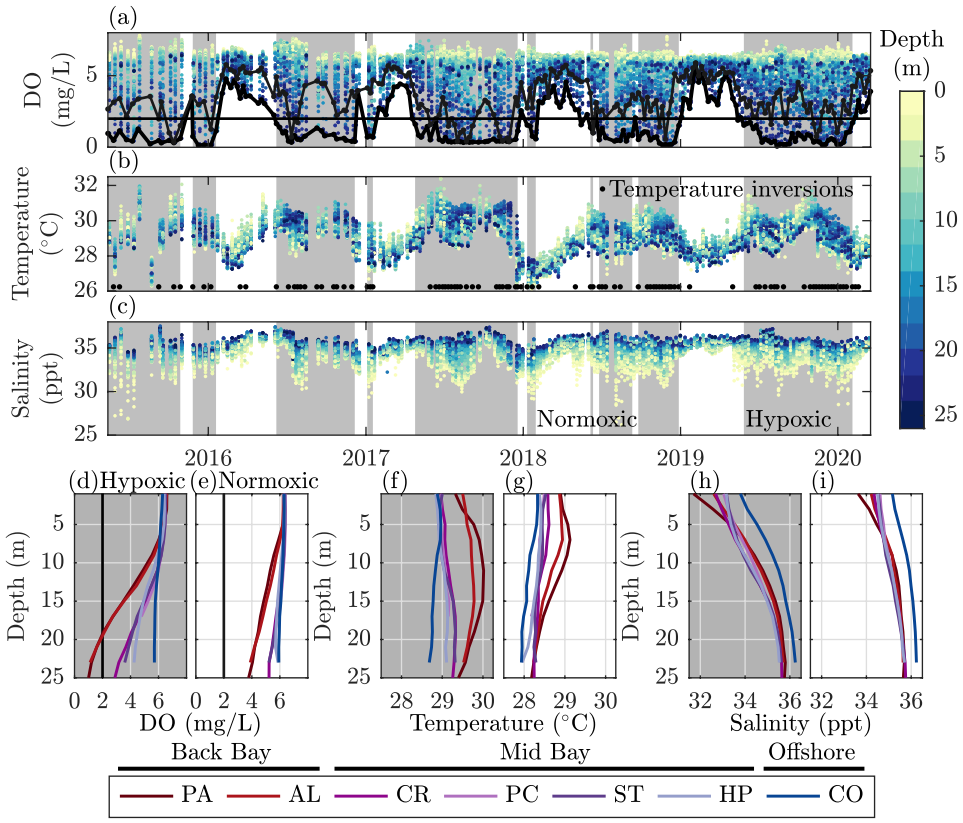

Figure 2.4. Profile time series from May 2015 to March 2020, at interior Bahía Almirante sites (all sites excluding offshore), with depth in color. Gray background indicates periods when at least one site is hypoxic (DO <2 mg/L), defined as the hypoxic period, whereas a white background indicates normoxic measurements (DO >2 mg/L) at all sites, defined as the normoxic period. (a) DO (mg/L), heavy black line: minimum DO; thin gray line: minimum DO excluding two back bay sites (Pastores and Almirante). (b) Temperature (°C), black dots denote profiles with a temperature inversion greater than 1°C anywhere in the water column; (c) salinity (ppt); (d-i) show ensemble average vertical profiles at each site during hypoxic (d, f, h) and normoxic (e, g, i) conditions for DO (d,e), temperature (f,g), and salinity (h,i). Sites are labeled in color as in Figure 2.1 and as identified in the legend. 2 mg/L DO line is shown for reference in (a,d,e).

than offshore and 0.8-0.9°C warmer than the other monitoring sites. While the thermal spatial gradient is diminished during the normoxic period, the back bay sites continue to exhibit temperature profiles that are warmer than the rest of the bay and that have near surface (<8m) temperature inversions.

The lowest surface salinities occur during the hypoxic period (Figure 2.4c,h,i), indicating stronger stratification. Additionally, there is a spatial gradient in surface

salinity, especially during the hypoxic period, leading to a horizontal gradient in vertical stratification, amplified during the hypoxic period, as average salinities at 20 m within the bay are consistent between the hypoxic and normoxic periods.

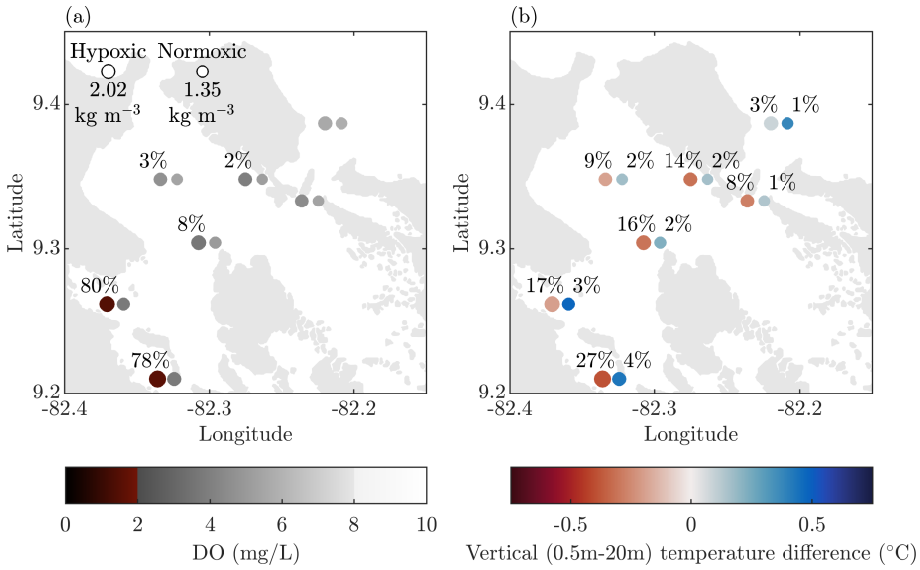

Figure 2.5. Spatial patterns of ensemble averages of: (a) DO at 20 m (indicated by color) during the hypoxic period (left bubble) and normoxic period (right bubble), as defined in Figure 2.4. Percentages indicate fraction of measurements that are hypoxic. If there are no incidents of hypoxia (i.e., 0%) the percentage is not included. (b): Vertical (0.5 m - 20 m) temperature difference (indicated by color) during the hypoxic period (left bubble) and normoxic period (right bubble). Red indicate temperature inversions. Percentages indicate percent of measurements that have vertical temperature differences greater than 1°C. Bubble size in both panels is scaled by the top-bottom density difference, with larger bubbles indicating greater stratification. Legend in (a) provides references of spatial-average, ensemble-averaged top-bottom density difference for the hypoxic and normoxic periods.

Seasonal hypoxia (Figure 2.5a) and temperature inversions (Figure 2.5b) follow similar spatial patterns; they are most intense and frequent in the back bay, where stratification is strongest, and decrease offshore. The offshore site and the site closest to a channel (Hospital Point) never experience hypoxia, while all sites experience temperature inversions during both the hypoxic and normoxic periods. The normoxic period typically has stable temperature stratification, with inversions in less than 5% of measurements at each site (Figure 2.5b, right bubble). During the hypoxic period, all sites experience

higher incidences of temperature inversions, and all, except the offshore site, exhibit a bulk temperature inversion in the ensemble average (Figure 2.5b, left bubble).

2.4.4 Dynamical drivers and co-occurrence of DO and temperature inversions

In order to develop a dynamical framework for hypoxia in Bahía Almirante, we consider physical environmental factors that influence hypoxia development and breakdown. This section examines evidence that high vertical stratification corresponds to low DO, temperature inversions, and high temperatures at depth. Lagged correlations are examined to explore the temporal relationships between environmental factors and water properties. The sampling interval prohibits consideration of lags shorter than one week; however, the time series length enables consideration of the relationships between parameters on weekly and longer time periods and provides a bulk sense of the dynamics in Bahía Almirante. Lags of up to five weeks were considered. Unless otherwise noted, the maximum correlation occurs with no lag. Confidence intervals found via bootstrapping ($n = 1000$) provide error bounds on the correlations and linear fits. While binned mean values are shown for illustrative purposes, all correlations reported correspond to raw data.

The dominant role of salinity on density variations in the bay suggests that precipitation will be important in determining vertical stratification. There is a statistically significant, weakly positive correlation ($r = 0.24$; $p < 0.05$) between weekly precipitation and vertical density difference lagged by one week (Supporting Information, Figure S3). The one week lag indicates that precipitation history is relevant and may also reflect a temporal delay in riverine freshwater inputs, although this delay may be between one day and one week. There is no statistical relationship between wind and vertical stratification.

The statistically significant negative correlation (r = -0.51; $p < 0.05$) between vertical stratification and DO indicates that low DO is linked to greater stratification (Figure 2.6a). Conversely, when the vertical density difference is weak, bottom waters are

more likely to be oxygenated.

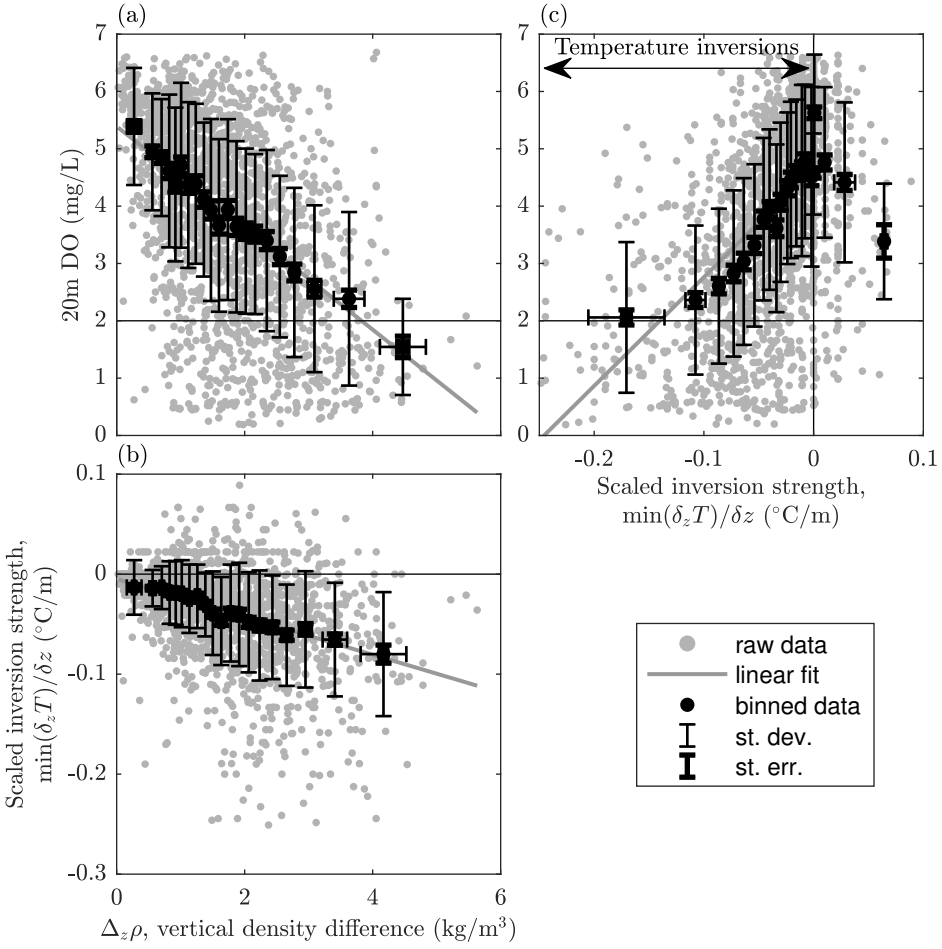

Figure 2.6. DO, temperature inversions, and stratification: Relationships between weekly sampled data including $\Delta_z \rho$, i.e. the vertical (20 m-0.5 m) density difference (kg/m^3), DO at 20 m (mg/L), and min($\delta_z T$)/δz, i.e. the most negative vertical temperature difference in the water column normalized by the difference in depths (°C/m), at the six interior sites. Outliers, absolute deviations greater than three scaled medians, are excluded. Gray points: raw data; black points: mean in 100 point bins; error bars: one standard deviation; heavy error bars: standard error.(a): 20 m DO vs. $\Delta_z \rho$. 35 outliers; 1.7%. For the raw data: r = -0.51; 95% confidence intervals = [-0.54 -0.47], $p < 0.05$. Fit slope = -0.88; confidence intervals = [-0.95 -0.82]. (b): min($\delta_z T$)/δz vs. $\Delta_z \rho$. 122 outliers, 6%. For raw data with inversions (i.e., min($\delta_z T$)/$\delta z < 0$; $n = 1746$), r = -0.38; 95% confidence intervals = [-0.41 -0.33], $p < 0.05$. (c): DO vs. min($\delta_z T$)/δz. 93 outliers; 4.4%. For raw data with inversions: r = 0.51; 95% confidence intervals = [0.48 0.54], $p < 0.05$. Fit slope = 19.0; confidence intervals = [17.3 20.6].

There is also a statistically significant negative correlation (r = -0.38; $p < 0.05$)

between vertical stratification and the magnitude of the most negative vertical temperature gradient normalized by its depth interval, $\min(\delta_z T)/\delta z$ (Figure 2.6b). This indicates that temperature inversion strength also increases with increased stratification. Temperature inversions co-occur with lower DO concentrations, while no clear relationship is evident between DO and positive $\min(\delta_z T)/\delta z$ (Figure 2.6c). This statistically significant relationship is not interpreted as causal because it is most likely a result of temperature inversions and hypoxia resulting from related dynamical conditions, in this case increased salinity stratification (Figure 2.6a,b).

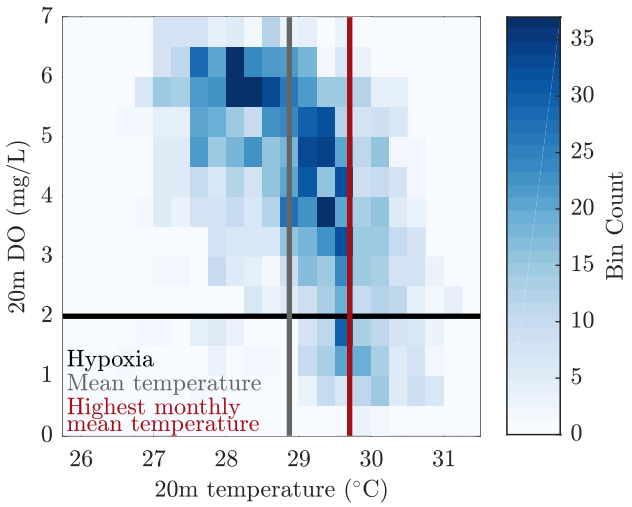

Figure 2.7. Histogram of DO vs. temperature: 2D histogram of weekly sampled DO at 20 m (mg/L) vs. weekly sampled temperature at 20 m (°C) at the six interior sites. Reference lines include: 2 mg/L DO (black), baywide average temperature (gray), and highest monthly mean temperature (red). Temperature bin widths: 0.5 °C, DO bin widths: 0.5 mg/L.

Using a technique developed by Goreau and Hayes (1994) to identify potential areas of coral bleaching based on satellite data, "hot spots" can be identified by regions with sea surface temperatures at least 1°C greater than the highest (i.e. warmest) monthly mean. The highest monthly baywide-mean temperature in Bahía Almirante is 29.7 °C at both 0.5 m and 20 m depth (Figure 2.7, red line). As conditions approach the lower right quadrant of Figure 2.7, organisms are more likely to experience metabolic stress. 18%

of data exceed the highest monthly mean temperature, and 16% are below the 2 mg/L hypoxia threshold, with 7% of the data occurring when both temperature exceeds the highest monthly mean and DO falls below the hypoxic threshold (i.e., lower right corner of Figure 2.7 defined by the red and black lines). At least one of these stressors is present for 27% of measurements. There are only eight data points (approximately 0.4% of all data) in the parameter space where thermal stress (exceeding the highest monthly mean temperature by +1°C; line not shown) co-occurs with hypoxic stress (<2 mg/L), as these benchmarks are defined. When considering only the back bay sites (Almirante; Pastores), 17% experience multiple stressors, and 1% of measurements exceed the highest monthly mean by +1°C. While this is illustrative for potential implications for organisms, this analysis considers the bay as a whole and does not account for species-specific thresholds or spatial distribution, nor tolerance shifts due to the presence of multiple stressors.

2.4.5 Heat budget

High residence times can be conducive to deoxygenation, and lateral advection is a possible mechanism of bottom water ventilation. Analysis of the bay heat budget allows assessment of the role of advection, provides residence time estimates, and explores the spatial and seasonal variations to further understand the patterns previously described. Shortwave radiation (Q_{SW}) dominates the net surface heat flux (Q_{SHF}), with peaks that occur during the solar maxima for the tropics (Figure 2.8a). Notably, there is an input of heat throughout the year.

A simplified integral heat budget for a control volume can be written as:

$$\langle \overline{\rho} \rangle \, C_p h A \frac{\Delta \langle \overline{T} \rangle}{\Delta t} = \overline{H}_S + \overline{H}_A. \tag{2.3}$$

Here C_p is the specific heat capacity (in units J/K kg), h is the average water depth, and A is the surface area. <> represents a volume average for the region of interest, and the

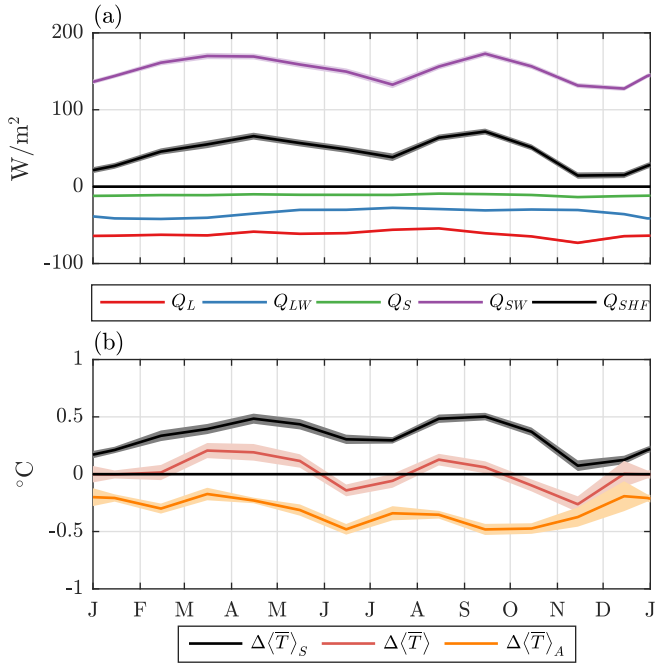

Figure 2.8. Annual pattern for: (a), surface heat flux (Q_{SHF}, black line) in Bahía Almirante, and its components: latent heat flux (Q_L, red line), long wave heat flux (Q_{LW}, blue line), sensible heat flux (Q_S, green line), shortwave heat flux (Q_{SW}, purple line). (b) the measured, normalized weekly change in water temperature ($\Delta\langle\overline{T}\rangle$, pink line), the weekly change in temperature due to the surface heat flux, assuming one-dimensional ($\Delta\langle\overline{T}\rangle_S$, black line), and the residual change in water temperature, assumed due to advection ($\Delta\langle\overline{T}\rangle_A$, orange line), where a positive value indicates heat transport into the bay and negative indicates heat export.

overbar indicates temporal averaging over a time scale Δt, such that $\langle\overline{\rho}\rangle$ and $\langle\overline{T}\rangle$ are the volume- and time-averaged density and temperature, respectively, $\overline{H}_S = \overline{Q}_{SHF}A$ is the net surface heat flux integrated across the surface, and $\overline{H}_A$ represents the net heat contribution due to all advective sources. The latter can include lateral fluxes across boundaries, input from rivers and heat fluxes due to precipitation.

The integrated heat budget in (2.3) then yields the temporal change in the bulk temperature which can be decomposed into surface heat flux and advective components:

$$\Delta\langle\overline{T}\rangle = \Delta\langle\overline{T}\rangle_S + \Delta\langle\overline{T}\rangle_A. \tag{2.4}$$

The weekly temperature change for a particular region, $\Delta\langle\overline{T}\rangle$, can be estimated using the weekly sampling observations, with $\Delta t = 1$ week. The contribution due to the surface heat flux, $\Delta\langle\overline{T}\rangle_S = \overline{Q}_{SHF}\Delta t/\left(\langle\overline{\rho}\rangle\, C_p h\right)$, can be estimated from the weekly averaged heat flux quantities (as described in the methods section). The change in temperature due to the advective flux, $\Delta\langle\overline{T}\rangle_A = \overline{H}_A\Delta t/\left(\langle\overline{\rho}\rangle\, C_p hA\right)$, is then estimated as the residual.

Figure 2.8b shows the annual average variations in the bay-wide (average of interior bay sites) weekly temperature change along with variations in $\Delta\langle\overline{T}\rangle_S$ and the residual, $\Delta\langle\overline{T}\rangle_A$, using equation (4). $\Delta\langle\overline{T}\rangle_S$ has two peaks in expected temperature increase and is positive throughout the annual cycle, reflecting the net surface heat influx. The observed temperature is consistent with a largely steady state thermal balance with periods of increasing and decreasing temperatures that are in phase with the surface flux. The difference, $\Delta\langle\overline{T}\rangle_A$, reflects a net outward advective heat flux (Figure 2.8b, orange line). Bahía Almirante thus acts as a net exporter of heat, consistent with the higher bay temperatures and as would be necessary to compensate for the net input at the surface, as is common at the tropics.

Precipitation and river flow contributions to the advective heat flux associated can be shown to be negligible, using observed rain estimates with reasonable temperature values. We assume that the advective heat flux is primarily through the three main channels (Figure 2.1) and can be written in terms of a time-averaged effective exchange volume flux $\overline{\Gamma}$, as

$$\overline{H}_A = 2\,\langle\overline{\rho}\rangle\, C_p \Delta T_X \overline{\Gamma}, \tag{2.5}$$

where $\Delta T_X = \overline{T}_{\mathrm{CO}} - \langle\overline{T}\rangle$ is the temperature difference between the interior bay and the offshore site, Colon. Using (2.5), we can calculate $\overline{\Gamma}$ as

$$\overline{\Gamma} = \frac{\Delta\langle\overline{T}\rangle_A}{2\Delta T_X}\frac{hA}{\Delta t}. \tag{2.6}$$

where $\Delta\langle\overline{T}\rangle_A$ is estimated using (2.4). This estimate of $\overline{\Gamma}$ indirectly incorporates the turbulent and tidal fluxes.

The seasonal variation in ocean-bay temperature difference, ΔT_X, remains negative over the year (on average, about -0.5°C; not shown) and is fairly constant, consistent with heat export. The resulting effective volume exchange $\overline{\Gamma}$ (not shown) then follows the pattern for $\Delta\langle\overline{T}\rangle_A$ (Figure 2.8b).

We can estimate a bulk residence time (t_r) for the bay using $\overline{\Gamma}$ as:

$$t_r = \frac{hA}{\overline{\Gamma}} = \frac{2\Delta T_X \Delta t}{\Delta\langle\overline{T}\rangle_A}. \tag{2.7}$$

There is no discernible seasonal pattern in t_r (not shown), but median monthly values in bulk residence times for the bay vary between 10-40 days. Residence times for subregions of the bay can similarly be calculated using Equation 2.7 with appropriate volume averages, with the surface heat flux assumed to be the same in each region. Median values are given in Supporting Information Table S2 for the mid bay to offshore, back bay to offshore and the full bay to offshore. Estimates for the mid bay are lower, i.e. shorter, than for the back bay as expected. The persistence of strong stratification and hypoxic events, especially at the back bay, reflects the spatial heterogeneity that is suggested by the residence time estimates, with shorter times near the entrances and much longer values towards the back bay, consistent with the results in Li and Reidenbach (2014).

2.4.6 Examination of a hypoxia breakdown event

The time series data in Figures 2.3 and 2.4 highlight considerable year-to-year and event-to-event variability, reflecting more complex dynamics associated with hypoxic event breakdown than is evident in the climatology. Here, we examine a specific breakdown event that illustrates potential mechanisms that can affect bottom water ventilation in Bahía Almirante.

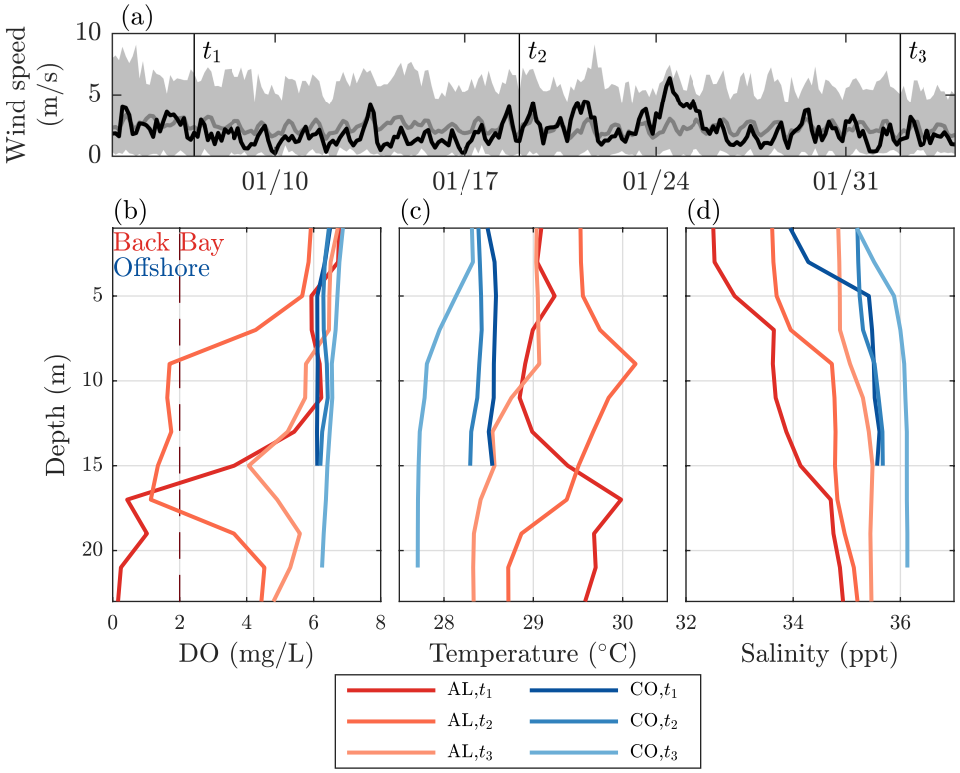

Figure 2.9. January 2016 hypoxia breakdown. (a) wind speed, 4 January - 4 February 2016 (black line), climatological mean (gray line), range over time series (gray shading), (b-d) profiles for (b) DO, (c) temperature, (d) salinity for Almirante (back bay, red) and Colon (offshore, blue). Time increases for lighter colors: 7 January 2016 (dark red and blue); 19 January (medium red and blue); and 2 February (light red and blue).

At the start of the period considered, a deep hypoxic layer (time t_1, 7 January 2016, Figure 2.9b; dark red) is warmer than the rest of the water column and offshore (Figure 2.9c; dark red) and has a higher salinity than the rest of the water column (Figure 2.9d; dark red). This suggests an isolated bottom layer at t_1, approximately 5-7m thick. The bottom layer in the back bay is oxygenated by the next measurement, (t_2, 19 January 2016); however, the mid-water column is hypoxic (Figure 2.9b; medium red), between 8-18 meters. The temperatures and salinities in the mid-water column at t_2 are similar to those of the bottom layer at t_1. The temperatures and salinities at depth are cooler and saltier at t_2 than t_1. By 2 February 2016 (t_3), the water column is normoxic (Figure 2.9b; light red), although there is remnant vertical structure in the DO profile. At t_3,

the water column is colder and saltier relative to t_2 in the back bay. Over the same time window, offshore water properties (2.9c,d; medium blue, light blue) are also cooler and saltier, while DO remains normoxic. By t_3, there is no meaningful temperature inversion and salinity stratification has weakened. Density profiles (not shown) indicate that the system is salinity stratified through this time period.

The time series of three-hour averaged wind speeds indicates that between t_1 and t_2, wind speeds appear to be typical for this time of year, between 0.2 m/s and 4.1 m/s, compared to the average range of 1.3 m/s to 3.3 m/s (Figure 2.9a). Between t_2 and t_3, there is a significant wind event, with wind speeds reaching 6.4 m/s, approaching the historical maximum for this time period.

In this example, the changes in deep water properties in the back bay are consistent with advective processes, suggesting that offshore influences play a role in governing the system. The hypoxic layer at the back bay site appears to be replaced by a deep intrusion of water with higher salinity and lower temperature, consistent with properties from the offshore site. The similarities between the water properties at depth during the first measurement (t_1) and in the mid-water column during the second measurement (t_2) suggests that the hypoxic layer was displaced upwards. It is notable that the deep water ventilation is coincident with light winds between t_1 and t_2. Changes near the surface are evident between t_2 and t_3, though salinity at depth continues to increase indicating that wind-driven mixing from the wind event between t_2 and t_3 does not extend to the bottom layer.

2.5 Discussion

Analysis of the hydrography of Bahía Almirante reveals an estuarine structure with regular, seasonal hypoxia at depth, often coincident with temperature inversions, where both are more prominent towards the back of the bay. Hypoxia occurrence and

temperature inversion events are correlated with seasonal changes in stratification. The following discussion examines the potential mechanisms for the onset and breakdown of hypoxic events.

2.5.1 Onset of hypoxic events

Freshwater inputs influence DO levels in Bahía Almirante via stratification. Conditions offshore remain normoxic indicating that hypoxia develops within the bay. The precipitation increase that begins in April/May (Figure 2.2b) is correlated with a surface freshening (Figure 2.2c) leading to increased vertical salinity stratification (Supporting Information, Figure S3), even while salinity at depth remains high and sometimes exceeds offshore values. Because Bahía Almirante's watershed is relatively small, direct precipitation is a critical freshwater source (Clark et al., 2022). Freshwater inputs into canonical estuaries are dominated by rivers, leading to a horizontal density gradient that drives exchange flows. In contrast, Bahía Almirante's rivers are small and dispersed, largely along the mainland, and direct rainfall results in a broad freshwater capping layer that extends offshore, which may lead to reduced baroclinic advection and consequently increased flushing timescales relative to those for equivalent riverine inputs.

Stratification's critical role in the onset and evolution of hypoxia is consistent with observations in temperate estuarine and coastal systems (Stanley and Nixon, 1992; Wiseman et al., 1997; Scully, 2013). In Bahía Almirante, the drawdown of DO at 20 m typically begins around April and continues through August, coincident with the surface freshening (Figure 2.2). This seasonal view further supports the idea that hypoxia develops after a period of elevated freshwater input which results in a strong, salinity-induced vertical stratification with an isolated deep layer. Continued biological oxygen demand from the respiration of organic matter within this isolated layer leads to hypoxic conditions. It is possible that a seasonal cycle in respiration may contribute to the observed patterns in hypoxia; however previous work indicates that there is not a seasonal signal in chlorophyll

concentrations (Collin et al., 2009). The lack of seasonality in primary productivity in Bahía Almirante may be similar to other tropical, oligotrophic systems, as solar radiation weakly varies throughout the year.

This analysis has demonstrated that stratification in Bahía Almirante is adequately strong for the formation and maintenance of hypoxic events. Nutrient dynamics were not considered in this analysis, but they may play a role in seasonal hypoxia in the bay. Regional coastal land use changes include banana cultivation and development (Cramer, 2013), and thus possible avenues for nutrient fluxes into Bahía Almirante include untreated sewage outfalls, river inputs, marine sources, groundwater, and atmospheric deposition. It can be inferred that nutrient loading would exacerbate the effects of the physical conditions that favor hypoxia (Rabalais et al., 2010), although the contribution of excess nutrients to hypoxia development in Bahía Almirante remains an open question. The precipitation patterns in Bahía Almirante that impact stratification, particularly the lack of a dry season, differ from other tropical regions; however, the seasonality in precipitation may also play a role in stratification, and thus DO dynamics, in other tropical estuaries.

2.5.2 Breakdown of hypoxic events

Despite interannual variability in the onset, duration, and termination of the hypoxic period, annual deoxygenation indicates that the driving forces of hypoxia also occur on a seasonal timescale. Seasonal averages (Figure 2.2) and the time series data (Figure 2.3) indicate that despite stratification weakening in September, hypoxia persists, occasionally for several months, suggesting that breakdown mechanisms, such as turbulent mixing or advection of oxygen-rich waters, are not present or strong enough in that period to ventilate deep waters. Seasonal hypoxia breakdown coincides with increased local and regional winds (Figure 2.2), suggesting that wind-driven mixing may be an important factor, although analysis (not shown) indicated no statistical relationship between wind and DO time series. Additionally, a strong wind event that followed one breakdown event

resulted in surface mixing but did not affect bottom water (Figure 2.9).

The high, near-bottom salinities observed in the back bay at the start of the event examined in Figure 2.9 are consistent with the salinity climatology (Figure 2.2c) and point toward a deep water renewal hypothesis for hypoxia breakdown. This model is commonly associated with ventilation in fjords where dense, salty water is isolated in deep regions and can only be refreshed by sufficiently dense water in adequate supply at the sill (Gade and Edwards, 1980). Deep water renewal occurs intermittently, typically when mixing of inflowing ocean water is weak and often varies on a spring-neap tidal cycle (e.g., Farmer and Freeland, 1983; Silva and Vargas, 2014). Deep water renewal, governed by the monsoon and the spring-neap phase of the internal tide, has been observed in Ambon Bay, Indonesia, a shallow-silled, tropical fjord (Salamena et al., 2021). Analysis of event persistence in Bahía Almirante based on hypoxia thresholds yields timescales that are potentially consistent with fortnightly processes (Supporting Information, Figure S1), though the weekly sampling scheme precludes resolution of spring-neap processes.

Exchange fluxes and residence times inferred from the heat budget analysis indicate that advection in Bahía Almirante is significant and persistent. It is important to note that this analysis considers the bay (or its subregions) in a volume-averaged sense and thus variations in circulation within the bay remains unresolved. Significant portions of the mid and back bay are deeper than the entrance channels (Figure 2.1). Ventilation of these deep regions requires advection of high density water (relative to the back bay), thus a salty, deep layer in the back bay will remain isolated despite strong advection through the channels if the necessary inflow density condition is not met. Advection at the bay entrances alone is thus unlikely to be sufficient to ventilate the back bay.

The salinity climatology (Figure 2.2c), which drives variations in density, provides an explanation for the seasonality in advection-driven hypoxia breakdown. Offshore salinity remains high throughout the year at depth, while surface salinity varies approximately coincident with the hypoxia cycle (and roughly following seasonal precipitation). If we

postulate a persistent mechanism for vertical mixing of incoming offshore water, associated with energetic flow through the channel entrances, tidal or otherwise, then the density of the inflowing layer will be reduced in proportion to the vertical stratification. Following this hypothesis, the climatologies in Figure 2.2 suggest that incoming water will thus have highest density, and therefore the highest potential for deep water renewal, between January and June and again in September-November. These periods coincide with the normoxic period and the period of intermittent ventilation, respectively.

While the lack of flow measurements prevents a comprehensive assessment of this ventilation model, a comparison of near-bottom salinity at Punta Caracol relative to Almirante shows a statistically significant relationship with the hypoxic state (Figure 2.10). Although there is considerable scatter, there is evidence that when Almirante near-bottom water is saltier than Punta Caracol (to the right in Figure 2.10), hypoxia tends to occur. In the context of the deep water renewal model, Punta Caracol serves as a proxy for the water that will resupply the stagnant, near-bottom water mass in the back bay. Ventilation in the back bay occurs only when the salinity difference, which follows the seasonal cycle (as shown in color), is weak.

While deep water renewal as a mechanism for ventilation is typically observed in fjords, it is a process that can also apply to shallow tropical systems, like Bahía Almirante. Further work is needed to examine this model, including potential mixing mechanisms and locations. These mechanisms would be likely to be modulated by tidal and subtidal flows, variations in inflow layer thickness and by effects of stratification on mixing mechanics. The potential for bottom water ventilation is also likely to be affected by vertical mixing within the back bay and by radiative heating, both of which will reduce the barrier for deep water renewal.

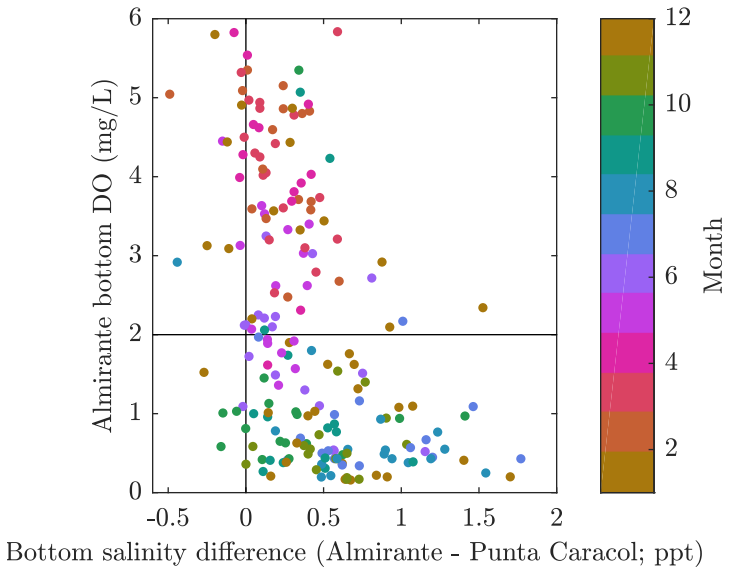

Figure 2.10. Almirante bottom DO vs. bottom salinity difference (Almirante - Punta Caracol). Data plotted are the near-bottom measurements for each high resolution profile (May 2015 - March 2020). Color indicates time of year. For raw data: r = -0.42; $p < 0.05$.

2.5.3 Co-occurrence of multiple stressors

Temperature inversions co-occur with low DO in bottom waters (Figure 2.6c), suggesting that when stratification is high, conditions are favorable for development of both temperature inversions and low DO. While increased temperature also reduces DO solubility, the observed temperature increases do not account for the magnitude of the DO reduction. The relationship between low DO and warmer bottom temperatures (Figure 2.7) implies that the temperature inversions are, at least in part, a consequence of accumulated radiative heating of the bottom layer over time. Figure 2.2d shows that temperature inversions on the annual timescale are coincident with near-surface water cooling; however, solar warming at depth, which has previously been shown to drive accelerated warming relative to the rest of a salinity stratified water column (Wells et al., 2012), likely contributes to formation of the observed temperature inversion in the bay (e.g., Harrison and Phizacklea, 1987) because seasonal bottom temperatures increase (Figure 2.2d). As such, temperature inversions and low-DO are consistent with long residence

times, which allow for heat accumulation and DO depletion. The co-occurrence between temperature inversions and hypoxia indicates that benthic organisms may face multiple stressors simultaneously, which can have exacerbating effects. Temperatures exceeding an organism's thermal tolerance increase oxygen demand, and deoxygenated waters may reduce the optimal thermal range (Vaquer-Sunyer and Duarte, 2011).

2.6 Summary

This study presents analysis of variability and seasonality of the hydrography and hypoxia for a tropical estuary system, Bahía Almirante, which experiences seasonal hypoxia at depth and frequent temperature inversions. The strongest, most persistent hypoxic events occur in the back bay, while the mid bay experiences intermittent hypoxia, and DO reductions at depth are common throughout the bay during the hypoxic period. Offshore DO values remain high, indicating that the sources of hypoxic waters do not originate from the open ocean. Temperature inversions exhibit a similar spatial pattern, with warmer temperatures at depth and stronger temperature inversions occurring in the back bay. They occur more frequently than hypoxia throughout the bay, including at the offshore site. Infrequent, relatively weak temperature inversions are also observed during the normoxic period. The common patterns in hypoxia and temperature inversions indicate that they are both related to the formation of an isolated deep layer in the bay. Seasonal averages suggest that strong vertical salinity stratification, that results from increased freshwater input, is a major contributing factor to the initiation of hypoxia. Hydrography indicates that the mechanisms that favor hypoxia are amplified in the back bay, where the strongest vertical stratification occurs.

The heat budget shows that there is net advective heat export from Bahía Almirante. The average residence time of 10-40 days likely does not represent the bay overall. For example, retention time is estimated to be longer in the back bay, consistent with the

persistence of significant stratification and hypoxia in the back bay. We present evidence through a case study that lateral advection can play a critical role in hypoxia breakdown. The relationship between near bottom DO and bottom salinities in the mid bay and back bay is consistent with deep water renewal as the mechanism for bottom water ventilation, as commonly observed in fjords. Our data shows no statistical relationship between wind and stratification or wind and DO, however, the relative contribution of advection and wind-driven mixing as well as the contribution of other mechanisms for vertical mixing (including convective cooling and interfacial shear) remains an open question.

Bahía Almirante shares characteristics with other tropical estuaries, including seasonal patterns in surface heat flux and freshwater flux. The net heat export and prevalent temperature inversions are expected in other tropical coastal embayments. The high, weakly seasonal, precipitation impacts seasonal stratification and is expected to play a similarly important role in other shallow tropical systems. The posited mechanism for hypoxia breakdown, deep water renewal, is not tropics-specific, however it poses an interesting potential mechanism for intermittent oxygen renewal in other tropical estuaries, and the governing processes require further study to be resolved.

The hypoxia and temperature inversions described above are of critical importance to the biological communities of Bahía Almirante. While this study does not address organismal responses, it suggests that physical dynamics in Bahía Almirante contribute to conditions that are known to be stressors for marine organisms. Identifying mechanisms that govern hypoxia and temperature inversions provides the context needed to evaluate whether similar processes occur in other shallow, tropical estuaries, as well as how they compare to temperate coastal systems.

2.7 Acknowledgements

We would like to thank Plinio Gondola and the environmental monitoring staff at STRI's Bocas del Toro Research Station and volunteers who have collected the long-term data set. We would also like to thank Steve Patton for the maintenance of the meteorological data. All data has been collected under permits from MiAmbiente and ARAP. AEA was supported by a Smithsonian Fellowship. This work was supported by a National Science Foundation grant, NSF OCE - 1924220 (RC), NSF OCE - 1924551 (GP), NSF OCE - 1924664 (KAD). No conflicts of interest.

Chapter 2, in full, is a reprint of the material as it appears in Limnology and Oceanography, 2022. Adelson, A.E., Altieri, A.H., Boza, X., Collin, R., Davis, K.A., Gaul, A., Giddings, S.N., Reed, V. and Pawlak, G., 2022. Seasonal hypoxia and temperature inversions in a tropical bay. *Limnology and Oceanography*, 67(10), pp.2174-2189. Used with permission. The dissertation author was the primary investigator and author of this paper.

2.A Supporting information

The following is the supporting information for Chapter 2.

2.A.1 Interannual variability

A linear fit to the bay-averaged weekly sampled temperature at 20 meters yields a slope of 0.06 °C/year, with an overall increase of 0.57 °C between 2010 and 2019. A linear fit to the bay-averaged weekly sampled salinity at 20 meters data yields a slope of 0.07 ppt/year, with an overall increase of 0.62 ppt between 2010 and 2019, and there is no significant trend in surface salinity.

There is significant interannual variability evident in the time series data in Figures 3 and 4. We define metrics to compare the relative intensity and persistence of hypoxic

events and temperature inversions.

Interannual variability in hypoxia

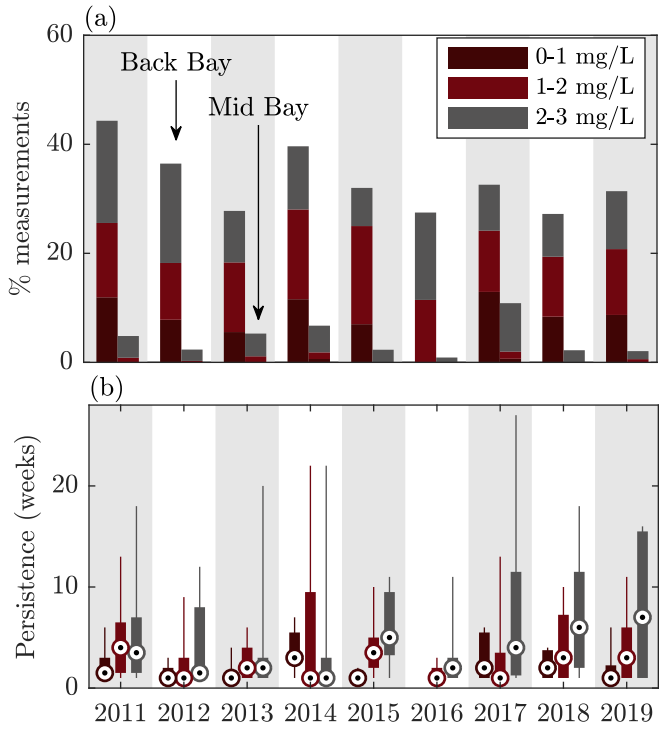

Figure 2.A.1. Indices of hypoxia, calculated for each hypoxia year (i.e. hypoxia year 2018: March 2018-February 2019). (a): the overall proportion of measurements that are anoxic (DO $<$ 1 mg/L), hypoxic (DO $<$ 2 mg/L), and low DO (DO $<$ 3 mg/L) within a hypoxic year (throughout the water column); within clusters, left bar represents back bay sites (Almirante; Pastores), right bar represents mid bay sites (Cristobal; STRI; Hospital Point; Punta Caracol). (b): the persistence of individual hypoxic events at the back bay sites (Almirante; Pastores) for the anoxic (DO $<$ 1 mg/L), hypoxic (DO $<$ 2 mg/L), and low DO (DO $<$ 3 mg/L) thresholds. Target denotes the median, bar denotes the 25th and 75th percentile, and whiskers denote range.

Over the time series, the baywide-average DO at 20m shows no significant trend, although there is interannual-variability in the severity, spatial extent, and persistence of hypoxic events. In order to elucidate year-to-year differences, we define a hypoxia year for Bahía Almirante as extending from March 1 to the end of February of the following year, to span a full hypoxic season, from the initial development (typically in April) through the full breakdown (typically in December/January). The percentage of DO measurements

(throughout the water column) below a selected threshold relative to the total number of measurements in a given hypoxia year, is used to provide a coarse view of the overall hypoxic volume (Figure 2.A.1a, Figure 2.A.2) . The average persistence of a hypoxic event is also considered at a nominally weekly resolution, determined by consecutive minimum DO measurements below a given threshold at each site (Figure 2.A.1b). These metrics have been subdivided by back bay (Almirante; Pastores) and mid bay (Cristobal; Hospital Point; Punta Caracol; STRI) sites and averaged in order to capture spatial differences. DO thresholds of 1 mg/L, 2 mg/L, and 3 mg/L are used in order to estimate the anoxic, hypoxic, and low-DO periods that have lethal and sub-lethal implications for marine organisms (Vaquer-Sunyer and Duarte, 2008).

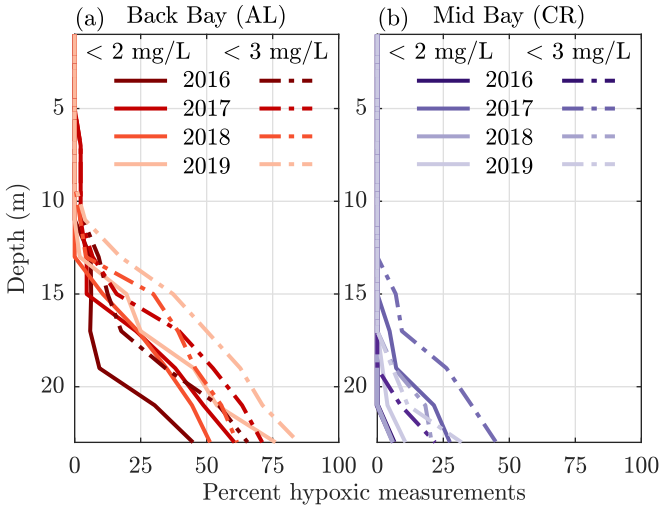

Figure 2.A.2. Proportion of hypoxic measurements at each depth bin for each hypoxia year (i.e. hypoxia year 2018: March 2018-February 2019) for two sites. (a): Almirante (representing the back bay);(b): Cristobal (representing the mid bay); 2016 lies behind 2018. Solid lines represent a threshold of 2mg/L, dashed lines are 3mg/L.

The metrics suggest that the hypoxia year 2017 was anomalously strong and widespread. The mid bay experienced a high percentage of low-DO (<3 mg/L) occurrences, with 10.9% of all measurements (Figure 2.A.1a) and 45% of measurements at Cristobal at 23m (Figure 2.A.2b). While the occurrence of low-DO measurements was high in the back bay in 2017 (32.6%), it was comparable with other hypoxia years, although a low-DO

episode persisted for 27 consecutive measurements in the back bay (spanning 33 weeks), the longest captured in the time series (Figure 2.A.1b). The persistent, widespread low-DO event was accompanied by the severest anoxia observed within a single hypoxia year, with 13.0% of all DO measurements below 1 mg/L in the back bay and an event in which anoxic conditions persisted for six weeks at both back bay sites. The depth to which the hypoxic layer shoals varied from year to year, with hypoxic measurements rare above 13 m, but in hypoxia year 2017, it was observed as shallow as 7 m (Figure 2.A.2). Recent studies in Bahía Almirante show that this shoaling can lead to sharp gradients of coral bleaching, where coral communities below a critical depth experience bleaching in the back bay (Altieri et al., 2017; Johnson et al., 2018).

Hypoxia year 2016, in contrast, was a relatively mild year. There were minimums in occurrence percentage for the anoxic and hypoxic DO thresholds in the back bay (0% DO <1mg/L and 22.5% DO <2mg/L), with no observed hypoxia and less than 1% of low-DO measurements in the mid bay (Figure 2.A.1). Hypoxia year 2016 had an average persistence at the 2 mg/L threshold of less than 2 consecutive weekly measurements, and the longest observed event was 3 consecutive weekly measurements. This minimum in hypoxic volume was further reflected in the depth view of the hypoxia occurrences (Figure 2.A.2a), where the hypoxic layer was less thick than other years and with a lower occurrence at all depths below 15m, where hypoxia is typically observed.

While hypoxia years 2016 and 2017 stand out as particularly mild and strong, respectively, other hypoxia years experience long low-DO events (hypoxia year 2013 had the longest persistent event with 20 consecutive measurements, spanning 22 weeks), persistent hypoxic events (hypoxia year 2014 with 22 consecutive measurements, spanning 24 weeks), and large low-DO volumes (44.3% of all measurements in hypoxia year 2011 were below 3 mg/L).

Analysis of interannual differences did not identify any clear correlations with variations in forcing mechanisms, including precipitation and wind stress, as resolution of

the intensity and longevity of low-DO events (and forcing) is limited by weekly sampling. Interannual changes in regional climate, larger scale offshore ocean conditions, and nutrient fluxes, not considered here, are other possible drivers for interannual variability in DO. These regional mechanisms may be affected by climatic teleconnections, including El Niño (Chen and Taylor, 2002). The most important drivers dictating the interannual variation in relative strength, persistence, and duration of hypoxic events remain undetermined.

Interannual variability in temperature inversions

The time series indicates a slight warming trend, suggesting that thermal stresses are increasing over the time frame of the observations considered here, consistent with regional (Glenn et al., 2015) and broader global patterns (Durack et al., 2018). Interannual variability in temperature is notably larger than the observed trend, with notable variations in the strength of temperature inversions. Statistics and indices for temperature inversions are considered for hypoxia years with profile data (2016-2019) in order to compare interannual strength and persistence (Table 2.A.1). Temperature inversions are defined as the largest continuous increase in temperature with depth (this definition for temperature inversions also seen in Figure 4b). For this analysis, temperature inversions are considered anywhere in the water column and must be at least -0.5°C in strength.

Table 2.A.1. Temperature inversion indices, including: strength (average and maximum), persistence (average and maximum), and frequency for hypoxia years 2016-2019. Temperature inversions are defined as the largest continuous increase in temperature with depth. They are considered anywhere in the water column and must be at least -0.5°C in strength.

Hypoxia Year	**Average strength** (°C)	**Maximum strength** (°C)	**Average persistence** (weeks)	**Maximum persistence** (weeks)	**Inversion frequency** (%)
2016	-0.89	-3.10	2.03	6	29.7
2017	-0.95	-3.38	2.77	15	30.1
2018	-0.92	-2.48	2.33	13	29.5
2019	-0.93	-2.32	2.32	12	33.8

For hypoxia years 2016-2019, the average strength, persistence, and frequency of temperature inversions is consistent, approximately -0.9°C and between 2 and 3 consecutive weekly measurements, respectively (Table 2.A.1); however, hypoxia year 2017, the year with the strong, widespread, and persistent hypoxic event, had the maximum inversion strength (-3.38°C) and longest inversion persistence (15 consecutive weekly measurements). While hypoxia year 2016, mild when considering the hypoxia indices, had a high inversion strength (-3.10°C), its longest temperature inversion event was only 6 consecutive weekly measurements, much shorter than the other years considered. The consistency between interannual hypoxia and temperature inversion metrics support the mechanistic link between these features, particularly the persistence and the link between hypoxia and temperature inversions both being related to long residence times in isolated bottom waters.

2.A.2 Precipitation and stratification

The dominant role for salinity in density variations for the bay suggests that precipitation will be important in determining vertical stratification. This relationship is evident in Figure 2.A.3 which shows a statistically significant, weakly positive correlation ($r = 0.24$; $p < 0.05$) between weekly precipitation (P_{7d})) and vertical density difference ($\delta_z \rho$) lagged by one week, for the six interior sites. The one week lag, which yields the maximum correlation, indicates that precipitation history is relevant and may also reflect a temporal delay in riverine freshwater inputs, although this delay may be between one day and one week. Similar analysis (not shown) indicates that the variations in stratification are largely associated with surface freshening that, in turn, correlates with precipitation. The relatively large scatter and weak correlation in Figure 2.A.3 is potentially due to high spatial variability in both surface salinity and in precipitation and/or freshwater discharge. This weak relationship may also be due to the fact that there is almost always a fresher surface layer and the addition of freshwater via precipitation may not contribute to a

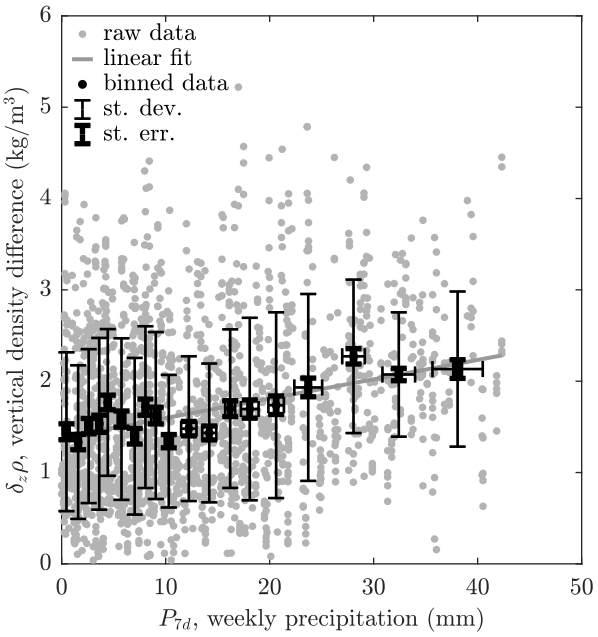

Figure 2.A.3. Stratification vs. precipitation: One week lagged $\Delta_z\rho$, the weekly sampled vertical (20m-0.5m) density difference (kg/m^3) vs. P_{7d}, the sum of the precipitation over the seven days prior to the corresponding density measurement, at the six interior sites (excluding offshore site Colon). Lag denotes that the vertical density difference is compared to the previous week's precipitation. Outliers, absolute deviations greater than three scaled medians, are excluded (161 outliers; 8%); additionally, data with unstable water columns are excluded ($n = 29$). Gray points: raw data; black points: mean in 100 point bins; error bars: one standard deviation; heavy error bars: standard error. For the raw data: $r = 0.24$; 95% confidence intervals = [0.20 0.29], $p < 0.05$. Linear fit slope = 0.021; confidence intervals = [0.017 0.025].

vertical salinity difference.

2.A.3 Spatially-variable residence time estimates

These bulk residence times provide context for how long water is in the bay. This analysis does not capture the spatial variability of residence time, beyond the bulk subregions shown in the table below. These results are consistent with the spatial patterns observed in hypoxia and temperature inversions - residence times are longer for the back bay than for the mid bay.

Table 2.A.2. Median residence times (days) for selected regions, with upper and lower quartile values and number of samples (N).

Region	t_r (days)	25%	75%	N
Mid-bay to Offshore	10.4	4.8	19.2	280
Back bay to Offshore	26.4	16.8	45.4	265
Full bay to Offshore	16.2	8.6	26.0	266

Chapter 3

Barotropic and baroclinic influences on a multi-inlet tropical estuary

3.1 Abstract

Bahía Almirante is a shallow, salt-stratified multi-inlet estuary on the Caribbean coast of Panamá. We conducted a two year intensive study, collecting time series of velocities and water properties, including temperature, salinity, and dissolved oxygen. There are time periods of strong subtidal net flow through the bay, where barotropic flow dominates the baroclinic component. This net flow through Bahía Almirante is driven by an alongshore pressure gradient. The subtidal barotropic velocity measured in Boca del Drago, an inlet that connects the estuary to the Caribbean Sea, correlates to an along-coast shelf current, with low frequency variations in velocity occurring on weekly timescales. Water properties indicate hydrographically distinct sub-basins, with a largely isolated inner bay. The inner bay site is commonly saltier and denser than the channels, and hypoxia can persist during periods of strong net flow. The outer bay exhibits properties more similar to conditions outside the bay during high flow events.

3.2 Introduction

Estuaries are fundamentally transitional bodies of water, with complex physics and biogeochemical processes producing highly variable conditions. Because estuaries are vulnerable to human activity, effective management plans are critical, particularly in developing regions (Le Moal et al., 2019; Vieillard et al., 2020), and understanding the hydrodynamics is an essential aspect of this endeavor. One commonality in estuaries is that buoyancy forces modify density within a system, creating horizontal density gradients (Geyer and MacCready, 2014). Typically this is in the form of a salinity gradient, and commonly estuaries have decreasing density from the ocean boundary towards the head, with barotropic forcing towards the ocean and a baroclinic forcing towards the head (Geyer, 2010).

While most of our understanding of estuaries comes from a canonical system with a single ocean inlet, and a predominant upstream freshwater inflow, coastal embayments with multiple inlets can have important hydrodynamic differences. Multiple-inlet estuaries have been studied on many coastlines, including the Wadden Sea in the Netherlands (Duran-Matute et al., 2016), the Ria Formosa in Portugal (Fabião et al., 2016), and the Intracoastal Waterway along the East coast of the United States (Waterhouse et al., 2011). Net residual circulation in these systems are often driven by tides, winds, or waves. Tides are modulated by the particular geometry of the multiple-inlet system and can lead to a net flow through the system (Waterhouse et al., 2011; Duran-Matute et al., 2016; Sheng et al., 1996). Local and/or remote winds can drive pressure gradients that can dictate net flow in multiple inlet systems (Fabião et al., 2016; Kang et al., 2017; Li, 2013). Finally, wave-driven setup can influence residual circulation (Orescanin et al., 2014) and wave-current interactions can impact net circulation within multiple-inlet systems (Mao and Xia, 2018). The net barotropic flow that can be established with multiple ocean connections can modify the typical baroclinic processes and influence water properties

within an estuary.

Moreover, the canonical estuarine system typically has a predominant freshwater inflow source (i.e., river) at the upstream estuarine head and most scientific efforts have been conducted along temperate coastlines. Thus tropical estuarine systems (where the climate leads to different precipitation, runoff, and heating patterns potentially departing from canonical temperate estuaries) are data-poor and underrepresented in the scientific literature (Vieillard et al., 2020). Because coastlines serve as home to a disproportionate share of the world's population and the tropics host much of the earth's biodiversity (Spalding et al., 2023), tropical estuaries are particularly important due to the confluence of environmental and societal factors (Oczkowski et al., 2020) and heavy reliance of tropical communities on coastal resources (Sale et al., 2014).

Reducing scientific bias in our understanding of estuarine dynamics is also important because coastal processes in the tropics can fundamentally differ from higher latitudes and can exhibit consider variability within this latitudinal band (Nittrouer et al., 1995). A recent study notes the value of considering the physics of tropical coastal areas in concert with biological interactions and social dynamics in order to best understand local and global drivers of change (Collin et al., in review), and therefore it is critically important to understand the circulation and physical dynamics of such a system. Efforts to understand the dynamics of tropical estuaries have been made in systems including the Upper Gulf of Thailand (Saramul and Ezer, 2014), and in Brazil, including the Amazon estuary (Menezes et al., 2009), the Caravelas estuarine system (Schettini et al., 2013), Itamaracá (Medeiros and Kjerfve, 2005), São Vicente, Santos and Bertioga estuarine channels (Moser et al., 2005), and Baía de Todos os Santos (Fonseca et al., 2024), and the Magdalena River in Colombia (Restrepo et al., 2018), among others, but there remains considerable need and opportunity for identifying critical processes to tropical estuarine function.

Estuaries are dynamic ecosystems, and a mechanistic understanding of the processes that govern these systems is critical to understanding residence times and the resulting

biogeochemical effects. Previous efforts have used dimensionless numbers to characterize the subtidal hydrodynamics of a tropical estuary (Tenorio-Fernandez et al., 2018). Residence times are critical to ecosystem function, and long retention times have been shown to correlate with regions of high sea surface temperature and thermal stress to marine life including corals (Li and Reidenbach, 2014). While local timescales will dictate the effects on benthic organisms and communities, bulk residence times can be considered to evaluate the relative influences of various mechanisms, including river discharge, tidal flushing, and estuarine circulation (Wang et al., 2004). Understanding these physical dynamics can characterize an estuary and provide the foundation for understanding how it may be affected by changes to global and local stressors.

We use extensive observations to describe the important physical processes in a tropical estuary. In this analysis, we examine velocity and water property observations from September 2019 to September 2021 in Bahía Almirante, a shallow, microtidal, multi-inlet tropical estuary on the Caribbean coast of Panamá (Figure 3.1) and leverage data from a long-term monitoring program (from late 2010 to present) and a global reanalysis product. After we describe the site, observations, and methods in Section 3.3, we describe water properties, resolve the relative influences of barotropic and baroclinic flows, and calculate residence a volume flux and residence times in Section 3.4. In Section 3.5, we discuss the hydrographically-distinct sub-basins of Bahía Almirante and the biological implications of residence times, describe the drivers of the barotropic flow through the estuary, and elucidate the resulting effects on water properties. This effort aims to shed light on the important mechanisms that dictate how Bahía Almirante functions in addition to elucidating some of the hydrodynamics that can influence other tropical estuaries and multi-inlet systems.

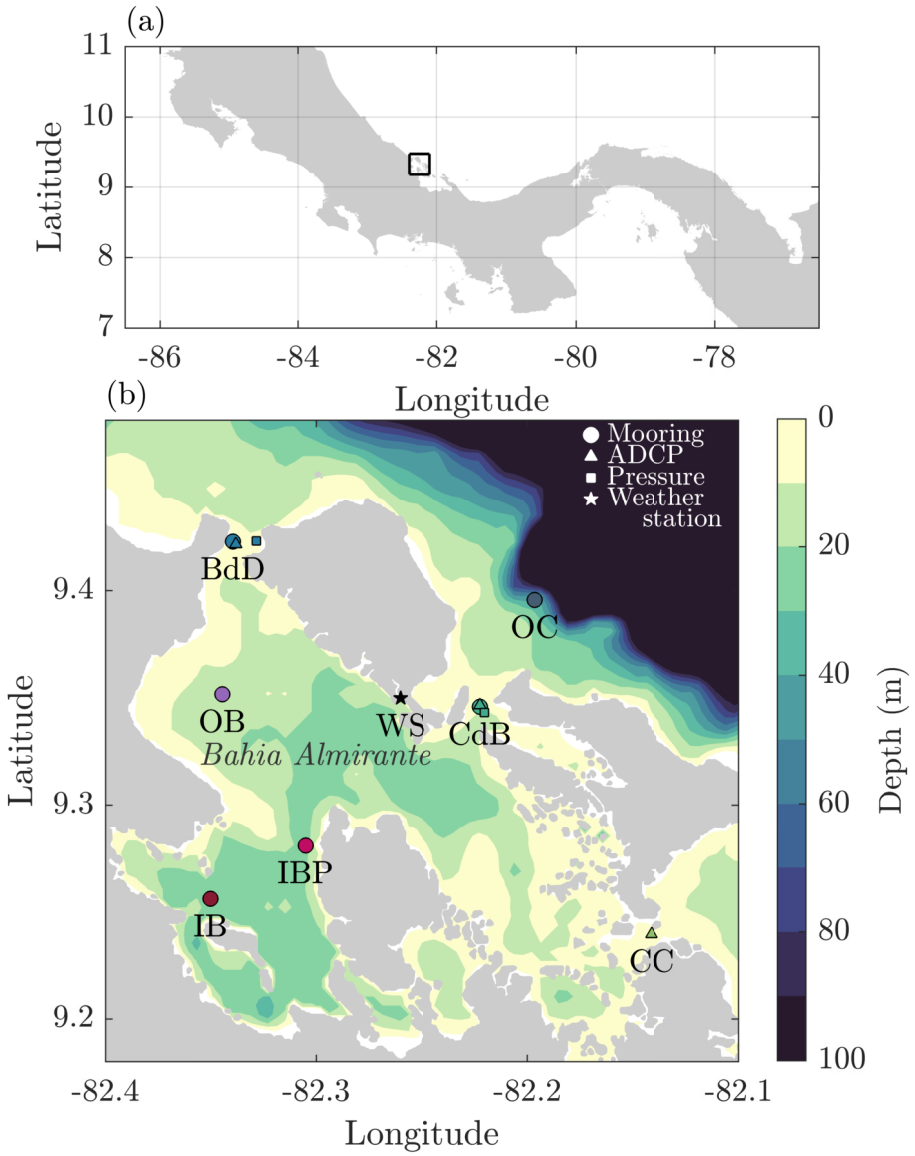

Figure 3.1. (a) Panamá Coast, with Bahía Almirante inset in box. (b) Site locations identified by color, used in subsequent figures. Mooring locations are shown in circles, bottom-mounted ADCP locations in triangles, and pressure sensor locations are shown in squares. Details on the moorings are included in the supporting information. Bathymetry in color.

3.3 Methods

3.3.1 Field site description: Bahía Almirante

Bahía Almirante is a shallow multi-inlet estuary on the Caribbean coast of Panamá, with a maximum depth of approximately 30 m (Figure 3.1). It has inlets to the north and northeast, Boca del Drago (BdD) and Canal de Bastimentos (CdB) respectively, that lead to the Caribbean Sea and two inlets that open into the Laguna de Chiriqui, Cayo Coral (CC) and another very small and shallow (<1 m) inlet to the southeast. While there are small, dispersed rivers into the bay along the mainland, the major river in the watershed is the Changuinola River, which outlets into the Caribbean Sea approximately 12 km northwest of the BdD inlet into Bahía Almirante.

Offshore conditions influence Bahía Almirante. There is a southeastward surface flow due to the Panamá-Colombia Gyre, that is modulated by westward-propagating Caribbean Current eddies (Kastner et al., in review). The Caribbean Sea has a well-mixed 50 m deep surface layer (Gallegos, 1996) and is influenced by the Intertropical Convergence Zone and other weather patterns (Kaufmann and Thompson, 2005). These offshore conditions are linked to seasonal trends in water temperature and salinity just outside of the bay (Adelson et al., 2022).

Seasonal meteorological and oceanographic patterns are evident within the estuary (Adelson et al., 2022). Bahía Almirante is salinity stratified throughout the year (Kaufmann and Thompson, 2005), such that temperature plays a largely passive role in stratification (Adelson et al., 2022). The vertical stratification strength is driven by the seasonal cycle in near-surface salinity, which is in turn dictated by freshwater inputs. Annual peaks in water temperature occur during the solar radiation maxima. The strongest vertical stratification is observed in the interior of the bay, where the lowest dissolved oxygen (DO) levels and the warmest temperatures are observed at depth and there are persistent temperature inversions (Adelson et al., 2022).

Bahía Almirante supports mangroves, seagrass beds, and coral reef ecosystems. There are documented mortality events associated with thermal stress (Neal et al., 2014) and hypoxia (Altieri et al., 2017; Johnson et al., 2021), and the threat from deoxygenation is expected increase with ocean warming (Altieri and Gedan, 2015; Breitburg et al., 2018; Stramma et al., 2010; Pezner et al., 2023). The system experiences seasonal hypoxia at depth and temperature inversions that have been linked to vertical salinity stratification driven by annual patterns in freshwater inputs, with spatial heterogeneity in the strength in these resultant biological stressors (Adelson et al., 2022).

3.3.2 Observations

An intensive instrument array was deployed from September 2019 to September 2021. Time series observations include current velocity, temperature, salinity, pressure, and DO data at strategic sites around Bahía Almirante (Figure 3.1). In this analysis, we consider data from a site outside of the estuary, Outer Colon (OC); the three major inlets into the bay, including Boca del Drago (BdD), Canal de Bastimentos (CdB), and Cayo Coral (CC); and three sites within the system: the outer bay (OB), the inner bay pass (IBP), and the inner bay (IB). These sites are listed from offshore to inshore, along the estuary.

The data presented here are from three deployments, from September 2019 - January 2020, January 2020 - October 2020, and November 2020 - September 2021, with instruments recovered and redeployed between each deployment. Due to field logistics, the exact location and depth of each deployment varied slightly. Subsurface moorings were deployed nearby at five of these sites: OC, BdD, CdB, IBP, and IB (all but the inlet CC), with conductivity, temperature, and depth sensors (CTD, SBE-37 SMP and SBE-37 SMP-ODO), temperature sensors (SBE-56), and optical DO measurements (PME MiniDOT or a CTD-integrated SBE-63), with depths ranging from 1 m above the bed (mab) to approximately 5.2 m below the surface. An additional subsurface mooring was

deployed at OB, with temperature and optical DO sensors. Some CTDs experienced significant sediment entrainment and/or biofouling, resulting in unrealistic conductivity and salinity measurements and those time periods were excluded from analyses.

Bottom-mounted, upward-looking acoustic Doppler current profilers (ADCP) were deployed in the three inlets, BdD, CdB and CC and are considered in this analysis, although additional ADCPs were deployed near the other mooring locations and another site in the arm of the bay between CdB and CC. All ADCP data were collected in beam coordinates. ADCP data were ensemble-averaged in 10-minute bins. Velocities were interpolated to 1 m vertical resolution and extrapolated to the bed (by assuming no flow at the bed and interpolating linearly) and the surface (by assuming constant velocity from the upper-most bin). Principal component analysis for each deployment was used to define along-channel and across-channel velocities.

Bottom-mounted pressure sensors (RBR Duets) were deployed near the major entrances, BdD and CdB. Details on the mooring layout, instrument sampling schemes, and deployment dates are included in the supporting information.

3.3.3 Long term monitoring

The Smithsonian Tropical Research Institute (STRI) conducts a physical monitoring program consisting of vertical profiles of salinity, temperature, along with other quantities not considered here. The intensive field campaign sites were selected to be adjacent to the monitoring sites to provide greater temporal resolution to the long-term context. This analysis includes measurements from a YSI multiparameter sonde, collected approximately weekly from May 2015 to present, at five sites in Bahía Almirante (Figure 3.1), which are approximately co-located with the OC, CdB, OB, IBP, and IB sites. Profile data were averaged into 2 m vertical bins as in Adelson et al. (2022). Density was calculated from measured salinity, temperature, and depth using Gibbs Seawater toolbox TEOS-10 (McDougall and Barker, 2011).

3.3.4 Meteorological and river data

STRI collects precipitation and wind speed and direction at a meteorological station (9.35°N, 82.26°W; WS on Figure 3.1). Variables are measured every 10 seconds with average values recorded every 15 minutes (Patton, 2023). Wind speed and direction are used to define the east and north components. STRI has gauged rivers flowing into Bahía Almirante and provides a daily flow (m^3 d^{-1}; Clark et al, in prep.). Further details about the gauged rivers can be found in Clark et al. (2022).

3.3.5 Analysis

All data were averaged into 10-minute intervals. Subtidal signals of time series were obtained by employing a Godin filter (Godin, 1973). Velocity data were decomposed into barotropic and baroclinic components. Barotropic velocities were estimated as the depth-mean velocity, and positive values indicate flow into Bahía Almirante. Baroclinic velocities were estimated as the residual. The baroclinic velocity magnitude is defined as

$$u_{BC} = -\left(\frac{u_{bott}}{|u_{bott}|}\right)\frac{1}{h}\int_{-h}^{0}|u(z) - u_{BT}|\mathrm{d}z, \tag{3.1}$$

where u is the along channel velocity, u_{bott}, is the depth-mean velocity of the bottom five meters, h is the water depth, and u_{BT} is the barotropic component of the velocity. The sign of the baroclinic flow magnitude is determined by the direction of the near bottom water; positive baroclinic flow represents inflow at depth, and outflow near the surface.

3.4 Results

Regional tides are mixed semidiurnal with microtidal amplitudes varying over a spring-neap cycle between 0.1 and 0.3 m. Harmonic analysis of pressure at BdD shows that principal lunar diurnal constituent (K1) and principal lunar semi-diurnal constituent (M2) are the dominant tidal components, followed by the O1 tide, a lunar diurnal constituent

(not shown). Tidal velocities in the inlets are typically within ± 0.22 m s^{-1} at BdD and ± 0.29 m s^{-1} at CdB (i.e. 2 standard deviations; not shown). Additionally, tidal velocities diminish towards the interior of the bay, with OB tidal velocity range of ±0.04 m/s.

Subtidal time series vary over a range of timescales (Figure 3.2), and spectra of 10-minute averaged velocities and pressure (not shown) indicate that there is no clear energy peak at the inertial frequency range corresponding to the latitudes of the Caribbean Sea. For reference, the inertial period is approximately 74 hours. There remains some structure that is subtidal but has higher periods (on the order of 2-5 days). Lagged correlations calculated between the barotropic velocity and north wind, east wind, wind speed, and wind direction yielded no significant correlations.

Comparisons between the weekly profiling data and the subsurface CTD time series show that the freshwater lens varies in thickness and is inconsistently captured by the near-surface CTDs. Additionally, previous work has established hypoxia originating at depth within Bahía Almirante (Adelson et al., 2022; Lucey et al., 2021), and thus we present water properties from approximately 1 mab to better understand the hydrography of the estuary (Figure 3.2 f-i). Density at 1 mab (25.7 m) at the inner bay site (IB) is relatively constant (mean and standard deviation: 1022.40 ± 0.26 kg m^{-3}; Figure 3.2 h). Outside the bay (OC) values at 2 mab (38.3 m) are higher but also 12.6 m deeper (1023.19 ± 0.31 kg m^{-3}). Near bottom densities in the channels (BdD and CdB) have more variation and are generally lower than IB and OC values (1022.15 ± 0.68 kg m^{-3}at BdD and 1022.33 ± 0.41 kg m^{-3}). This pattern is mirrored in salinity (Figure 3.2 g), which has the dominant contribution to density variability, with IB bottom salinity (35.54 ± 0.24 psu) near oceanic values (OC: 36.00 ± 0.34 psu) and relatively constant. Bottom salinity in the channels are lower, on average, and more variable (35.28 ± 0.48 psu at CdB and 34.94 ± 0.87 psu at BdD).

A seasonal signal in water temperature is exhibited at all sites; near-bottom water temperatures vary by more than 2°C in the bay over the time series (Figure 3.2 f), again

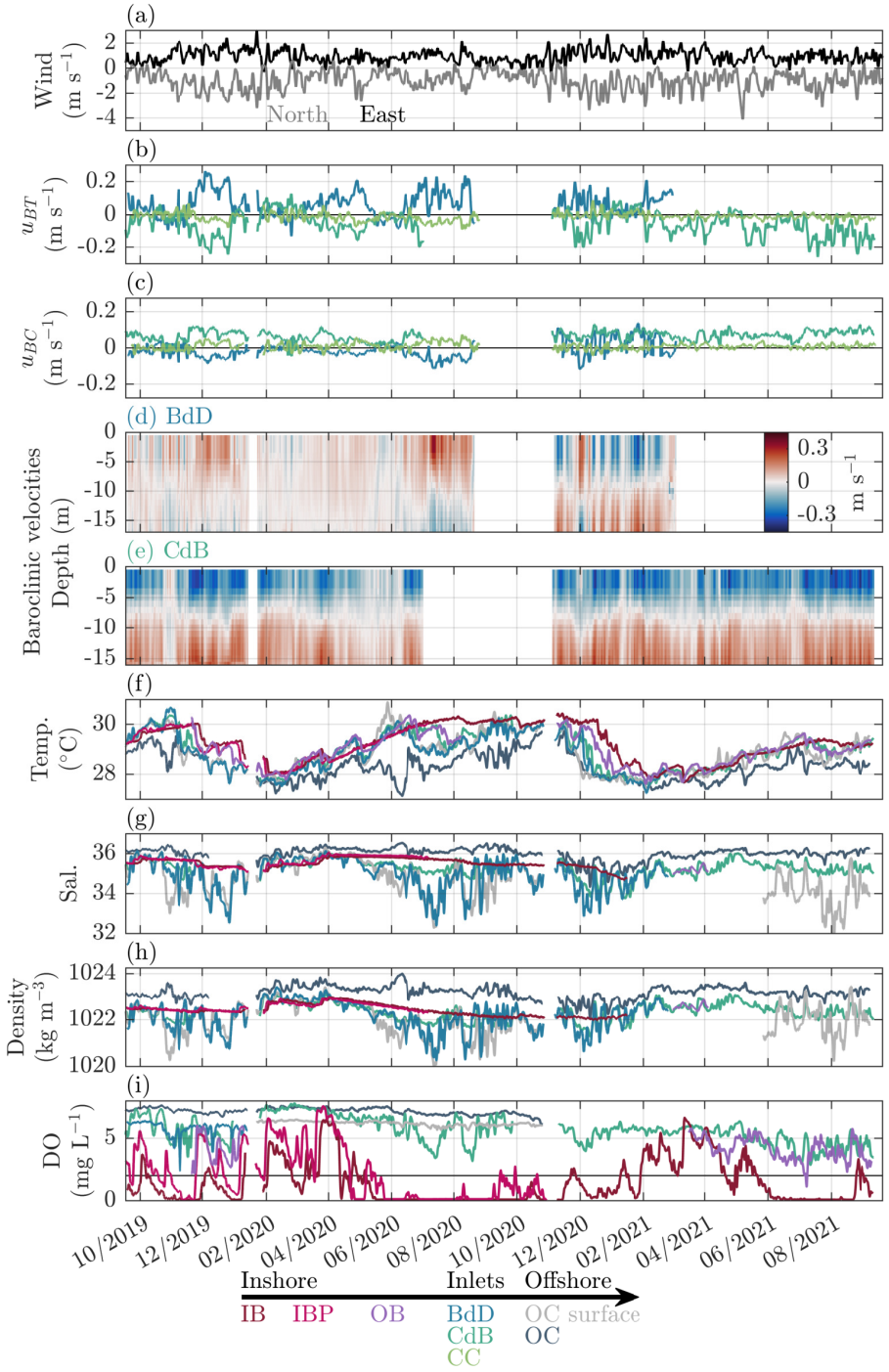

Figure 3.2. Subtidal time series of (a) wind components (east in black; north in gray; m s^{-1}); (b) barotropic velocity (m s^{-1}); (c) baroclinic velocity magnitude (m s^{-1}); (d) baroclinic velocity at BdD (m s^{-1}); (e) baroclinic velocity at CdB (m s^{-1}); (f) temperature (°C); (g) salinity (psu); (h) density (kg m^{-3}); (i) DO (mg L^{-1}); at sites (indicated by color) around Bahía Almirante (Figure 3.1). Water properties show near bottom data, with near surface (light gray line) shown for OC only. Time series at IB and IBP overlap considerably in panels (f), (g), and (h).

with more variation in the channels (28.89 ± 0.82 °C at BdD and 28.96 ± 0.75 °C at CdB) than at IB (29.23 ± 0.73 °C), while the warmest near-bottom water temperatures are typically observed at IB and IBP. The seasonality in water temperature is consistent with long-term annual patterns (Adelson et al., 2022).

Near-bottom waters at IB are anoxic (DO < 0.1 mg L^{-1}) and hypoxic (DO < 2 mg L^{-1}) 49.4% and 76.4% of the time series, respectively, with mean DO of 1.11 mg L^{-1} (Figure 3.2 i). The near bed layer at IB and IBP is fully anoxic over nearly the full time span between mid May to mid October 2020, and the hypoxia is interrupted by sporadic reoxygenation events. There is no observed hypoxia outside the bay (7.14 ± 0.29 mg L^{-1}), and near bottom channel DO values (5.78 ± 0.73 mg L^{-1} at BdD and 6.20 ± 1.24 mg L^{-1} at CdB) are slightly reduced, as compared to outside the bay, and exhibit hypoxia 0.2% and less than 0.1% of the time respectively, indicating that oxygen drawdown occurs within the bay. OB average near bottom DO (4.16 ± 1.40 mg L^{-1}) is typically between IB and the channels. Over the course of its more limited time series, 5.2% of measurements are hypoxic.

3.4.1 Barotropic and baroclinic subtidal flows

Subtidal velocity measurements in the inlets show the presence of a barotropic net flow through the bay (Figure 3.2 b). The direction changes over the course of the time series, with periods of inflow at BdD and outflow at CdB, limited periods of outflow at BdD and inflow at CdB, and periods with weak net flow. The barotropic flow at CC is generally correlated with flow at CdB. The most common barotropic flow regime is inflow (positive velocity) at BdD and outflow (negative velocity) at CdB, with magnitudes up to 0.275 m s^{-1}.

While tidal velocities in the channels are similar in magnitude to the subtidal barotropic velocity during the time periods of weak net flow, over the course of the full time period, the direction of the 10-minute averaged depth-averaged flow is reversed from

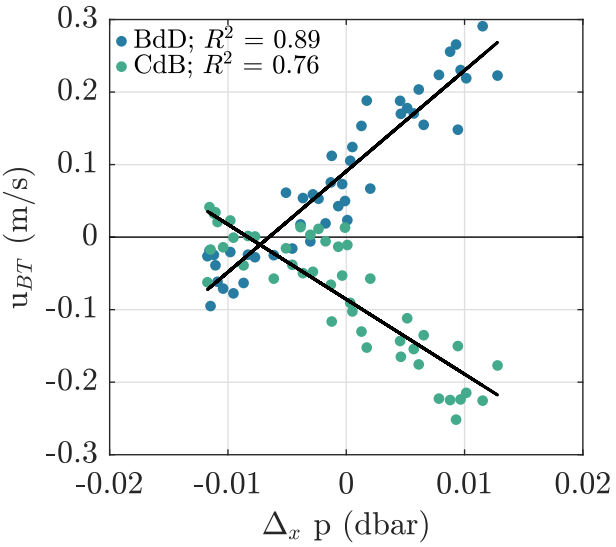

Figure 3.3. Barotropic velocity vs. channel pressure difference. Subtidal alongshore pressure difference, as measured between the two channels, and subtidal barotropic velocities for BdD (blue) and CdB (green), with linear fits. R^2 values reported in the figure, with $N_{eff} = 46$ and $p < 0.0001$ at each channel, where N_{eff} is the effective degrees of freedom accounting for the subtidal filter. Flow into the bay is positive.

the subtidal depth-averaged flow 23% of the time at BdD, 29% of the time at CdB, and 30% of the time at CC, indicating that the tides are not reversing the direction of the flow for a substantial portion of this time series. ADCP site selection was constrained by appropriate bottom type, and there may be localized flow effects due to bottom topography that result in steering of the flow at BdD in particular as well as indicators of hydraulic control, leading to complications in accurately estimating the along-channel flow.

The net pressure difference, $\Delta_x p$, measured between BdD and CdB correlates to the subtidal, barotropic flow through the bay described above (Figure 3.3). The measured pressure difference reflects anomalies in time but does not account for any constant pressure gradient between the channels. Correlations are strong at both the entrances, with a relationship that indicates the typical pattern of inflow at BdD and outflow at CdB.

The vertical structure of the along channel baroclinic flow at CdB largely reflects the typical estuarine circulation (i.e., positive/towards the bay near the bottom), with

occasional reversals. The baroclinic velocity at BdD is much weaker and variable in direction for the first two deployments (Oct 2019 - Aug 2020) but exhibits a stronger, canonical, estuarine exchange during the last deployment (Dec 2020 - Mar 2021) (Figure 3.2 c,d,e).

Baroclinic flow magnitudes are compared to scaling estimates for estuarine exchange that are based on a tidally averaged momentum balance between baroclinic pressure gradient and friction (Hansen and Rattray Jr, 1966). The resulting scaling differs slightly for bottom-driven friction versus interfacial baroclinic shear, which scales with the square root of the along-estuary density difference $(\Delta_x \rho/\rho_0)^{1/2}$. A stronger correlation was evident with the latter and is shown in Figure 3.4, which compares the baroclinic velocities in the two main inlets (i.e. BdD and CdB) with $(\Delta_x \rho/\rho_0)^{1/2}$ the square root of the depth-averaged (i.e. mean of near-surface and near-bottom densities) along-estuary density difference, defined as $\rho_{inlet} - \rho_{IB}$, normalized by reference density $\rho_0 = 1023$ kg m^{-3}. We maintain the sign of the density difference in the square root, such that when the inlet is denser than IB, the quantity is positive.

At BdD, baroclinic velocities are most strongly correlated with the scaling estimate during time periods of weak barotropic flow (Figure 3.4). This includes periods with a negative along-estuary gradient where the resulting baroclinic exchange is reversed (i.e. out at the bottom). The correlation weakens with increased barotropic flow indicating that the baroclinic component is disconnected with the up-estuary density gradient, especially for strong positive barotropic flow (i.e. inflow). At CdB, correlation improves somewhat for lower velocities, but correlations were generally higher for the full time series. This channel also exhibits more typical estuarine exchange (Figure 3.2 e). The correlation between the observed subtidal baroclinic flow and frictional estuarine scaling indicates that the exchange is generally determined by the larger scale along-estuary density differences, as expected for an estuarine system damped by interfacial friction; however, the estuarine function of the bay is significantly modulated by the net barotropic flow strength, particularly at the

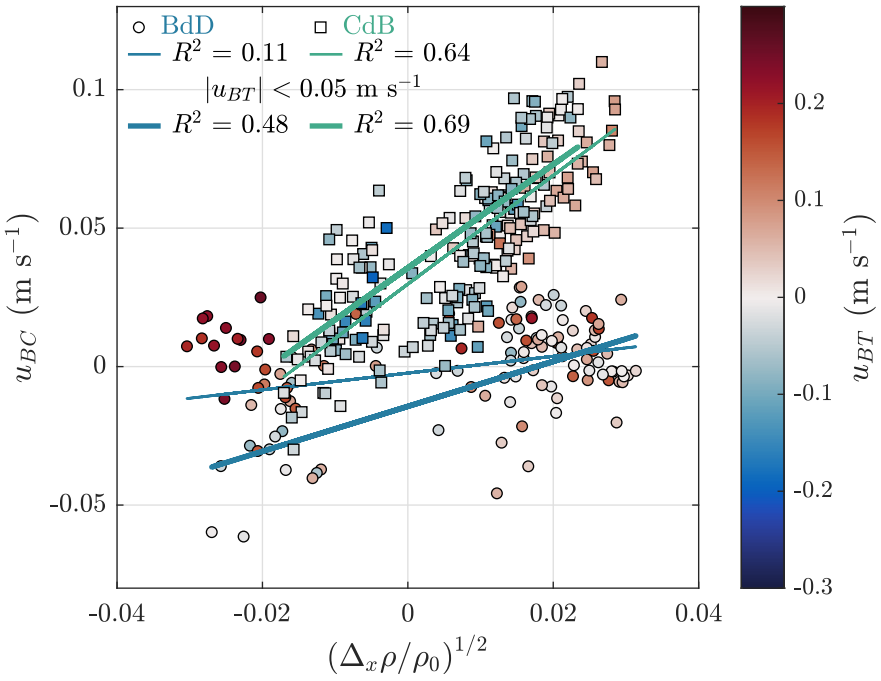

Figure 3.4. Baroclinic velocity (m s^{-1}) vs. scaling estimate for estuarine circulation, $(\Delta_x \rho/\rho_0)^{1/2}$, the square root of the along-estuary depth-averaged density difference between each of the two major inlets and IB (maintaining sign such that this quantity is positive when BdD/CdB > IB). Circles indicate BdD, and squares indicate CdB. Points are colored by the magnitude of the barotropic velocity. Linear fits are shown and correlations are calculated for all data (BdD: $R^2 = 0.11$, $N_{eff} = 124$, $p < 0.001$; CdB: $R^2 = 0.64$, $N_{eff} = 224$, $p < 0.0001$) and for the subset with $u_{BT} < 0.03$ m s^{-1} (BdD: $R^2 = 0.48$, $N_{eff} = 38$, $p < 0.0001$; CdB: $R^2 = 0.69$, $N_{eff} = 60$, $p < 0.0001$). N_{eff} is the effective degrees of freedom accounting for the subtidal filter.

BdD channel, where inflow tends to occur (Figure 3.2 b).

We can determine when the subtidal barotropic flow dominates the baroclinic exchange by considering their relative contributions in terms of the local hydraulic state in the channels. Observations in the channels indicate that the baroclinic flow component can often be characterized by a two-layer flow, generally typical estuarine exchange (out near the surface, in near the bottom) at CdB, and often in the opposite sense at BdD (Figure 3.2 c,d,e). If we approximate flow in the channels as comprising two layers, an internal barotropic Froude number can be defined as $Fr = u/\sqrt{g'h}$, where u is the barotropic

velocity at the narrowest point, $g' = g(\rho_2 - \rho_1)/\rho_0$, is reduced gravity, with ρ_1 as the density measured in the channel near the surface ($\approx$ 5.2 m at BdD, 7.3 m at CdB), ρ_2 as the near bottom density in the channel ($\approx$ 21.7 m at BdD, 20.2 m at CdB), and ρ_0 is a reference density (1023 kg m^{-3}). This definition of the Froude number represents the strength of the barotropic flow relative to a locally defined baroclinic exchange (Armi and Farmer, 1986; Pawlak and Armi, 1997). A strong barotropic flow can lead to an arrested wedge either upstream or downstream of a channel constriction, at which point the flow in the channel will be unidirectional and the internal Froude number exceeds a critical value ($Fr \approx 0.544$, (Pawlak and Armi, 1997)). In this case, hydraulic theory yields dynamics that are similar to those for a single layer hydraulically controlled flow but based on the reduced gravity, g'. For weaker barotropic flow ($|Fr| < 0.544$) the wedge extends upstream (relative to the barotropic flow) and an interface can be observed at the control point, with flow in both directions (Pawlak and Armi, 1997). The bathymetry in the two primary channels in Bahía Almirante (BdD and CdB) is complex and the ADCP locations are not precisely in the narrowest section, but if we proceed using measurements as representative velocities we can calculate the associated Fr at both channels.

The directionality and strength of the barotropic flow relative to that of the baroclinic exchange can be quantified using a Barotropic Flow Metric (BFM) defined as

$$BFM = \frac{|u_{in}| - |u_{out}|}{|u_{in}| + |u_{out}|}, \tag{3.2}$$

where u_{in} is the integral of the inward velocities and u_{out} is the integral of the outward velocities, such that when $BFM = 1$, there is unidirectional flow into the estuary, when $BFM = -1$, there is unidirectional flow out of the estuary, and when $BFM = 0$, there is pure exchange flow. At other values, there is bi-directional flow in the along-channel direction. The BFM is calculated using subtidal velocity profiles in each channel and compared with the internal barotropic Froude number, Fr, in Figure 3.5.

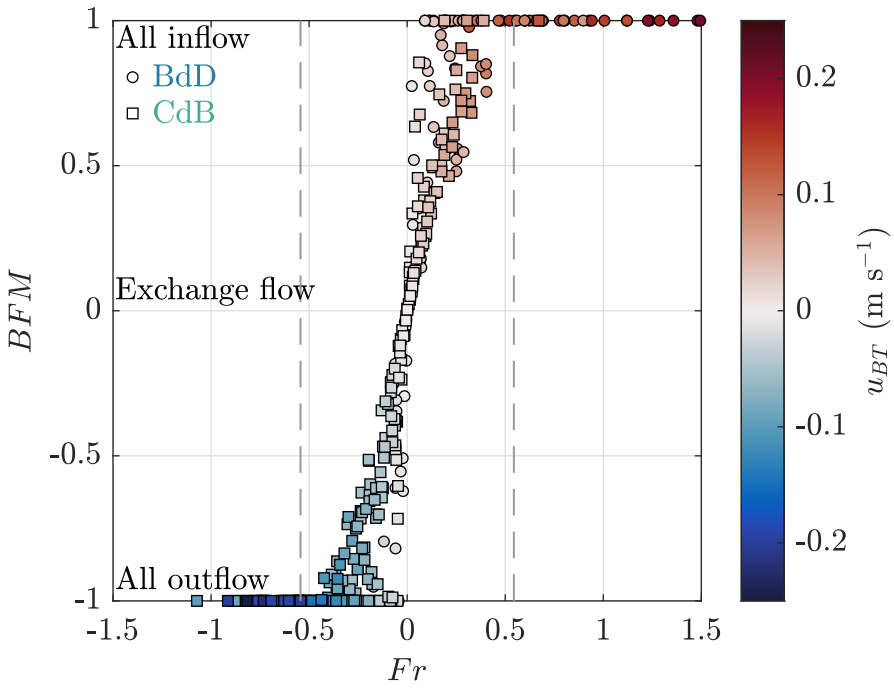

Figure 3.5. Barotropic flow metric ($BFM = |u_{in}| - |u_{out}|/|u_{in}| + |u_{out}|$) vs. the internal Froude number with the barotropic velocity (m s^{-1}) in color, measured in the two main channels (BdD and CdB). Critical $Fr = .544$ shown in black line.

During time periods of strong net flow (high $|Fr|$), the water column tends to be unidirectional (i.e. $|BFM| = 1$), consistent with hydraulic theory, where the barotropic flow through the system overwhelms the baroclinic exchange. During these periods, Bahía Almirante does not exhibit the exchange flow associated with canonical estuaries due to the strength of the barotropic flow. For very strong barotropic flow ($|Fr| > 1$), two layer theory indicates that an arrested wedge will be swept downstream of the narrowest section (relative to the barotropic flow). In this case, the local vertical density difference is no longer relevant and the Froude number definition is no longer applicable. Here we expect $|BFM| = 1$, as evident in Figure 3.5.

The critical transition value derived from hydraulic theory ($Fr \approx 0.544$) strictly applies only for idealized frictionless flow, but it provides a good prediction in both channels for the point at which bi-directional exchange is no longer present (Figure 3.5). Periods with bi-directional flow ($|BFM| < 1$) only occur when the barotropic velocity is weak ($|Fr| < 0.544$), indicating that baroclinic information can propagate during these conditions and an exchange flow can occur.

There are some periods with weak barotropic flow and $|Fr| < 0.544$, when the flow remains unidirectional with $|BFM| = 1$, with 56% of the points with $|BFM| = 1$ correspond to Froude numbers less than the critical value. These are likely periods when the vertical density structure in a channel is determined solely by conditions upstream (relative to the barotropic flow) so that baroclinic structure propagates in the same sense as the barotropic net flow. There are no points with the Froude number less than the critical value with unidirectional flow. Overall, unidirectional flow ($|BFM| = 1$) is well-predicted by $|Fr| > 0.544$, and baroclinic exchange occurs only for $|Fr| < 0.544$ indicating that the observations are largely consistent with hydraulic theory in both channels.

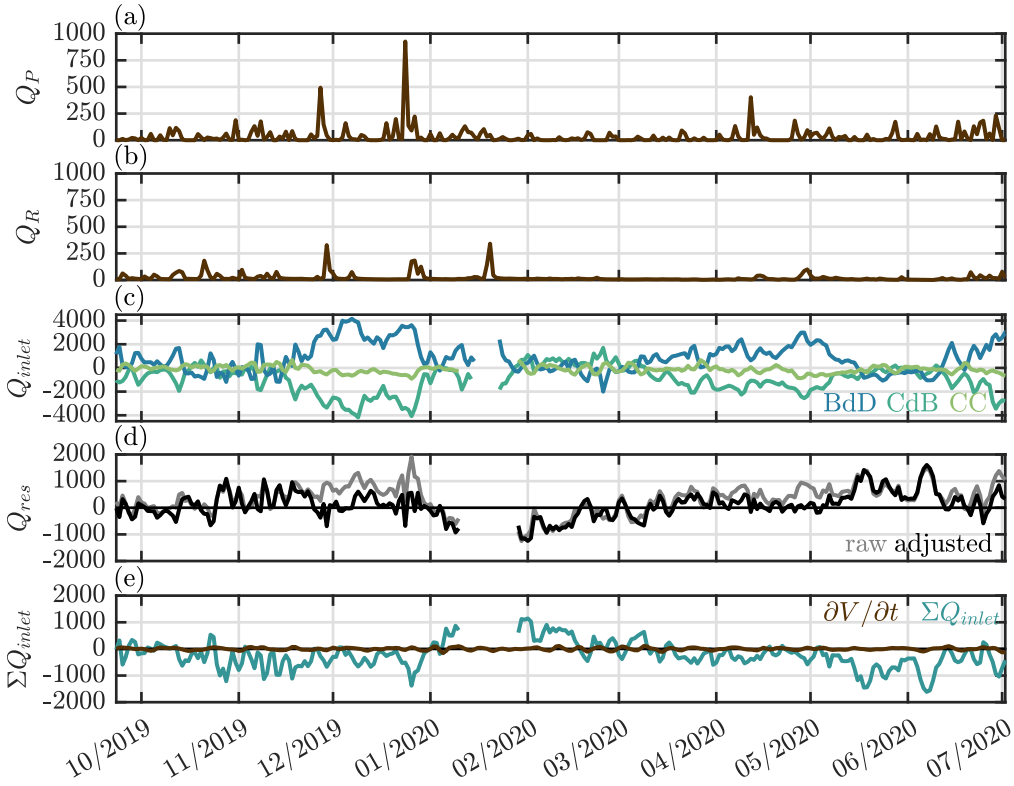

Figure 3.6. Subtidal time series of volume flux (m^3 s^{-1}) components:(a) precipitation (Q_P); (b) river discharge into Bahía Almirante (Q_R), (c) adjusted fluxes through inlets (Q_{inlet}, with Q_{BdD} in blue, Q_{CdB} in dark green, Q_{CC} in light green), (d) residual, with the sum of the fluxes in gray and the least squares linear adjustment in black, and (e) storage ($\partial V/\partial t$) and the sum of the inlet volume fluxes shown in panel (c).

3.4.2 Volume flux and residence times

We calculate a volume budget,

$$\frac{\partial V}{\partial t} = Q_R + Q_P + \Sigma Q_{inlet} + Q_{res}, \tag{3.3}$$

where volume fluxes contributing to volume (i.e. V) changes with time, $\partial V/\partial t$ (i.e., storage), include river flow, Q_R, precipitation, Q_P, flow through the inlets, such that $\Sigma Q_{inlet} = Q_{BdD} + Q_{CdB} + Q_{CC}$, and a residual, Q_{res}. The riverine volume flux was calculated via measurements from gauged rivers and scaled to account for ungauged rivers (Clark et al., in prep). Precipitation at WS is assumed to be representative of the spatially-averaged rainfall; therefore precipitation was integrated over the surface area of the estuary to find the volume flux. We assume cross-channel uniformity at the inlets. The storage term is calculated from a subtidal sea surface height time series within Bahía Almirante located at WS (Patton, 2023).

We estimate the magnitude of evaporative volume flux

$$Q_E = A\frac{Q_{lat}}{L\rho} \tag{3.4}$$

where A is the surface area of the bay, Q_{lat} is the latent heat flux calculated in Chapter 2, $L = 2.5 \times 106$ J kg^{-1} is the latent heat of vaporization, and ρ is assumed to be reference density of 1023 kg m^{-3}. We calculate an evaporative heat flux that ranges from -23.8 to -2.3 m^3 s, with a mean of -8.2 $\pm$ 2.6 m^3 s^{-1} (standard deviation). Typical values account for 2.6 to 7.3% of the residual and are likely within the error associated with the other volume flux measurements, and thus the evaporative volume flux is neglected in this analysis.

Fluxes through the inlets (Q_{BdD}, Q_{CdB}, and Q_{CC}) provide the largest contributions to the net volume flux (Figure 3.6 c, e). Over the time series, the magnitude of the

freshwater volume fluxes is less than 5% of the magnitude of the total fluxes through Bahía Almirante 84% of the time, and 91% and 97% for precipitation and rivers alone, respectively. The storage term (Figure 3.6 c; brown) is much smaller than the residual. The inlets that connect to the open ocean, BdD and CdB, are deeper than CC and generally account for larger volume fluxes, with CC contributions typically 50% or less than the flux through CdB. During time periods of high net flow through the bay, volume flux estimates through the channels reach values over 4000 m^3 s^{-1}. The patterns in the volume fluxes reflect the patterns in the velocities described above, with the direction of the flow typically in at BdD and out at CdB during the time periods of high net flow through the bay. The sum of the volume fluxes through the inlets is typically negative (Figure 3.6 e; green) and is the primary contributor to the residual (Figure 3.6 d).

The volume budget does not close, likely due to inestimable error in the inlet terms (Figure 3.6 d, gray). This is likely due to the assumption of cross-channel uniformity, however we are unable to quantify this error due to data set limitations. Consequently, we calculate least squares coefficients for the volume flux components and use them to minimize error, setting the coefficient for $Q_{CdB} = 1$ to force nonzero coefficients. The remaining volume flux in the adjusted calculation is considered to be Q_{res} (Figure 3.6 d, black).

Coefficients for the least square linear adjustment are as follows:

$$\frac{\partial V}{\partial t} = Q_{CdB} + 1.17Q_{BdD} + 0.76Q_{CC} + 4Q_P + 1.26Q_R. \tag{3.5}$$

The coefficients are order one, suggesting that the values estimated here are reasonable. Notably, the factor multiplying the precipitation volume flux is 4. This larger adjustment may reflect spatial variation in rainfall patterns observed across the Bahía Almirante region (Clark, unpublished data), suggesting that the meteorological station at STRI underpredicts the precipitation in other regions of bay. This could be driven by

topographic precipitation due to the Cordillera de Talamanca, mountains approximately 60 km to the west which reach altitudes greater than 3400 m. The least squares linear adjustment to minimize the residual is correlated with the magnitude of the volume flux through the inlets, ($R^2 = 0.80$) and consequently minimizes error more effectively during time periods of strong net flow. With or without the adjustment, Q_{res} is typically positive, indicating an overestimate of the fluxes out of Bahía Almirante.

We calculate a bulk flushing time of Bahía Almirante based on the volume exchange through the channels, through the full estuary volume

$$T_{Ex} = \frac{V}{Q_{Ex}}, \tag{3.6}$$

where $Q_{Ex} = Q_1 - Q_2$, and Q_1 is the volume flux into the estuary and Q_2 is the volume flux out of the estuary, maintaining the positive in / negative out sign convention. Alternative methods for residence times were also considered (i.e. tidal prism, freshwater fraction), and are included in the supporting information.

The residence time is calculated using the 10-minute averaged,adjusted volume flux estimates (i.e. using the linear coefficients from the least squares fit), as well as an estimated bay volume of 6.76 $\times 10^9$ m^3. The median flushing time is 17.3 days, with lower and upper quartiles of 12.7 and 24.6 days, respectively. Seasonality cannot be assessed due to limited data coverage in all volume flux quantities over the course of the study period, with insufficient data from early July 2020 to early November 2020 or after early March 2021.

3.5 Discussion

The observations described above reveal characteristics of Bahía Almirante that are consistent with canonical frictional estuaries along with some important differences. In particular, the presence of multiple entrances allows for residual barotropic flows

that often dominate over baroclinic estuarine exchange. The flow through the inlets is linked to an alongshore pressure gradient, indicating that offshore influences can dictate the circulation of Bahía Almirante. In addition, water density at IB is commonly high relative to typical values in the channels, consistent with the description given by (Adelson et al., 2022) and suggests that there are time periods when the inner bay operates as a hydrographically-distinct sub-basin.

3.5.1 Water properties within Bahía Almirante

Previous observations in Bahía Almirante show that the bay is strongly salt-stratified with surface salinities that generally increase oceanward as expected for a typical shallow estuary (Adelson et al., 2022). However, the near-bottom salinity and density often show a decrease from IB to the inlets at BdD and CdB (Figure 3.2 g,h), with higher variances in these quantities at the inlets. Reversed density gradients have been observed in other tropical estuaries (Valle-Levinson and Schettini, 2016) resulting from the influence of wet and dry seasons, although this does not appear to play the dominant role in setting the near-bed along-estuary density gradient in Bahía Almirante.

The reversed density gradient is driven by offshore influences. Near surface density observations at 7 m at the Outer Colon station (OC; Figure 3.2 h; light gray line) outside of CdB, show a clear correlation with near-bottom density at the BdD inlet ($R^2 = 0.74$) and a somewhat weaker correlation with near-bottom density at CdB indicating that the deep inflow in these channels is modulated by offshore near-surface densities as it enters the system, likely via vertical mixing. The density outside the bay is likely influenced significantly by the Changuinola River, with an outlet into coastal waters 12 km to the northwest of the BdD inlet that provides a large freshwater source (Clark et al., 2022) and results in noticeably decreased near-surface salinity at OC.

Previous work shows that the near surface salinities are lowest in the inner bay, and surface salinities throughout Bahía Almirante are linked to precipitation patterns (Adelson

et al., 2022). The along-estuary gradients also reflect the diffuse freshwater inputs into the bay. Freshwater enters the system through a series of flashy rivers distributed around the bay as well as via direct precipitation (Clark et al., 2022; Adelson et al., 2022). These freshwater sources are of comparable magnitude, while the contribution of groundwater is unknown. Due to these diffuse freshwater inputs, vertical salinity gradients are reinforced without driving significant vertical mixing.

Some estuaries are comprised of hydrographically distinct basins, with the outer basins serving as the oceanward boundary condition for the interior basins (Smith and Hollibaugh, 2006). In Bahía Almirante, the water temperature, salinity, density, and DO time series in Figure 3.2 f-i show that near-bottom water properties of the inner bay sites commonly deviate from those in the inlets suggesting that the hydrography is often disconnected from these sources. Between reoxygenation events at IB, DO decreases, water temperature steadily increases, and salinity slightly decreases, indicating that the bottom water mass is largely isolated from the channels which exhibit much higher variability. Thus, the water properties point towards persistent isolation events during which the inner bay is hydrographically distinct from the outer bay.

There are step changes in near-bottom IB salinity and water temperature that correspond to sharp increases in DO (Figure 3.2 f,g,i), suggesting that lateral advection intermittently refreshes IB bottom waters during brief periods of connectivity with the outer bay, consistent with previous work that indicate similar reoxygenation mechanisms (Adelson et al., 2022); however, there is no clear relationship between channel velocities and these refreshment events (Figure 3.2 b,f,g,i). IB water properties show evidence of isolation, as described previously (i.e. decreased DO, stable or linearly decreasing salinity, linearly increasing temperature) through time periods of high net flow, and refreshment events can occur during time periods of low net flow. When reoxygenation occurs, IB water properties approach those of the inlets, suggesting that the isolated layer has been refreshed by water originating outside the bay (Figure 3.2 f-i). While coastal influences

are observed in the outer bay, there is evidence of inner bay isolation periods.

3.5.2 Flow through the estuary

The configuration of Bahía Almirante's channels features multiple locations for exchange with the ocean. Unlike the canonical, single inlet estuary, multiple inlets allow for net residual circulation through the system, which can be driven by density gradients, tides, freshwater inputs, winds, barotropic pressure gradients, and bathymetric effects (Buijsman and Ridderinkhof, 2007; Waterhouse et al., 2011; Duran-Matute et al., 2016). In Bahía Almirante, the subtidal residual barotropic flow shows significant variability, with time periods of strong and weak net flow on timescales of weeks, along with significant fluctuations at shorter timescales (Figure 3.2 b).

The baroclinic flow is density-driven, akin to canonical estuarine circulation (Figure 3.4), though it is generally smaller than the barotropic flow. The along-estuary density difference influences the flow during time periods of weak flow at the typically inflowing channel (BdD) and more consistently at the outflowing channel (CdB; Figure 3.4). The strong inflow mutes the density signal for the inlet that typically has inflow (BdD), but the density within the estuary impacts the predominantly outflowing inlet (CdB). Furthermore, the BFM indicates that there are significant time periods that Bahía Almirante does not behave like a typical estuary (Figure 3.5), such that the buoyancy-driven flows are dwarfed by the barotropic signal. Periods of reversed baroclinic flow at BdD (Figure 3.2 c) tend to coincide with very low OC densities (i.e., outside the bay) and are likely associated with offshore stratification driven by influence of nearby river inputs (i.e. Changuinola River). Densities at depth are more variable and frequently lower at the north inlet (BdD) than in the interior of the bay (IB; Figure 3.2 h), likely due to the influence of the Changuinola River on the water density outside of the BdD inlet, as previously discussed.

Measurements of the pressure difference between BdD and CdB show a strong correlation with the strength of the net flow through the two primary inlets (Figure 3.3),

consistent with a frictional momentum balance; however, the dynamics that govern this along-coast pressure difference remain unresolved. The observed barotropic flow shows little correlation with local wind variability (Figure 3.2 a) or with spring-neap tidal changes (not shown). Local winds and barotropic channel velocity time series appear to have similarities, however the overall relationship is weak (Figure 3.2 a,b; $R^2 = 0.22$). The low frequency variations in the mean barotropic velocity are not reflected in the winds however, indicating that on longer timescales, these flows are not driven by local winds.

To shed further light on potential driving mechanisms that influence the alongshore pressure gradient and examine relationships with offshore conditions, we examine output from an assimilative global model. We use 3-hourly global reanalysis velocity output at a 1/12 degree resolution from the Hybrid Coordinate Ocean Model (HYCOM) Global Ocean Forecasting System (GOFS) 3.1 reanalysis product, GLBv0.08-53.X (Chassignet et al., 2007). From the output, we calculate depth-averages over the top 50 m, which spans 14 vertical levels, with 2 m resolution from the surface to 12 m and 5 m resolution from 15 m to 50 m and consider a spatial-averages over 25 grid cells up to 4 grid cells off the coastline, with latitudes ranging from 9.32 to 9.52 °N. and longitudes from -82.48 to -81.84 °E. Among several dynamic quantities examined (sea surface height, temperature, along and cross-shore currents), the strongest correlation with the observed channel flow was obtained with along-coast velocity ($R^2 = 0.40$; Figure 3.7). The low-frequency flow structure is particularly well-represented by the model velocities. The alongshore flow has a statistically significant correlation with the pressure difference between the channels ($R^2 = 0.64$), showing that these quantities are linked, and further investigation is required to elucidate the mechanisms that drive the variations in the alongshore current and pressure gradient.

Low frequency variability in the along-coast currents in the vicinity of Bahía Almirante has been shown to be related to the life cycle of westward propagating anticyclonic eddies in the Caribbean Current along the northern part of the Caribbean basin (Kastner

et al, in review). The low-frequency variation occurs at roughly 3-4 months (Figure 3.7) and is comparable to the timescale for Caribbean Current eddies (116 $\pm$ 31.5 days; Kastner et al, in review). Variability at higher frequencies could be related to mesoscale structures or more local atmospheric processes.

The observed relationship between our field observations and the HYCOM reanalysis product provides a valuable link between small scale observations and a global scale model and indicates that global model data can be useful in resolving local processes in data-poor regions like the Caribbean Sea.

3.5.3 Effect of barotropic flow on water properties

IB water properties are uncoupled from the barotropic net flow, as noted in Section 3.5.1; however, we can anticipate that the barotropic flow will have some influence on water properties throughout other regions of Bahía Almirante. In order to examine this relationship more closely, we consider mean profiles of temperature and salinity calculated for time periods of high and low flow (Figure 3.8). We leverage the correlation between the offshore, along-coast velocity and the velocity measured in the channel (Figure 3.7), using the HYCOM alongshore velocity as a proxy for flow through the channels in order to make use of the long-term weekly monitoring profile data, that extends from May 2015 to April 2023.

To classify flow regimes, we consider the 7-day low pass-filtered HYCOM along-coast velocity time series with a threshold of 0.15 m s^{-1} to differentiate periods of high and low flow and calculate conditional averages. In order to remove potential biases due to seasonal trends in temperature, salinity, and velocity, we sub-sampled the data evenly for each month of the year, randomly selecting 5 samples per month (i.e., the minimum number of samples in a given month for a given flow condition) per flow condition with replacement, repeating 100 times and calculated a mean of those profiles. The resulting average profiles for high and low flow are shown for each site in Figure 3.8 in temperature-salinity space

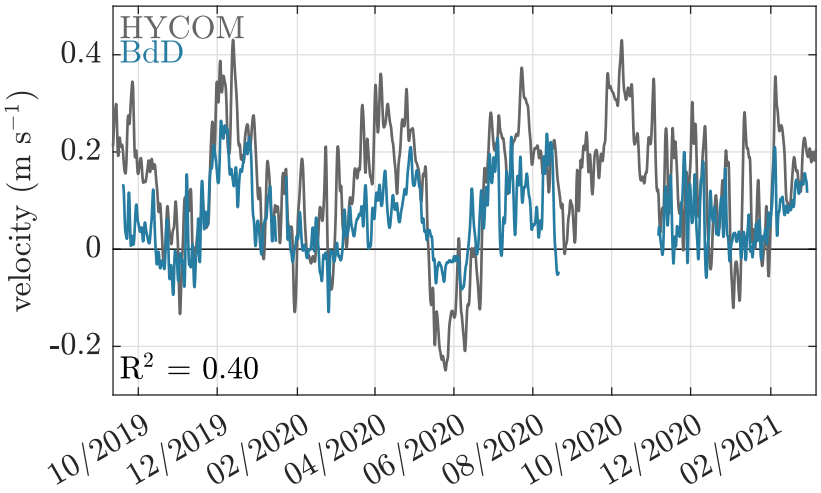

Figure 3.7. Time series of measured depth-mean velocity (m s^{-1}) in a channel (BdD; blue) and offshore, alongshore current (m s^{-1}) from HYCOM (gray); $R^2 = 0.40$.

with the sub-sampled data shown in transparent points.

The generally horizontal orientation of each profile reflects the dominant salinity stratification. Along-estuary differences in water properties noted previously (Figure 3.2 f-i) are evident, with water temperature increasing toward the interior of the system (dark red) for both the low flow and high flow ensemble averages. Average IB near-bottom salinity (dark red) is higher than the inlet (CdB; green) for both ensemble averages while near-surface salinities are lower reflecting the horizontal gradients described previously. Profile data was not obtained at BdD as part of the weekly monitoring program until more recently and are not included. Note that the outer bay (OB; purple) profiles are at a shallower site and consequently do not capture the larger scale along-estuary structure at depth.

There are significant differences in water properties during time periods of high net flow and low net flow through the system (Figure 3.8). Most notably, OB (purple) shows a large shift in temperature with properties more closely resembling conditions outside the bay (gray) during time periods of high net flow while water properties, particularly temperature, shift towards IB (dark red) during low flow periods. The high flow profiles

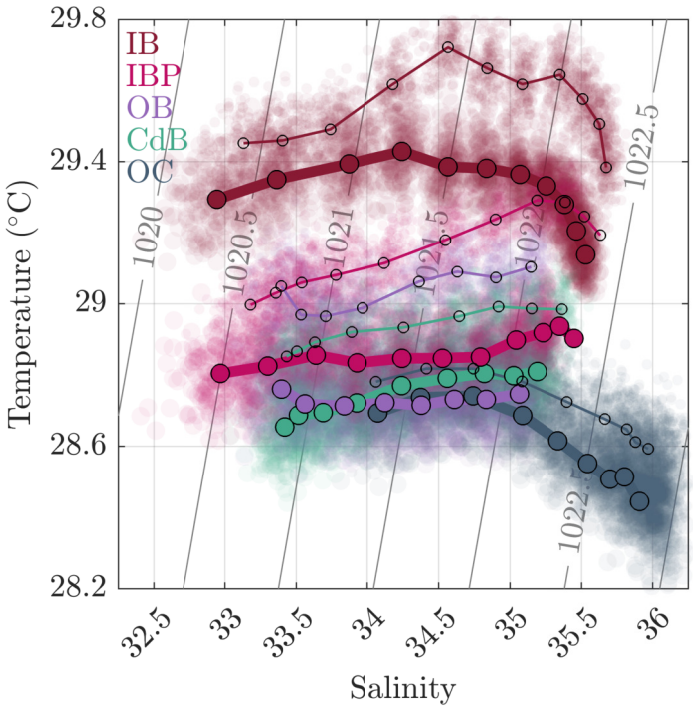

Figure 3.8. Ensemble mean profiles in temperature-salinity space for high flow conditions (large circles) and low flow conditions (small circles) for the sampling sites (color in Figure 3.1). Data sub-sampled evenly throughout the year.

for the inlet (CdB; green) and IBP (pink) also show pronounced shifts toward properties outside the bay. IB shows a pronounced shift near the surface but only a minimal response at depth, consistent with the weak relationship noted earlier. A temperature difference between the high and low flow conditions at the site outside the bay (OC; gray) persists in the conditional averaging, despite the uniform seasonal sampling scheme. This indicates a link between alongshore flow and temperature; however, it does not account for the larger temperature differences between high flow and low flow time periods that occur within the bay. The conditional averages during high flow and low flow time periods show that the barotropic flow affects the water properties in the outer bay, with less connectivity to the inner bay.

3.5.4 Residence time

The volume flux sheds light on how Bahía Almirante functions. Like many estuaries, the magnitude of the volume fluxes through the channels is much larger than the precipitation or riverine components (Figure 3.6), suggesting that changes in the flow regime are critical to setting the water properties within the bay. Freshwater fluxes via rivers and precipitation are much smaller than the water exchanged through the inlets, but during time periods of low net flow, they can play a meaningful role in the residual volume flux. The volume flux described here is illustrative, and results should be interpreted with caution because there are limitations on this analysis. Storage within the system is much smaller than the residual with the least squares linear adjustment, however there is likely considerable error associated with the assumptions in the volume fluxes through the channels, particularly the cross-channel uniformity assumption. The single mooring in each channel means that the cross-channel velocity structure cannot be resolved. As a sensitivity analysis, we also calculated volume fluxes assuming parabolic fits across the channel, which decreases the estimates by one third, yielding correspondingly longer residence times.

The bulk flushing time (17.3 days), as estimated from the volume flux through the channels, is comparable in magnitude to previous estimates from a bulk heat budget of the bay, where median monthly estimates yielded results of 10-40 days (Adelson et al., 2022). Alternative methods for calculating residence times are also considered including the freshwater fraction method and the tidal prism method (see supporting information), and produce median residence times of up to 54.2 days. Previous work has shown that bulk formula approaches can vary significantly in different tidal and river discharge conditions (Lemagie and Lerczak, 2015); therefore, differences in bulk flushing times are expected. Residence times provide context for the dynamics of Bahía Almirante, but it is important to note the implications for marine communities will depend on localized retention times. While the bulk residence time cannot provide insight into localized biogeochemical processes, it varies in time and can provide insight into temporal patterns in biologically-important consequences of increased retention times, including oxygen depletion and warming.

Previous spatially-variable residence time estimates (Li and Reidenbach, 2014; Adelson et al., 2022) support longer retention in the inner bay relative to the outer bay. The persistent IB hypoxia indicates that there are important ecological implications to this physical process in Bahía Almirante. The along-estuary differences in water properties suggest varying residence times for sub-basins, and previous work has estimated residence times for subregions of the bay based on a heat budget, with annual mean residence times of approximately 10.4 days for the outer bay, and 26.4 days for the inner bay (Adelson et al., 2022). With the higher residence time in the inner bay, there is a longer timescale for biogeochemical and physical processes to modify the water column. This is shown in the DO time series, in which oxygen drawdown occurs at IB and IBP (Figure 3.2 i). The persistent hypoxia, particularly the long anoxic event in 2020, indicates that the bulk residence time estimates do not capture the lengths of low-oxygen events. Therefore, the DO spatial patterns are consistent with longer residence times in the inner bay. Due to the strong vertical stratification in the system, these residence times are more pronounced

at depth, with the near-bottom time series indicating DO reductions and temperature increases relative to the upper water column (not shown). Elucidating the hydrodynamic controls on refreshment intermittency is critical to a better understanding of oxygen dynamics in this tropical system.

Above, we consider DO to be a proxy for water age, as the residence time is sufficiently long for oxygen consumption to occur at depth. Temperature can also be indicative of the water age, as radiative heating can warm the water column, and therefore higher temperatures can indicate longer residence times. The temperature offset in the ensemble mean profiles (Figure 3.8) throughout the water column during the time periods of low flow reflect longer retention within the estuary. Furthermore, temperatures steadily warm at IB and IBP (Figure 3.2 f) during the time periods that are concurrent with DO drawdown and hypoxia, further indicating stagnation periods over which warming can occur. Residence times can have important implications for ecosystem health, depending on the local transport mechanisms and timescales associated with biogeochemical processes, and warming and DO are stressors that co-occur during long retention times within Bahía Almirante.

3.5.5 Summary

This study presents analysis on the relative influences of the barotropic and baroclinic flow on Bahía Almirante, a tropical multi-inlet estuary. A strong, often dominant, net barotropic flow through BA is driven by an alongshore pressure gradient. While wind may play a role in setting up this pressure gradient or driving subtidal fluctuations on the order of 2-5 days, correlation with an along-coast flow as estimated from HYCOM suggests that offshore influences are dictating the flow regime within Bahía Almirante, that fluctuates on timescales of weeks to months. Furthermore, this correlation indicates that global models can resolve key aspects of coastal dynamics, which can be used to provide insight into data-poor regions like the Caribbean Sea.

The strength of the net flow dictates the dominant mechanics of the estuary. During periods with strong net flow, we see hydraulic control in the channels and a unidirectional, subtidal flow, typically into the estuary at BdD and out at CdB. During periods with weaker net flow, the baroclinic flow scales with the gravitational estuarine exchange theory.

The inner bay is a more isolated basin with a generally distinct water mass. Strong net flow through the bay dictates outer bay water properties while providing little direct influence on IB. Consequently, there are hydrographically distinct sub-basins within the system, and therefore spatially-variable residence times. Bulk residence times estimates are illustrative of the relative influences of the components of the volume fluxes, dominated by fluxes through the inlets, with smaller contributions from freshwater sources.

Previous work has shown that lateral advection is a mechanism for reoxygenation in Bahía Almirante, suggesting that an influx of sufficiently dense water into the bay is necessary for hypoxia breakdown (Adelson et al., 2022). Quantifying the residual net fluxes and transport through the bay, as well as characterizing the mixing within Bahía Almirante that sets the oceanward boundary condition for the inner bay, where hypoxia is most extreme and persistent, is therefore critical for developing a mechanistic understanding of hypoxia in this system. The analysis here shows that the inner bay is a hydrographically distinct sub-basin, with intermittent exchange with the outer bay, suggesting that the outer bay serves as the control point for refreshment within the system. Tropical estuaries are understudied relative to their temperate counterparts and describing the dominant processes that govern Bahía Almirante is a step towards addressing this knowledge gap, as well as progress in developing a mechanistic understanding of tropical systems and how they are similar to and differ from temperate estuaries.

3.6 Acknowledgements

We would like to thank Plinio Gondola and the environmental monitoring staff at STRI's Bocas del Toro Research Station and volunteers who have collected the long-term data set. We would also like to thank Steve Patton for the maintenance of the meteorological data. We would also like to thank the people who helped in the field, including Isabella Arzeno-Soltero, Ximena Boza, Viviana Bravo, Sebastian Castillo, Carolina Cesar, Antonia Helwig, Cynthia Pena, Max Rintoul, Duncan Wheeler, Jennifer Yin, and all the folks who keep the STRI Bocas station running.

All data has been collected under permits from MiAmbiente and ARAP. AEA was supported by a Smithsonian Fellowship. This work was supported by a National Science Foundation grant, NSF OCE - 1924220 (RC), NSF OCE - 1924551 (GP), NSF OCE - 1924664 (KAD). No conflicts of interest.

Chapter 3, in part, is currently being prepared for submission for publication of the material. Adelson, A.E. Collin, R, Davis, K.A., Giddings, S.N., Kastner, S.E., and Pawlak, G., Barotropic and baroclinic influences on a multi-inlet tropical estuary. The dissertation author was the primary investigator and author of this paper.

3.A Supporting information: Deployment details

The tables in Chapter 3 Appendix A provide information about the locations, depths, and sampling schemes for the instruments deployed in the three field campaigns in Bahía Almirante that provide the observations for the data analysis presented in this research.

3.B Supporting information: Residence time estimates

We compare residence time estimates, using the freshwater fraction, tidal prism, and flushing time methods to calculate time series of residence times. The freshwater fraction method yields a residence time using the estuary volume, the freshwater inflow rate, and the estuary and ocean salinities

$$T_{fw} = \left(\frac{S_O - S_{avg}}{S_O} \right) \frac{V}{Q_R}, \tag{3.7}$$

where S_O is the oceanic salinity, S_{avg} is the average estuarine salinity, V is the estuary volume, and Q_R is the freshwater fluxes into the estuary.

The tidal prism residence time is defined as

$$T_{TP} = \frac{V}{P} T_T, \tag{3.8}$$

where the tidal prism, $P = \eta A$, is calculated using the tidal range (η) and surface area (A) and T_T is the tidal period. We calculate the tidal range from the pressure gauge time series and use the M2 tidal period (12.42 hours).

We calculate a flushing time based on the volume exchange through the channels,

$$T_{Ex} = \frac{V}{Q_{Ex}}, \tag{3.9}$$

where $Q_{Ex} = Q_{in} - Q_{out}$, and Q_{in} is the volume flux into the estuary and Q_{out} is the volume flux out of the estuary. This residence time estimate is calculated using the ten minute-averaged and Godin-filtered data to estimate flushing times.

Median residence time estimates range from 17.3 - 54.2 days (Table 3.B.1), with time variations over the course of the year (not shown). These residence time estimates

are for the full bay volume and thus represent the bulk properties. The longest median residence times result from the freshwater fraction method. The tidal prism method does not account for the net flow through the system which results from the multi-inlet nature of Bahía Almirante. Finally, the residence time estimate from the subtidal exchange volume flux is nearly double the residence time of the same method that also considers tidal velocities.

The residence time estimates yield varying results (Table 3.B.1), which is not inconsistent with the nature of methods. Previous work has shown that bulk formula approaches can vary significantly in different tidal and river discharge conditions Lemagie and Lerczak (2015), and thus the differences bulk flushing times are expected. The flushing time calculated using the exchange through the channels on the tidal timescale is comparable to previous estimates from a heat budget Adelson et al. (2022) and is shorter than similarly computed flushing time using the subtidal volume flux, indicating that tidal velocities meaningfully contribute to the flushing time. In contrast, the residence times estimated from the freshwater fraction method are much longer, which potentially reflects that much of overall volume flux through the system is driven by flow through the channels. Finally, because the tidal range of Bahía Almirante is small, the residence time estimated from the tidal prism is also relatively long. The residence times listed here should be interpreted with caution, as there is considerable, unquantified error associated with the components of the volume flux, as broad assumptions have been made about cross-channel uniformity with respect to the volume fluxes through the channels. Furthermore, previous work has cautioned that all transport timescale depend on underlying assumptions and that no single metric can account for all processes Monsen et al. (2002). Thus, we provide these estimates to indicate that different methods yield results that are similar in magnitude and can provide a rough approximation of an expected bulk residence time.

Comparisons of transect data (not shown) and the the salinity data collected at 7 m indicate that the near surface data does not always capture the near-surface freshwater lens,

and thus the bulk estimate of estuarine salinity used in the freshwater fraction residence time estimate may be an overestimate.

Table 3.A.1. Sampling information for the ADCPs deployed in the channels of Bahía Almirante, Boca del Drago (BdD), Canal de Bastimentos (CdB), Cayo Coral (CC). All data were collected from Teledyne-RDI Workhorses.

Frequency (Hz)	**Date (MM/DD/YY)**	**Coordinates (°N; °W)**	**Depth (m)**	**Sampling information**
		BdD ADCP		
1200	09/17/19-01/16/20	9.42178; 82.33797	22.1	0.4 Hz; 36 0.5-m bins
1200	01/22/20-08/24/20	9.422721; 82.337814	24.6	0.4 Hz; 20 1-m bins
600	11/04/20-02/24/21	9.422870; 82.339408	20.3	0.5 Hz; 17 1-m bins; (10 min bursts every 20 min; in-line in mooring)
		CdB ADCP		
1200	09/13/19-01/15/20	9.34664; 82.2223	18.0	0.5 Hz; 17 1-m bins
600	01/21/20-07/03/20	9.346671; 82.222252	18.2	0.4 Hz; 23 1-m bins
600	11/02/20-09/14/21	9.346671; 82.222252	18.2	0.4 Hz; 20 1-m bins; (10 min bursts every 20 min)
		CC ADCP		
1200	09/21/19-01/11/20	9.23965; 82.14136	13.7	0.5 Hz; 36 0.5-m bins
1200	01/22/20-08/26/20	9.239624; 82.141435	13.1	0.4 Hz; 36 0.5-m bins
1200	11/03/20-09/18/21	9.239685; 82.141374	13.0	0.25 Hz; 36 0.5-m bins; (10 min bursts every 30 min)

Table 3.A.2. Sampling scheme information for moored instruments, excluding ADCPs. Sampling rates provided for CTDs, thermisters, MiniDOTs, MiniDOT wipers, and RBR duets for each of the three field campaigns (FC).

Instrument	**Sampling rates (s)**		
	FC 1	**FC 2**	**FC 3**
CTD (SBE-37-SMP-ODO)	300	300	600
CTD (SBE-37-SMP)	60	60	120
Thermisters (SBE 56)	3	3	5
MiniDOT	60	60	60
MiniDOT wiper	7200	7200	3600
RBR Duet	1	1	2

Table 3.A.3. Deployment information for IB subsurface mooring (9.25601°N, 82.35°W; location did not change between deployments), including instrument types and depths. See accompanying table for sampling schemes.

FC 1: 9/13/19-01/16/20	
Instruments	**Depth (m)**
CTD (SBE-37-SMP-ODO)	7.3
Thermister chain (SBE 56)	
(8 units every 2 m)	9.3-23.3
(1 unit)	24.7
CTD (SBE-37-SMP-ODO)	25.7
FC 2: 01/27/20-10/29/20	
Instruments	**Depth (m)**
CTD (SBE-37-SMP-ODO)	6.7
Thermister chain (SBE 56)	
(9 units every 2 m)	7.6-23.6
CTD (SBE-37-SMP)	25.4
MiniDOT and wiper	25.9
FC 3: 11/07/20-09/12/21	
Instruments	**Depth (m)**
MiniDOT and wiper	6.8
CTD (SBE-37-SMP)	7.0
Thermister chain (SBE 56)	
(9 units every 2 m)	8.6-24.6
CTD (SBE-37-SMP-ODO)	25.6

Table 3.A.4. Deployment information for IBP subsurface mooring (9.28092°N, 82.30498°W; location did not change between deployments), including instrument types and depths. Mooring was only deployed in FC 1 and FC 2. See accompanying table for sampling schemes.

FC 1: 9/17/19-01/13/20	
Instruments	**Depth (m)**
CTD (SBE-37-SMP)	4.6
MiniDOT and wiper	4.6
Thermister chain (SBE 56)	
(10 units every 2 m)	6.5 - 24.5
CTD (SBE-37-SMP-ODO)	26.4
MiniDOT and wiper	26.4
FC 2: 01/27/20-10/29/20	
Instruments	**Depth (m)**
CTD (SBE-37-SMP-ODO)	5.5
Thermister chain (SBE 56)	
(10 units every 2 m)	6.6-24.6
CTD (SBE-37-SMP)	26.0
MiniDOT and wiper	26.5

Table 3.A.5. Deployment information for OB subsurface mooring (9.3517°N, 82.34438°W; location did not change between deployments), including instrument types and depths. See accompanying table for sampling schemes.

FC 1: 11/18/19-01/13/20	
Instruments	**Depth (m)**
Pressure sensor (SBE 39)	7.0
MiniDOT and wiper	7.0
Thermister chain (SBE 56)	
(6 units every 2 m)	8.2-18.2
MiniDOT and wiper	18.2
FC 2: 01/21/20-10/29/20	
Instruments	**Depth (m)**
MiniDOT and wiper	6.0
Pressure sensor (SBE 39)	7.0
Thermister chain (SBE 56)	
(6 units every 2 m)	8.2-18.2
MiniDOT and wiper	18.2
FC 3: 11/07/20-09/11/21	
Instruments	**Depth (m)**
MiniDOT and wiper	6.9
CTD (SBE-37-SMP)	6.9
Thermister chain (SBE 56)	
(6 units every 2 m)	7.1-17.1
CTD (SBE-37-SMP-ODO)	18.1

Table 3.A.6. Deployment information for CdB subsurface mooring, including instrument types and depths. See accompanying table for sampling schemes.

FC 1: 9/13/19-01/14/20	
9.34597°N; 82.2224°W	
Instruments	**Depth (m)**
MiniDOT and wiper	7.2
CTD (SBE-37-SMP)	7.3
Thermister chain (SBE 56)	
(4 units every 2.8 m)	10.6-19.0
CTD (SBE-37-SMP)	21.4
MiniDOT and wiper	21.5
FC 2: 01/24/20-10/27/20	
9.345821°N; 82.222588°W	
Instruments	**Depth (m)**
CTD (SBE-37-SMP)	7.5
MiniDOT and wiper	7.6
Thermister chain (SBE 56)	
(5 units every 2 m)	9.7-17.7
CTD (SBE-37-SMP)	19.5
MiniDOT and wiper	19.7
FC 3: 11/09/20-09/13/21	
9.345769°N; 82.222593°W	
Instruments	**Depth (m)**
MiniDOT and wiper	7.1
CTD (SBE-37-SMP)	7.1
Thermister chain (SBE 56)	
(6 units every 2 m)	8.7-18.7
CTD (SBE-37-SMP-ODO)	19.7

Table 3.A.7. Deployment information for BdD subsurface mooring, including instrument types and depths. See accompanying table for sampling schemes. Note that the FC 3 mooring failed, and the only instruments recovered were the ADCP and CTD. There is a near surface measurement station in this inlet with deployment information in a separate table.

FC 1: 9/16/19-01/15/20	
9.42291°N; 82.33939°W	
Instruments	**Depth (m)**
Thermister (SBE 56)	14.2
Thermister (SBE56)	17.0
CTD (SBE-37-SMP-ODO)	19.9
Thermister (SBE 56)	22.6
FC 2: 01/22/20-10/28/20	
9.422873°N; 82.339435°W	
Instruments	**Depth (m)**
Pressure sensor (RBR Duet)	9.7
Thermister chain (SBE 56)	
(5 units every 2 m)	11.7-19.7
CTD (SBE-37-SMP-ODO)	21.5
FC 3: 11/04/20-02/24/21	
9.422870°N; 82.339408°W	
Instruments	**Depth (m)**
ADCP	20.8
CTD (SBE-37-SMP)	20.8

Table 3.A.8. Deployment information for OC subsurface mooring, including instrument types and depths. See accompanying table for sampling schemes.

FC 1: 9/11/19-01/16/20	
9.39569°N; 82.19661°W	
Instruments	**Depth (m)**
CTD (SBE-37-SMP)	7.8
MiniDOT and wiper	7.9
Thermister chain (SBE 56)	
(6 units every 5 m)	12.6-35.6
MiniDOT and wiper	39.3
CTD (SBE-37-SMP)	39.4
ADCP	39.7
FC 2: 01/20/20-10/27/20	
9.395689°N; 82.196542°W	
Instruments	**Depth (m)**
CTD (SBE-37-SMP-ODO)	6.9
Thermister chain (SBE 56)	
(6 units every 5 m)	11.9-36.94
CTD (SBE-37-SMP)	38.2
MiniDOT and wiper	38.2
ADCP	38.6
FC 3: 11/06/20-09/09/21	
9.39333°N; 82.201516°W	
Instruments	**Depth (m)**
CTD (SBE-37-SMP)	6.4
Thermister chain (SBE 56)	
(7 units every 3 m)	7.2-25.2
CTD (SBE-37-SMP)	27.2
MiniDOT and wiper	27.3

Table 3.A.9. Deployment information for bottom-mounted instruments, including pressure sensors (RBR Duets), CTDs (SBE-37-SMP), and MiniDOTs and wipers.

Instrument	**Dates (MM/DD/YY)**	**Coordinates (°N; °W)**	**Depth (m)**
CdB pressure sensor (RBR Duet)	FC 1: 9/14/19-01/08/20	9.34327; 82.22029	7.6
BdD pressure sensor (RBR Duet)	FC 1: 9/14/19-01/09/20	9.42329; 82.32823	5.2
BdD bottom station			
CTD (SBE-37-SMP)	FC 1: 9/17/19-01/09/20	9.41938; 82.33559	5.5
CTD (SBE-37-SMP) MiniDOT and wiper	FC 2: 9/22/19-10/28/20	9.419339; 82.335623	5.3
CTD (SBE-37-SMP) MiniDOT and wiper pressure sensor (RBR Duet)	FC 3: 11/04/20-09/14/21	9.419339; 82.335623	5.3

Table 3.B.1. Residence time estimates via various methods. Median values reported, as well as the 25% and 75% quartiles.

Method	**Median (days)**	**25%**	**75%**
Exchange volume flux	17.3	12.7	24.6
Subtidal exchange volume flux	33.2	22.4	46.9
Tidal prism	48.7	41.7	58.0
Freshwater fraction	54.2	18.1	136.3

Chapter 4

Deep water renewal episodes dictate hypoxic state of a shallow tropical estuary

4.1 Abstract

Global changes including deoxygenation have detrimental effects on marine biological communities. Tropical ecosystems are particularly vulnerable, and thus there is a critical need to understand the dynamics and drivers of low oxygen events in the tropics. From September 2019 to September 2021, we conducted an intensive study of Bahía Almirante, a shallow, multiple-inlet tropical estuary, in the Bocas del Toro region on the Caribbean coast of Panama, which has experienced documented hypoxia and warming events that have resulted in coral bleaching and die offs. Time series observations include water velocity, temperature, salinity, and dissolved oxygen. In the inner bay, dissolved oxygen concentrations at depth drops to hypoxic levels on seasonal timescales, with slow salinity decreases consistent with weak vertical mixing of an isolated, stagnant bottom water mass. Reoxygenation events occur with (1) inflow at depth and (2) inflow density that exceeds the bottom layer density in the inner bay, exhibiting events that are mechanistically similar to deep water renewal commonly observed in fjords. In fjords, diapycnal mixing drives density reduction of the stagnant water mass which contributes to

refreshment. In Bahía Almirante, warming of the isolated bottom water mass via radiative heating also contributes to density reduction, a novel mechanism in deep water renewal dynamics. Variations in renewal timescales calculated using density variability statistics outside of the bay highlights the role of density outside the bay in the dissolved oxygen seasonal cycle inside Bahía Almirante. Finally, we compare timescales and intermittency of oxygen drawdown within the bay and deep water renewal events to understand the regular, seasonal deoxygenation that occurs within this estuary and identify potential commonalities with other shallow systems.

4.2 Introduction

Oxygen losses are occurring throughout the global ocean, including open seas, coastal regions, and semi-enclosed systems, such as estuaries (Limburg et al., 2020). While deoxygenation is well studied in the open ocean and temperate regions (Breitburg et al., 2018), there have been fewer studies in tropical coastal systems (e.g., Altieri et al., 2017; Kealoha et al., 2020; Hughes et al., 2020; Nelson and Altieri, 2019; Pezner et al., 2023), reflecting a scientific bias towards temperate regions (Vieillard et al., 2020). Low dissolved oxygen (DO) can have significant effects on ocean organisms and ecosystems, and hypoxia is commonly defined as DO < 2 mg L^{-1}, although physiological impairment and reduced ecosystem function can occur above this threshold (Vaquer-Sunyer and Duarte, 2008). Given the likely underestimate of DO-driven coral reef mortality (Altieri et al., 2017), it is critical to understand the processes that govern hypoxia in tropical systems.

While anthropogenic eutrophication is commonly linked to deoxygenation (Breitburg et al., 2018), physical mechanisms can also contribute to hypoxia, with or without excess nutrient fluxes. When a pycnocline prevents vertical exchange in a stratified system and bathymetry restricts horizontal exchange, continued biological oxygen demand (BOD) can lead to deoxygenation (Gade and Edwards, 1980).

Deep water renewal describes the general process by which new water is injected into a stagnant basin, generally separated by a sill from the surrounding region (Inall and Gillibrand, 2010). It has long been identified as a mechanism for hypoxia reprieve in fjords (Gade and Edwards, 1980) and more recently, deep tidally-influenced lagoons (Kelly et al., 2017) and a tropical systems with sill (Salamena et al., 2021). This intermittent exchange is a function of coastal density at the sill height and the density reduction within the basin (Stigebrandt, 2012).

Longitudinal density gradients are key to deep water renewal, where a water mass of an adequate density class and volume is required at the sill height to refresh water within the enclosed basin (Gade and Edwards, 1980). Typically, density reductions of the stagnant water mass must occur to lead to longitudinal density gradients favorable for this exchange. This is frequently achieved via diapycnal mixing, which can also oxygenate waters (Gade, 1973; Gade and Edwards, 1980; Stigebrandt, 2001). Fluctuations in the density field at the sill are affected by various physical processes, including tides, winds, offshore conditions, and variations in freshwater inputs (Gade and Edwards, 1980). These factors can influence the barotropic and baroclinic flows over a sill, and the relative changes in these flows also contributes to the intermittency of deep water renewal. In Ambon Bay, Indonesia, a shallow-silled tropical system, the phase of the monsoon and the spring-neap phase of the internal tide lead to variations in flushing volumes (Salamena et al., 2021).

In the paradigm in which deep water renewal relieves hypoxia, there are two factors that are critical to consider, the frequency of deep water renewal episodes, which provide oxygenated waters to isolated bottom waters, and the timescale for oxygen depletion (Gillibrand et al., 2006). Their relationship determines the propensity for hypoxia in bottom waters (Fennel and Testa, 2019). If the timescale for refreshment is shorter than that of oxygen depletion, then we can expect that bottom waters will remain oxygenated or that other mechanisms will determine local DO dynamics, including horizontal advection of low DO water. If deep water renewal occurs on a longer timescale than hypoxia

development, then we can expect anoxia to be a regular feature of the system. If these two are on similar timescales, the system experiences intermittent hypoxia. If at least one of the timescales varies in time, renewal may occur on a spring-neap, seasonal, or another forcing timescale.

Adelson et al. (2022) describe physical forcings that lead to hypoxia development in Bahía Almirante, a shallow estuary with mangrove, coral reef, and sea grass communities (Collin et al, in review). While measured nutrient inputs into the bay are minimal, there are likely urban point sources that have not been measured (Clark et al., 2022). There are favorable physical conditions for hypoxia development, as high freshwater inputs leads to strong vertical stratification that isolates bottom waters, leading to DO drawdown and hypoxia (Adelson et al., 2022). There remains open questions about the processes that drive hypoxia termination within Bahía Almirante and mechanistically similar tropical estuaries.

Few datasets of tropical estuaries exist, and we combine intensive field campaign data with long-term weekly monitoring data to examine the dynamics important to re-oxygenation in this tropical estuary. We use observations from September 2019 through September 2021 of physical parameters including currents, density, salinity, water temperature, DO, wind, solar radiation, as well as long-term data from a spatial program, including salinity, water temperature, and DO profiles and Secchi depths (Figure 4.1). We describe the site and observations in Section 4.3. In Section 4.4, we show that deep water renewal is the primary mechanism for reoxygenation of near-bottom waters in the inner bay of Bahía Almirante (Section 4.4.1 and Section 4.4.2). We then delve further into the isolation periods when hypoxia develops (Section 4.4.3), estimate vertical eddy diffusivity, which allows us to calculate a predicted temperature and density change due to diapycnal mixing. We compare these values to measurements and estimate the relative contributions of diapycnal mixing and radiative heating to density reduction (Section 4.4.4). We then compare a DO drawdown timescale to a renewal timescale to show that this system tends

towards hypoxia (Section 4.4.5). In Section 4.5, we discuss the implications of the deep water renewal framework and adapting dynamics that have long been described in as a reoxygenation mechanism in fjords (Gade, 1973) to a shallow tropical estuary with gentle bathymetry (Section 4.5.1). We show that radiative heating of the bottom layer can significantly contribute to density reduction of the isolated water mass, a novel mechanism in this critical deep water renewal process, which may be important in deep water renewal in other shallow, tropical systems (Section 4.5.2). We discuss what drives the deep water renewal intermittency and DO drawdown timescale (Section 4.5.3). We attribute the DO seasonality in Bahía Almirante to the density field outside of the estuary (Section 4.5.3) and hypothesize that shoaling of the near-bottom hypoxic layer causes episodic die-off events (Section 4.5.5).

4.3 Observations and methods

4.3.1 Site description

Bahía Almirante is a shallow (30 m) tropical, multi-inlet estuary in the Bocas del Toro region of Panamá (Figure 4.1). It has two inlets to the Caribbean Sea, Boca del Drago (BdD) and Canal de Bastimentos (CdB). The multiple inlets allow for a net barotropic flow through Bahía Almirante, which is associated with alongshore pressure gradients (Chapter 3).

The estuary is salinity-stratified throughout the year (Kaufmann and Thompson, 2005), which leads to isolation of the bottom layer. Bahía Almirante experiences seasonal hypoxia at depth and temperature inversions that have been linked to vertical salinity stratification driven by annual patterns in freshwater inputs, with spatial heterogeneity in the strength in these resultant biological stressors, with effects particularly strong in the inner bay (Adelson et al., 2022). Previous work has also shown that the inner bay is often isolated, particularly at depth, due to limited exchange (Chapter 3).

Hypoxia has been linked to die offs and coral reef mortality within the system in an episodic sense (Altieri et al., 2017; Johnson et al., 2021); however, our previous work shows that hypoxia occurs seasonally at depth in Bahía Almirante (Adelson et al., 2022), with instances of Low-DO waters at depths as shallow as 4 m (Adelson et al., 2022; Lucey et al., 2021). Beyond the documented mortality events, significant sub-lethal effects on reef animals, including sea urchins, have been observed when they are subjected to DO levels common in Bahía Almirante (Lucey et al., 2020a, 2021). In Bahía Almirante, hypoxia and warming have been linked to reduced larval bivalve concentrations (Weinstock and Collin, 2021) and zooplankton abundance (Weinstock et al., 2022), which has implications for the ecosystem function.

4.3.2 Dataset description

We use data from a two-year observational campaign that took place from September 2019 - September 2021. This dataset has three major deployments (September 2019 - January 2020, January 2020 - October 2020, and November 2020 - September 2021) with instruments recovered and redeployed at approximately the same location, given field logistics. In this analysis, we consider data at five sites, a site outside the bay (OC), the two inlets to the Caribbean Sea (BdD and CdB), inner bay pass (IBP), and the inner bay (IB), as shown on Figure 4.1.

In this analysis, we largely focus on the bottom water mass, because this is where hypoxia has been shown to occur in the system (Adelson et al., 2022). We consider data from subsurface moorings outfitted with temperature sensors (SBE-56), conductivity, temperature, and depth (CTD) sensors (SBE-37 SMP and SBE-37 SMP-ODO), and optical DO sensors (PME MiniDOT and CTD-integrated SBE-63). The depths of the near-bottom CTDs are: OC - 3 meters above bed (mab), CdB - 1 mab, BdD - 3 mab, IBP - 1 mab, and IB - 1 mab. These measurements are assumed to be representative of the bottom layer. The only near-surface CTD considered in this analysis is at OC,

with a median depth of approximately 8 meters. Some CTDs experienced significant sediment entrainment and/or biofouling, resulting in unrealistic conductivity and salinity measurements and those time periods are excluded from analyses. We also use data collected from upward-facing acoustic Doppler current profilers (ADCPs; Teledyne RDI Workhorse and Sentinel V) in the channels, CdB and BdD. Principal component analysis for each deployment was used to define along-channel and across-channel velocities. All data are ensemble-averaged in 10-minute bins. For further description of the dataset used in this analysis, see Chapter 3.

We use meteorological data, collected by the Smithsonian Tropical Research Institute's (STRI) Physical Monitoring Program at the Bocas del Toro Research Station in Panamá (Patton, 2023), including wind speed and direction and solar radiation from a weather station at STRI (WS on Figure 4.1).

This analysis also considers data from STRI's spatial water sampling program, including processed vertical salinity, temperature, and DO profiles collected by YSI multiparameter sonde (Adelson et al., 2022) and Secchi depths. These measurements are taken nominally weekly from May 2015 to present. The sites are approximately co-located with the mooring locations shown in Figure 4.1, with further information on this dataset in Adelson et al. (2022). We calculate density and depth of maximum stratification from measured salinity, temperature, and depth using Gibbs Seawater toolbox (McDougall and Barker, 2011).

4.4 Analysis

4.4.1 Deep water renewal framework

Deep water renewal requires sufficiently dense water entering the bay in sufficient supply to refresh the bottom layer in the inner bay. We develop a simple framework to identify time periods when these conditions are met and comparing these instances to

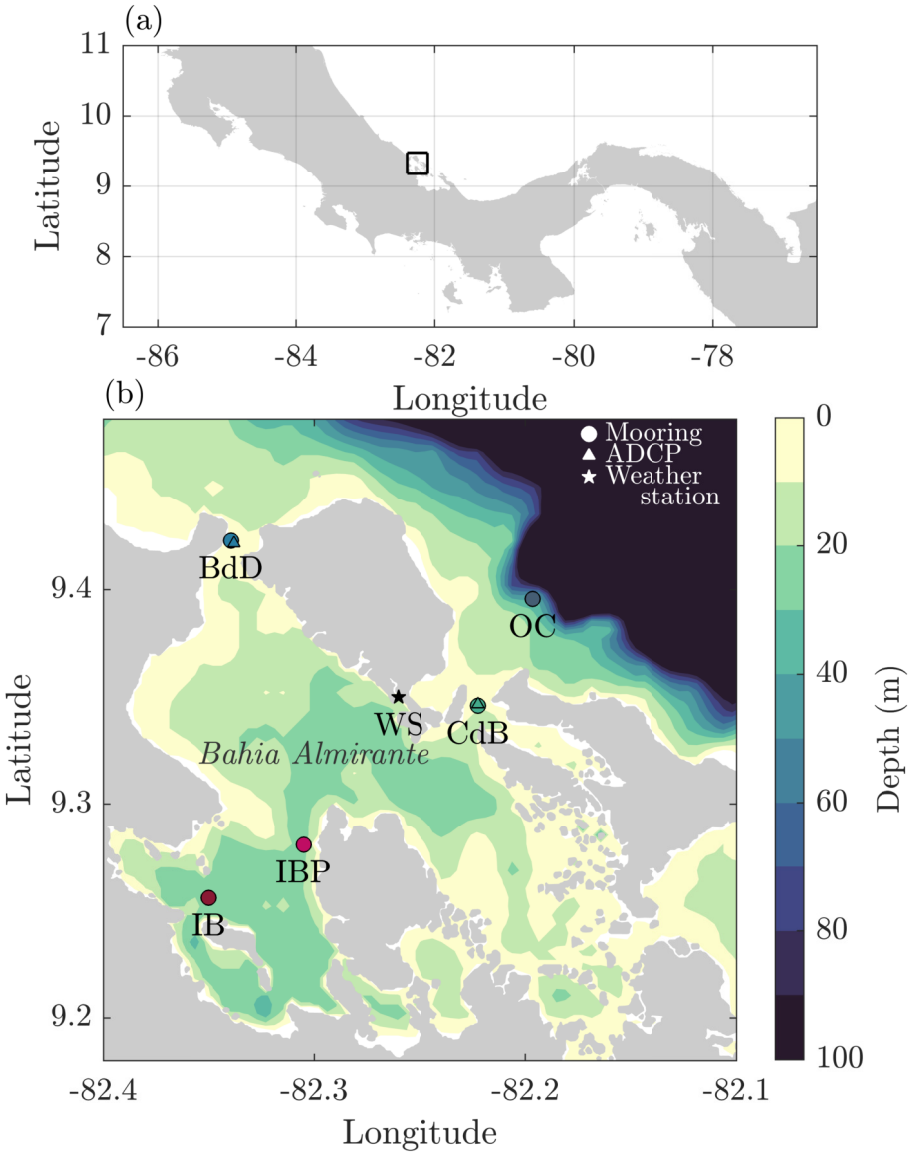

Figure 4.1. (a) Panamá Coast, with Bahía Almirante inset in box. (b) Site locations identified by color, used in subsequent figures. Mooring locations are shown in circles and bottom-mounted ADCP locations in triangles. Details on the moorings are included in the supporting information in 3. Bathymetry in color.

the DO time series (Figure 4.2 c). We apply a 7-day low-pass filter in this analysis to attenuate higher frequency variations.

We define an along-estuary bottom density difference ($\rho_{inlet} - \rho_{IB}$), with densities measured by CTDs in the inner bay (IB) and each of the inlets (BdD and CdB), such that this quantity is positive when the inlet density exceeds the inner bay density (i.e., when

it leads to a along-estuary density gradient conducive to IB bottom-water replacement; Figure 4.2 a). We consider the near bottom velocity in each of the inlets, which is an average of the bottom 5 m of the vertically-interpolated along-channel velocity, defined such that flow into the bay is positive and consistent with a flow direction consistent with deep water renewal (Figure 4.2 b). When there is insufficient data for this framework to apply, the time series is transparent in Figure 4.2 (i.e., color is less saturated). When both of the conditions are met (i.e., both values are positive) simultaneously at one or both of the inlets, the time series in each panel of Figure 4.2 is shaded.

Deep water renewal conditions are met preceding all significant reoxygenation events for the time period considered (Figure 4.2 c). When they are met for at least 24 hours, there is a minimum DO increase of 0.7 mg L^{-1} within 7 days of termination of deep water renewal conditions. Furthermore, there is a statistically significant relationship between the length of time that these conditions are met and the ensuing change in DO ($R^2 = 0.53$; $p < 0.0001$), such that when deep water renewal conditions are met for longer periods, there is a greater DO increase (See supporting information, Figure 4.A.1).

4.4.2 Role of wind

Wind-driven vertical mixing is a common mechanism for reoxygenation in estuaries (Stanley and Nixon, 1992; Scully, 2010). Bahía Almirante is a strongly-stratified system (Kaufmann and Thompson, 2005; Adelson et al., 2022), and the stratification may limit the depth to which wind-driven mixing can penetrate. We calculate the maximum stratification depth from the weekly monitoring profiles (Figure 4.3). The mean maximum stratification depth is 5.7 m, and 95% of estimates are 13.4 m or shallower, which shows that Bahía Almirante is rarely well-mixed throughout the water column.

To evaluate the role that wind plays in the water column in Bahía Almirante, we estimate a mixing length scale L_Z, akin to a Monin-Obukhov length, (Farmer and Freeland,

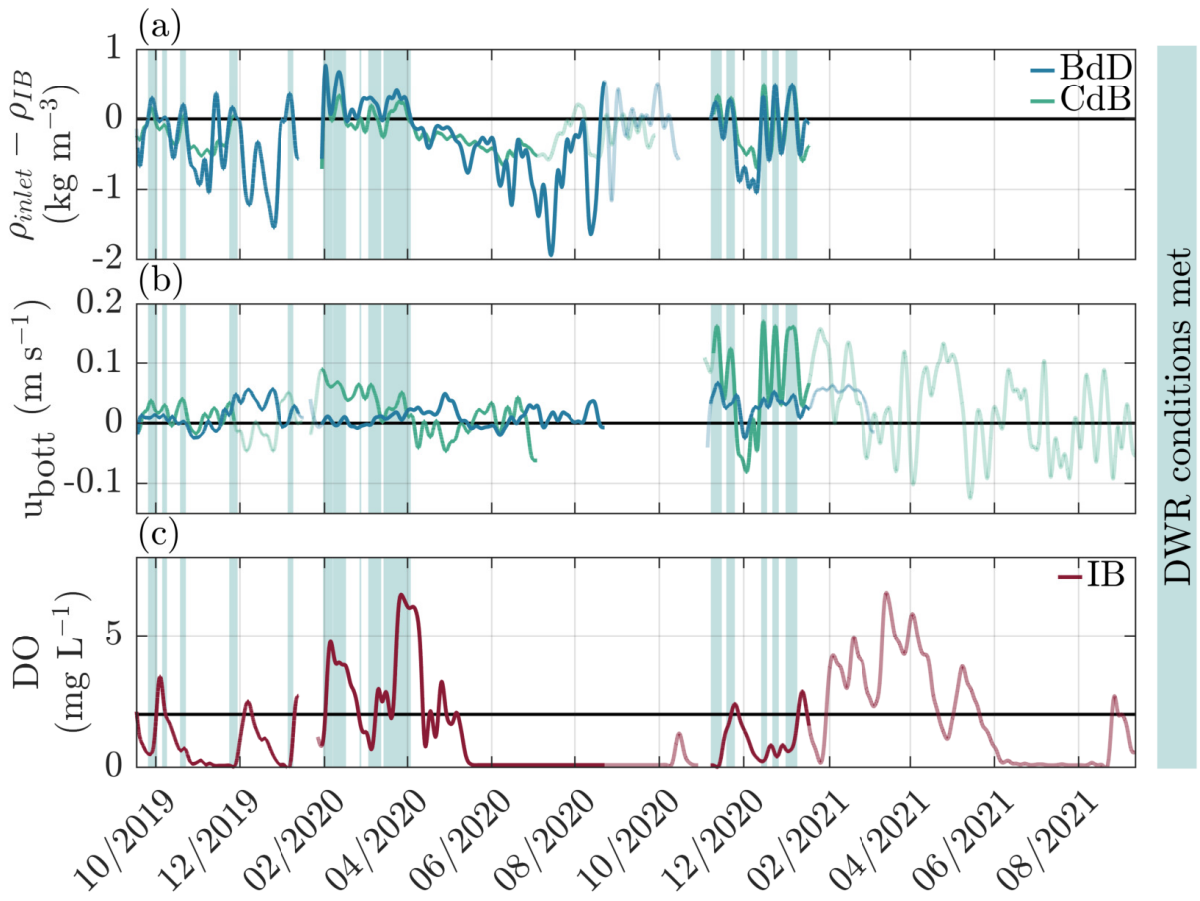

Figure 4.2. The deep water renewal framework. (a) The along-estuary density difference ($\rho_{inlet} - \rho_{IB}$; kg m^{-3}) for BdD and CdB. When this quantity is positive, the deep water renewal condition for density is met; (b) the near-bottom velocity (u_{bott}; m s^{-1}) in the inlets. When this quantity is positive, the deep water renewal condition for velocity is met; (c) DO (mg L^{-1}) at IB, with 2 mg L^{-1} hypoxia threshold shown in black for reference. All data are low-pass filtered. The transparent (i.e., lighter) time series indicates time periods when there is not sufficient data for this framework. Shading indicates when both deep water renewal conditions are met at one or both of the channels (i.e., when both the quantities in panel (a) and (b) are positive at one or both channels).

1983). We define

$$L_z = \gamma \frac{u_*^2}{\kappa g \Delta\rho/\rho}, \tag{4.1}$$

where g is the gravitational acceleration constant, $\Delta\rho$ is the difference between density at level z' and the average density above level z', ρ is density at level z', and $\kappa = 0.4$, a constant, γ is an unknown constant, and u_* is the shear velocity from the wind, i.e.,

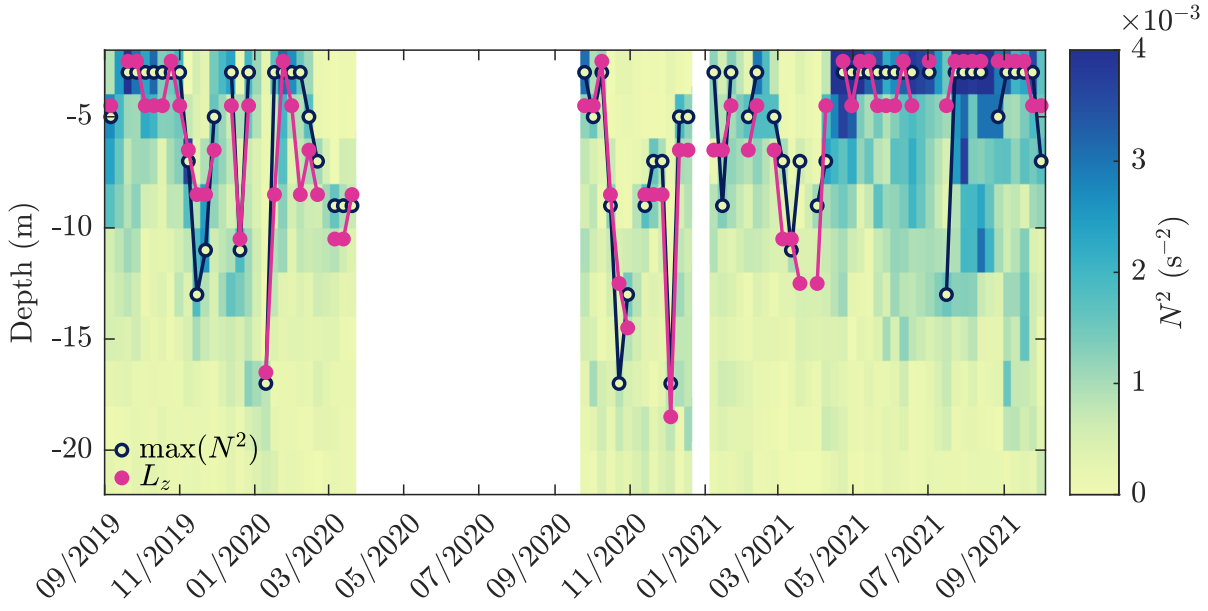

Figure 4.3. Comparison of maximum stratification depth and mixing length scale. N^2 in color, calculated from the weekly monitoring data collected near IB, with maximum value shown in dark line. Mixing length scale, L_z shown in pink.

$u_*^2 = \tau_{wind}/\rho_0 = \rho_a C_D U_{10}^2/\rho_0$. We assume an air density, $\rho_a = 1.3$ kg m^{-3}, and a drag coefficient, $C_D = 0.0013$, and we use the wind speed from STRI meteorological station (WS on Figure 4.1).

L_z is correlated with ($R^2 = 0.69$) and similar to the depth of maximum stratification (Figure 4.3), with a mean of 5.6 m and 95% of estimates 12.2 m or shallower. It is important to note that we expect these quantities to be correlated, because the mixing length estimate depends on the stratification. The similar magnitudes of the maximum stratification depth and the mixing length indicates that the unknown factor γ is of order unity.

Other analyses examining correlations of wind with DO and density have not yielded significant results. The wind's role is therefore generally limited to the upper part of the water column in Bahía Almirante. While wind-driven mixing may play a role in the DO dynamics in the upper part of the water column (typically limited to 13 m or less) and may be modulating the pycnocline height, there is no evidence that it drives reoxygenation at depth.

4.4.3 Isolation periods

The inner bay experiences concurrent step changes in temperature, salinity, and DO at depth, which is consistent with lateral advection as the mechanism for reoxygenation (Figure 4.4). The time periods between these events are characterized by DO drawdown and slow, steady changes in temperature, salinity, and density, suggesting water mass isolation. During these periods, the salinity decrease indicates that vertical mixing is modifying the bottom layer, however the continued DO drawdown or anoxia suggests that this vertical mixing is insufficient to reoxygenate the bottom layer. The following analysis quantifies the vertical mixing that occurs during isolation periods and explores the important physical mechanisms in water property modification.

Identifying isolation periods

We identify periods that have the isolation characteristics, including decreasing DO or anoxia, and slow changes in density, salinity, and temperature, allowing for some local advection leading to higher frequency variations. Due to the requirements to calculate vertical mixing parameters that are described below, we must only consider periods when the intensive observational campaign and the ongoing monitoring data overlap. We are further limited by a monitoring hiatus due to the COVID-19 pandemic and an instrument failure from the moored IB CTD.

Considering 60-minute averaged salinity and temperature data, we identify local maxima, that typically occur after sharp DO increases, to signify isolation onset (Figure 4.4). While all time series have high frequency variations, we consider the water mass isolated between step changes in temperature and/or salinity and calculate linear fits to capture the slow changes caused by vertical mixing. We compare the periods to the DO time series to confirm there is DO drawdown. We are able to define four isolation periods with sufficient data for the following analysis (Figure 4.4, shading).

The isolation events with sufficient data have durations which range from 19.9 to

56.5 days. Table 4.1 lists all four of these events and the associated parameters of interest that are detailed below. It is outside the scope of this analysis to consider intra-event differences because the sample size is small. We provide the values for individual events to illustrate possible values for this system.

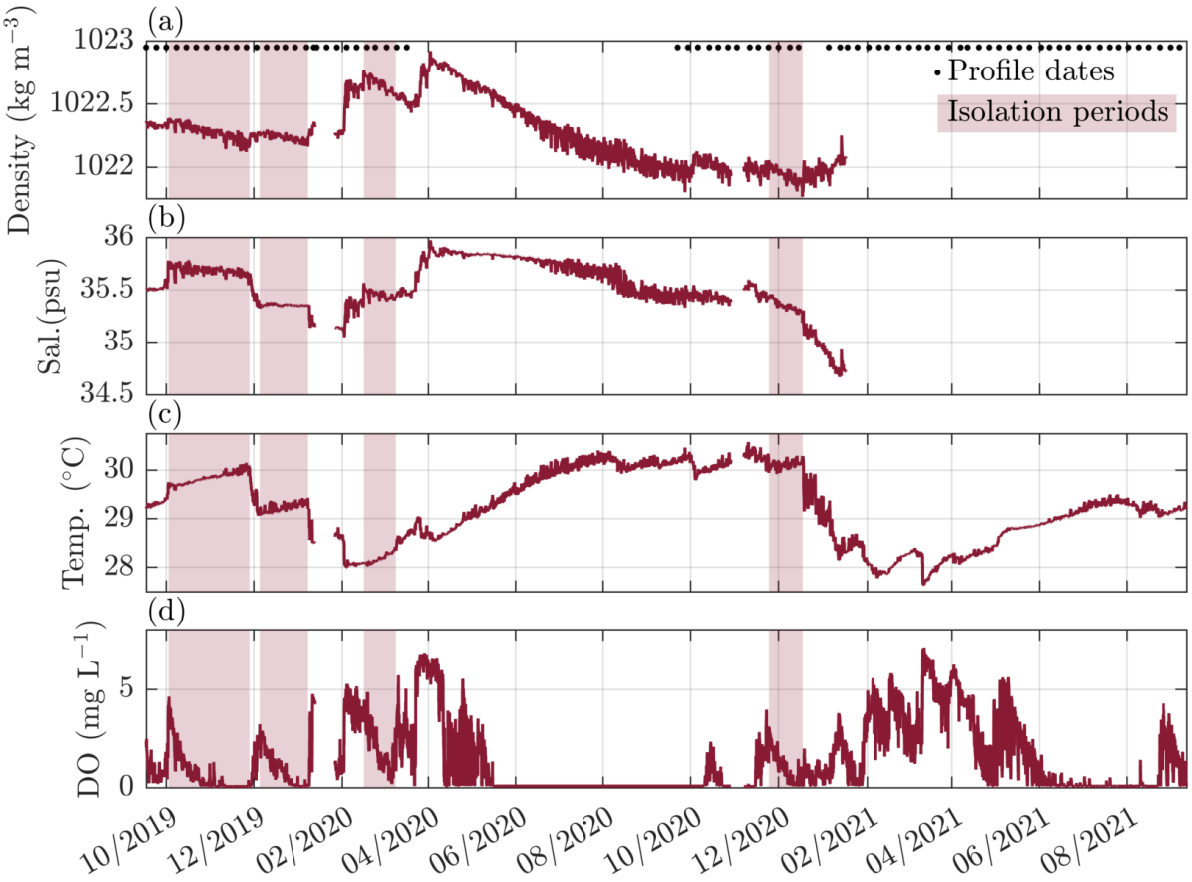

Figure 4.4. Isolation event identification using water property time series. (a) density (kg m^{-3}), (b) salinity (psu), (c) temperature (°C), (d) DO (mg L^{-1}). Black dots on panel (a) indicate monitoring profile dates. Shading indicates isolation periods identified for the analysis shown in Table 4.1.

Estimating vertical eddy diffusivity, K_z

During isolation periods, we assume that conservative scalar quantities such as salinity are changed only through vertical mixing. We can therefore estimate a 1-D salt budget for the bottom layer, following Gade (1973) and Gargett (1984), and revisited in

Stigebrandt (2012).

Considering an isolated slab of bottom water during a period between refreshment events, conservation of salt can be written as

$$\frac{\partial S}{\partial t} = \frac{1}{A}\left[\frac{\partial}{\partial z}\left(AK_z\frac{\partial S}{\partial z}\right)\right], \tag{4.2}$$

where S is salinity, A is the horizontal surface area, and K_z is the vertical diffusivity. Assuming A is constant, the equation simplifies to

$$\frac{\partial S}{\partial t} = \frac{\partial}{\partial z}\left(K_z\frac{\partial S}{\partial z}\right). \tag{4.3}$$

We can estimate a horizontally-averaged K_z by integrating from the bottom ($z = -H$) to some level z',

$$K_z|_{z=z'} = \frac{1}{\frac{\partial S}{\partial z}|_{z=z'}}\int_{-H}^{z'}\frac{\partial S}{\partial t}\mathrm{d}z, \tag{4.4}$$

assuming there is no diffusive flux through the bottom and that $\partial S/\partial t$ is constant within the layer of interest, then

$$K_z|_{z=z'} = \frac{1}{\frac{\partial S}{\partial z}|_{z=z'}}\frac{\partial S}{\partial t}(H - z'). \tag{4.5}$$

We estimate $\partial S/\partial t$ by conducting a linear fit to the near-bottom salinity measured by the moored CTD over each isolation event. The error associated with this quantity is assumed to be the standard error of the linear regression. We estimate $\partial S/\partial z$ using the STRI monitoring data, fitting a line to processed salinity profile data from 15 m to the bottom. We use this method to calculate a vertical salinity gradient for every profile taken during each isolation event, then time-average to find a single $\partial S/\partial z$ for each isolation event. Errors for each $\partial S/\partial z$ are again assumed to be the standard error of the linear fit and are propagated to calculate an error associated with the mean $\partial S/\partial z$ for each event

(Thomson and Emery, 2014). These quantities are integrated over the bottom 2 meters to estimate K_z as in equation 4.5, assuming the measured $\partial S/\partial t$ is representative of the bottom layer. The error associated with K_z is estimated by propagating the errors in the intermediate quantities (Thomson and Emery, 2014).

Table 4.1. Estimates for each of the four identified isolation events with sufficient data, including duration, vertical eddy diffusivity, K_z, measured $\partial T/\partial t$, estimated $(\partial T/\partial t)_{dia}$ due to diapycnal mixing, residual $(\partial T/\partial t)_{res}$, and the possible $(\partial T/\partial t)_{rad}$ due to radiative heating. The table also includes measured $\partial \rho/\partial t$, predicted $(\partial \rho/\partial t)_{dia}$ due to diapycnal mixing, and the residual $(\partial \rho/\partial t)_{rad}$, attributed to radiative heating.

Event	1	2	3	4
Duration (days)	56.5	33.8	19.9	23.6
K_z (m^2 s^{-1}; $\times 10^{-6}$)	2.26 ± 0.79	0.15 ± 0.10	4.07 ± 1.0	1.05 ± 0.31
$\partial T/\partial t$ (°C s^{-1}) ($\times 10^{-7}$)				
Measured	0.771 ± 0.003	0.720 ± 0.010	1.437 ± 0.011	0.556 ± 0.021
Diapycnal mixing	0.29 ± 0.10	0.04 ± 0.020	0.28 ± 0.05	0.27 ± 0.07
Residual	0.48 ± 0.10	0.68 ± 0.02	1.16 ± 0.05	0.29 ± 0.08
Radiative heating	1.11	0.90	1.44	0.99
$\partial \rho/\partial t$ (kg m^{-3} s^{-1}) ($\times 10^{-8}$)				
Measured	-3.74 ± 0.02	-2.59 ± 0.03	-8.35 ± 0.09	-7.37 ± 0.09
Diapycnal mixing	-2.11 ± 0.34	-0.31 ± 0.05	-4.53 ± 0.18	-6.38 ± 0.26
Radiative heating	-1.62 ± 0.34	-2.29 ± 0.06	-3.81 ± 0.17	-0.99 ± 0.26

During the isolation periods, the bottom layer vertical diffusivity estimates range from 1.5×10^{-7} m s^{-2} to 4.07×10^{-6} m s^{-2}, with three of the four K_z estimates on the order of 10^{-6} (Table 4.1). For reference the molecular diffusivity of salt is 10^{-8} m s^{-2}, indicating that mixing of the bottom layer is very weak. The low vertical diffusivity estimates show that the isolated bottom layer is very slowly modified by vertical mixing.

Diapycnal mixing and radiative heating contributions to temperature

For an isolated layer (i.e., no advection), the rate of change in temperature is given by

$$\frac{\partial T}{\partial t} = \frac{\partial}{\partial z}\left(K_z \frac{\partial T}{\partial z}\right) + \frac{1}{\rho C_p}\frac{\partial Q_{rad}}{\partial z}, \tag{4.6}$$

where ρ is the average density and $C_p = 4200$ J kg^{-1} K $^{-1}$, is the is the heat capacity, and Q_{rad} is the radiative heating flux. The terms on the right hand side indicate that the rate of change in temperature in the bottom layer is a function of vertical mixing with the overlying water column and radiative heating. Therefore, we can decompose the total rate of change in temperature into diapycnal mixing and radiative heating components,

$$\frac{\partial T}{\partial t} = \left(\frac{\partial T}{\partial t}\right)_{dia} + \left(\frac{\partial T}{\partial t}\right)_{rad}. \tag{4.7}$$

The moored CTD is used to estimate $\partial T/\partial t$, using the same technique described above for salinity. The measured $\partial T/\partial t$ represents the overall rate of temperature change in the bottom layer during the isolation events (Table 4.1).

If we assume that the eddy diffusivity is the same for temperature and salinity, then we can write the write the diapycnal mixing term in equation 4.7 in a form that is analogous to equation 4.3,

$$\left(\frac{\partial T}{\partial t}\right)_{dia} = \frac{\partial}{\partial z}\left(K_z \frac{\partial T}{\partial z}\right). \tag{4.8}$$

We use the K_z values from the salt budget (Table 4.1). To estimate $\partial T/\partial z$, we use temperature sensors from the temperature chain installed on the mooring, leveraging the greater temporal resolution. We assume a linear $\partial T/\partial z$, as measured between the temperature sensor 5 mab and 1 mab. We then time-average $\partial T/\partial z$ to find a single quantity for each isolation event and assume the error is associated with the standard deviations of the measured quantities.

The residual rate of temperature change (i.e., $(\partial T/\partial t)_{res} = \partial T/\partial t$ - $(\partial T/\partial t)_{dia}$)

is assumed to be associated with radiative heating. We compare the magnitude of this residual to possible radiative heating amounts following Wells et al. (2012), calculating bulk estimates to find the magnitude of this contribution to the temperature change.

We begin by estimating solar radiation as a function of depth, using Beer's law for the light intensity attenuation,

$$I(z) = I_0 e^{kz}, \tag{4.9}$$

where I is the light intensity, i.e., the radiation energy passing through an area per time and thus equivalent to the radiation flux, Q_{rad}, and $I_0 =$ is the incident radiation, which is estimated from the average short wave solar radiation over each isolation event using data from the STRI weather station (WS on Figure 4.1), and an albedo of 0.05 (Fairall et al., 1996). The attenuation coefficient is k, and z is the light path distance, using $z = 26$ m as the maximum depth. To calculate k, we follow Pilgrim (1987),

$$k = \frac{1.53}{SD}, \tag{4.10}$$

where SD is the Secchi depth. We use the mean Secchi depth (9.72 m) over the full monitoring time series at IB, in order to get an approximate magnitude of the light attenuation, as we cannot evaluate homogeneity in water column clarity. We can then estimate the rate of change in temperature due to radiative heating,

$$\left(\frac{\partial T}{\partial t}\right)_{rad} = \frac{kI}{\rho C_p}, \tag{4.11}$$

where ρ is the average bottom density during each isolation event. This serves as a back of the envelope quantity to compare the magnitude of the residual $\partial T/\partial t$, as data limitations preclude more precise estimates.

The measured $\partial T/\partial t$ during isolation events range from 5.6×10^{-8} °C s^{-1} to 1.44×10^{-7} °C s^{-1}, while the temperature rate of change due to diapycnal mixing ranged

from 4×10^{-9} °C s^{-1} to 2.9×10^{-8} °C s^{-1}. During all isolation events, the calculated temperature change due to diapycnal mixing is significantly lower than the measured temperature change during each of the isolation events, suggesting there must be an alternate mechanism to account for the excess heating. This residual is well-accounted for by the radiative heating amounts estimated from the model in equation 4.11 (Table 4.1).

4.4.4 Density reduction of the bottom layer

Density reduction of the isolated bottom water is a critical component of deep water renewal (Gade, 1973; Gade and Edwards, 1980; Stigebrandt, 2001; Gillibrand et al., 2006). Without density reduction, bottom waters would become progressively more difficult to exchange as longitudinal density gradients would be adverse for renewal. In fjords, the typical mechanism for density reduction is diapycnal mixing (Gade, 1973). While we have adapted this reoxygenation mechanism from fjords, Bahía Almirante is much shallower, and therefore radiative heating can play in important role through the full water column. The analysis above shows that that the bottom layer can experience warming through surface heat fluxes and observed temperature inversions provide further evidence (Adelson et al., 2022; Neal et al., 2014) .

Assuming pressure effects are negligible given the shallow water depth, density can be approximated as a linear function of temperature and salinity from the equation of state. The rate of change of density can therefore be written as

$$\frac{\partial \rho}{\partial t} \approx \rho_0 \left(-\alpha \frac{\partial T}{\partial t} + \beta \frac{\partial S}{\partial t} \right), \tag{4.12}$$

where ρ_0 is a reference density, α is the thermal expansion coefficient, and β is the haline contraction coefficient. By considering the rate of density change in this way, we can decompose $\partial\rho/\partial t$ into its diapycnal mixing and radiative heating components, in an analogous fashion to equation 4.7.

We can estimate the density change due to diapycnal mixing for the bottom layer in Bahía Almirante by again assuming a 1-D vertical balance during the isolation periods. We use the measured $\partial S/\partial t$ and the rate of temperature change due to diapycnal mixing calculated via equation 4.8 to find $(\partial\rho/\partial t)_{dia}$, following the equation of state (Equation 4.12),

$$\left(\frac{\partial \rho}{\partial t}\right)_{dia} \approx \rho_0 \left(-\alpha \left(\frac{\partial T}{\partial t}\right)_{dia} + \beta \frac{\partial S}{\partial t}\right), \tag{4.13}$$

The radiative heating contribution to the rate of density change is estimated by assessing the thermal contribution to density change in equation 4.12, considering the residual $\partial T/\partial t$ in Table 4.1. While we also report $(\partial T/\partial t)_{rad}$ values in Table 4.1, the primary purpose is to confirm that the residuals can reasonably be attributed to a temperature change due to radiative heating.

As with temperature and salinity, we calculate $\partial\rho/\partial t$ by a linear fit to the density time series from the moored CTD. The measured $\partial\rho/\partial t$ and the components attributed to diapycnal mixing and radiative heating (assumed to be the residual) are in Table 4.1.

Due to the decomposition described above, we can estimate the relative contributions of diapycnal mixing and radiative heating to density reduction of the bottom layer. For three of the events, the measured density reduction during isolation is much larger than that predicted by diapycnal mixing (Table 4.1 and supporting information, Figure 4.A.3). During two of the four isolation events, density reduction due to each of the mechanisms is of a similar magnitude (Events 1 and 3, with 43% and 46% of density reduction due to radiative heating, respectively), whereas during Event 4, diapycnal mixing accounts for 87% of the density reduction. In contrast, radiative heating provides 89% of the total density reduction in Event 2. While there is significant variability, it is apparent that for this tropical system, radiative heating can significantly contribute to density reduction.

4.4.5 Timescale estimates for DO state of Bahía Almirante

In order to characterize the DO state of the estuary, we will examine the relative timescales of oxygen drawdown and refreshment via deep water renewal. Fennel and Testa (2019) compare a timescale to hypoxia occurrence to the water residence time, identifying a nondimensional number that requires the DO drawdown timescale to be less than the residence time for hypoxia to occur. We adapt this framework for the more episodic Bahía Almirante system where the stagnation period of the isolated system is governed by deep water renewal events. We compare the DO drawdown timescale, τ_{hyp} and the renewal timescale τ_{DWR},

$$\mathcal{T} = \frac{\tau_{hyp}}{\tau_{DWR}}, \tag{4.14}$$

defined such that if $\mathcal{T} > 1$, the system tends towards normoxia, and if $\mathcal{T} < 1$, the system tends towards hypoxia.

DO drawdown timescale

The DO drawdown timescale is a function of the net DO consumption rate of the bottom layer. We assume that there is negligible net lateral transport of oxygen. In a vertically averaged lower layer, following (Officer et al., 1984),

$$\frac{\partial C}{\partial t} = -R_d + R_v, \tag{4.15}$$

where C is the oxygen concentration (mg L^{-1}), R_d is the oxygen demand (mg L^{-1} s^{-1}) due to internal and boundary sinks, and R_v is the vertical oxygen exchange rate with the surface layer (mg L^{-1} s^{-1}). The oxygen demand can be parameterized as:

$$R_d = k_d C, \tag{4.16}$$

where k_d is a rate constant for oxygen demand (Borsuk et al., 2001). R_d is temperature-dependent, and we assume that any temperature-dependence would be captured in the k_d parameter. This requires that temperature effects on DO solubility are negligible in the inner bay, where hypoxia is most severe and bottom water temperatures are warmest (Adelson et al., 2022). We estimate DO solubility of the bottom water mass (Garcia and Gordon, 1992), and find that it changes by 4% over the course of the time series. Furthermore, DO levels approach saturation only when the bottom waters are normoxic and are at most 32% saturated when the inner bay meets the hypoxic threshold (See supporting information, Figure 4.A.2). Consequently, we assume that temperature effects on DO solubility are minimal.

We assume that the vertical oxygen exchange rate scales linearly with the DO concentration difference from the surface (Officer et al., 1984; Borsuk et al., 2001),

$$R_v = k_v(C_S - C), \tag{4.17}$$

where C_S is the surface concentration and k_v is the vertical exchange coefficient. We can combine equations (4.15), (4.16), and (4.17) as

$$\frac{\partial C}{\partial t} = -k_d C + k_v(C_S - C). \tag{4.18}$$

We can solve this equation to find that

$$C(t) = \frac{k_v C_S}{k_d + k_v}\left(1 - \mathrm{e}^{-(k_v + k_d)t}\right) + C_0 \mathrm{e}^{-k_d t}, \tag{4.19}$$

where C_0 is the DO concentration of the renewal water. If the oxygen demand is much greater than the vertical exchange as it is in the bottom layer of a strongly stratified,

isolated bottom layer, (i.e., $k_d \gg k_v$),

$$C(t) = C_0 \mathrm{e}^{-k_d t}, \tag{4.20}$$

We then use k_d to estimate an e-folding DO drawdown timescale, such that

$$\tau_{hyp} = \frac{1}{k_d}. \tag{4.21}$$

We find a mean and standard deviation τ_{hyp} of 11.4± 3.7 days from 22 drawdown events at IB and IBP, with estimates ranging from 3.4 to 19.2 days (See supporting information, Figure 4.A.4). We observe DO drawdown during all months of the year, with the exception of July and August, which is typically anoxic throughout the time series. While there is a limited sample size and coverage throughout the year, there is no clear annual pattern in DO drawdown, further suggesting no strong temperature control.

Renewal timescale

The renewal timescale is episodic in nature with intermittent renewal events separated by periods of isolation. We rely on frameworks developed in high latitude systems like fjords to estimate duration of isolation periods. Aure and Stigebrandt (1990) provide a timescale for deep water renewal episodes, τ_{DWR}.

$$\tau_{DWR} = \frac{R_{DWR}}{\partial\rho/\partial t}, \tag{4.22}$$

where R_{DWR} is the density reduction required to completely refresh basin waters and $\partial\rho/\partial t$ is the rate of density reduction in the basin. Gade (1973) assumes that density in the basin reduces linearly with time. Here, we use the estimated $\partial\rho/\partial t$ described in Section 4.4.4.

R_{DWR} is fundamentally linked to the offshore density field at the sill depth, although

there are other influences, including channel geometry and mixing (Gade, 1973; Stigebrandt et al., 1996). Because the offshore density ultimately sets the inner-bay bottom density, if we consider statistics over long time periods, we can attribute the likelihood of refreshment to the offshore density standard deviation. If there is little variability in offshore density, then offshore conditions will regularly be sufficient for deep water renewal to occur, whereas higher variability reduces the likelihood of adequate density available.

A number of studies have considered parameters for R_{DWR} (e.g., Gade (1973); Darelius (2020)) which depends on the offshore density standard deviation, σ_ρ, at sill height. Gillibrand et al. (2006) consider various Scottish fjords and lochs to develop the equation,

$$R_{DWR} = \sigma_\rho \log_{10}(N_s + 10), \tag{4.23}$$

which includes a mixing factor, $\log_{10}(N_s + 10)$, where N_s is the number of sills between the basin and the open ocean, included to account for variations in mixing between systems, hereby attributed to mixing at sills. This provides a statistical framework for estimating R_{DWR} in fjords, and we use this formulation in our adaptation to estimate τ_{DWR}. We calculate R_{DWR} using $N_s = 1$, as well as $N_s = 0$ because the bathymetry is subtle in the system, finding timescales of $\tau_{DWR} = 173.8$ days and $\tau_{DWR} = 166.9$ days, respectively. This mixing parameter changes the resulting estimate by 4%, which is likely well within error associated with this estimate.

Observed events and timescale comparison

For comparison to the renewal timescale, we consider isolation events between the onset of DO drawdown and the beginning of reoxygenation, confirming that water temperature signal (i.e., the other most comprehensive time series) is consistent with isolation of near bottom waters (i.e., no step changes).

We identified 9 isolation events in the inner bay, fewer than the number of DO

drawdown events because we required onset and reoxygenation to occur without any gaps in the time series. Additionally, we consider only IB, omitting IBP because events are not independent between the two locations. The isolation event lengths ranged from 15.1 days to 194.6 days, with a mean of 56.1 days (See supporting information, Figure 4.A.4).

In order to gain insight into the hypoxic state of Bahía Almirante, we estimate DO drawdown and renewal timescales. The deep water renewal timescale (τ_{DWR}=166.9 days) is within the range of observed isolation events (15.1 days to 194.6 days) and much longer than the DO drawdown timescale (τ_{hyp} of 11.4± 3.7 days), such that $\mathcal{T} < 1$ and consequently, Bahía Almirante tends towards hypoxia.

4.5 Discussion

4.5.1 Deep water renewal in Bahía Almirante

We attribute reoxygenation of near-bottom waters in Bahía Almirante to deep water renewal, showing that an important reoxygenation mechanism in fjords is also applicable in shallow tropical systems. While wind-driven mixing is a common reoxygenation mechanism in temperate estuaries, we find that the wind mixing length L_z reaches insufficient depths to reoxygenate the stagnant bottom layer. Therefore, wind-driven vertical mixing is unlikely to play a role in reoxygenation at depth in Bahía Almirante.

Using the framework highlighted in Figure 4.2, based on the signs of the velocity and along-estuary density difference, we capture almost all of the observed reoxygenation events. The positive correlation between the length of time that deep water renewal conditions are met and the change in DO further suggests that lateral advection leads to renewal within Bahía Almirante (See supporting information, Figure 4.A.1). This simple framework shows that the near-bottom velocity and the along-estuary density difference are sufficient to identify when reoxygenation will occur in this system, without considering the volume flux and mixing that occurs along the estuary, which play a role in the supply

and modification of the near bottom water.

Our previous work shows that there is often a subtidal net flow through Bahía Almirante, typically inflow at BdD and outflow at CdB, and that during time periods of weak net flow, estuarine exchange plays an important role in the inlet velocities (Chapter 3). During deep water renewal conditions, the velocity and along-estuary density difference are favorable at both channels 75% of the time. The relationship between channel densities indicates that they are subjected to the same influences. Due to predominant net barotropic flow and the structure of two-layer estuarine exchange (i.e., inward flow in the bottom layer), the velocity condition is met at one or both of the inlets 81% of the time when the data is sufficient to apply this framework. Therefore, the along-estuary density difference is the more stringent condition. However, it is important to note that during time periods when we do not have velocity data, the along-estuary density difference condition is met, yet there is no accompanying reoxygenation (i.e., August-September 2020), illustrating that the velocity condition is critical as well.

To further strengthen the evidence for deep water renewal as the primary mechanism for reoxygenation in Bahía Almirante, we identify reoxygenation onsets in order to examine the conditions in Bahía Almirante that precede hypoxia termination. Of the nine reoxygenation events with sufficient data, seven are preceded by deep water renewal conditions met at one or both of the channels. The two exceptions occur during April 2020, which is the typically normoxic season (Adelson et al., 2022) and are possibly due to local advection of low-DO water, as the drawdown rates differ from other hypoxic events. Therefore, reoxygenation is typically preceded by deep water renewal conditions as well, indicating that it is typical mechanism for the termination of hypoxic events.

Mixing that modifies the density of the incoming water mass typically controls whether or not deep water renewal can occur; it is the density of the water mass at the sill of a fjord that determines if it will be sufficient to refresh the bottom water mass (Geyer and Cannon, 1982). The success of this scheme suggests that density modifications between

the measurements taken in the inlets and the inner bay are minimal. It is important to note that the measurement locations were constrained by field conditions and are located inside the channels. It is possible that there is considerable mixing that occurs within the channel oceanward of the inlet measurements. The bottom density in the channels (measured at $\approx$ 20 m) is strongly correlated to the $\approx$ 7 8 density at the site outside the bay (OC), suggesting that the deeper waters in the channels is modulated by shallower waters outside the bay, likely via vertical mixing (Chapter 3).

Bahía Almirante has mildly-sloping bathymetry, which may also contribute to the efficacy of the framework. Mixing in fjords often occurs at sills (Geyer and Cannon, 1982), and the relatively smooth bathymetry of Bahía Almirante may allow for the framework to apply while neglecting mixing of the inflow. The reoxygenation events have no apparent relationship with the spring-neap tidal cycle, which is consistent with limited role of within-estuary mixing in refreshment due to deep water renewal.

Deep water renewal is a common mechanism for reoxgyenation in high latitude fjords, and while the process has been observed in deep Scottish lochs (Kelly et al., 2017), as well as a tropical fjord with a sill (Salamena et al., 2021), it has not been previously identified as a reoxygenation mechanism in tropical estuaries. This study's results suggest that deep water renewal could be a refreshment mechanism in other coastal, tropical systems that suffer from hypoxia.

4.5.2 Diapycnal mixing and radiative heating

During isolation events, we see that mixing of the lower layer is slow (i.e., K_z is small), resulting in a stagnant bottom water mass at depth in the inner bay. We estimate K_z with a factor of ten difference between the minimum and maximum (Table 4.1). As noted previously, we provide the estimates for the individual isolation events in order to show a range of possible values, but preliminary analysis has not yielded clear results for the intra-event differences, and instead we focus on the commonalities.

There is always a significant deficit between the measured $\partial T/\partial t$ and estimated $(\partial T/\partial t)_{dia}$ due to diapycnal mixing. The bulk estimates of radiative heating can account for this difference (Table 4.1). Future work with direct observations of light attenuation in the water column would confirm this attribution. This is a novel density reduction mechanism for deep water renewal, and it may play a significant role in other shallow, tropical systems where radiative heating reaches the near bottom layer.

4.5.3 Timescales

Our estimates show that the DO drawdown timescale is shorter for Bahía Almirante than the deep water renewal timescale, (i.e., $\mathcal{T} < 1$), and therefore the system tends towards hypoxia. The DO time series supports this (Figure 4.2 c), as there is net DO consumption and persistent anoxia through much of the two year field campaign. The timescales as estimated have limitations and should be interpreted with caution.

We calculate an average τ_{hyp} for the system from DO time series measured 1 mab at IB and IBP. The estimates are based on the assumption that the bottom layer is well-mixed; however if the net DO consumption is due to sediment oxygen demand and there is a vertical DO gradient within the bottom layer, then the $\partial DO/\partial t$, and therefore τ_{hyp} is somewhat reliant on the distance of the measurement above the bed. The DO profiles from the monitoring data do not have sufficient vertical resolution to evaluate the DO profile on smaller scales, and the dependency of τ_{hyp} on the depth of the DO measurements is unknown.

Ultimately, the DO drawdown estimates (2.3-14.4 mmol m^{-2} d^{-1}) are consistent with published values of benthic diffusive oxygen fluxes (3.2-9.8 mmol m^{-2} d^{-1}), albeit in a very different system of the Oregon continental shelf (Reimers et al., 2012). Because we have not directly measured benthic fluxes, we cannot accurately compare our net DO drawdown estimates to sediment fluxes in tropical systems. Further study on the nature of oxygen demand in Bahía Almirante and direct calculations of DO fluxes will provide

estimates that can be more directly comparable to oxygen fluxes measured in tropical systems.

The renewal timescale, τ_{DWR}, is a statistical approach first developed in fjords (Gade, 1973). We compare to the estimates by Gillibrand et al. (2006) because the stagnation period in their formulation can be less than a year and reoxygenation occurs within every year of the long-term time series (Adelson et al., 2022). The deep water renewal timescale, τ_{DWR}, depends on the variability of the offshore density and must be applied on timescales sufficiently long to sample the distribution of offshore density. The annual hypoxia indicates that one year is an acceptable period to accumulate representative statistics. Ultimately, the renewal timescale of 173.7 days is a factor of three larger than the mean isolation event length, 56.1 days, reflecting that there is an unknown scaling factor in this timescale, however the timescale estimate falls within the range of observed events. It is important to note that there is a large range in isolation lengths observed in Bahía Almirante; however, the deep water renewal timescale applies as a mean over long time.

If there are changes in the offshore density variance with climate change, then the tendency of the state of the bay will change, and we can use similar analyses to understand the effects on Bahía Almirante (Darelius, 2020). Ultimately comparing DO drawdown timescales to retention times is illustrative of the state of the bay (Fennel and Testa, 2019), and we provide a metric that can apply in other tropical systems that experience episodic isolation, in contrast to constant refreshment.

Finally, radiative heating also plays an important role in the density renewal timescale. Excess warming significantly contributes to density reduction, and without this contribution, hypoxia would persist for significantly longer in Bahía Almirante because radiative heating accelerates density reduction, as shown in equation 4.23, and accounts for a 43%, 89%, 49%, and 13% of the overall density reduction for the isolation events respectively.

4.5.4 Seasonality

Previous work has shown that hypoxia develops seasonally within Bahía Almirante (Adelson et al., 2022), which links hypoxia development to increases in stratification; however the driver of the seasonal DO increases in the inner bay has remained undetermined. Collin et al. (2009) shows that there is no clear annual pattern in chlorophyll *a* concentrations, providing some evidence that there is not a strong seasonality in primary production in Bahía Almirante. Estimates for τ_{hyp} from deoxygenation events at IB and IBP suggest that the DO drawdown timescale does not drive the hypoxia seasonality. There is a broad range (3.4 to 19.2 days, with all but two estimates within 7.9 - 16.1 days), and annual coverage is incomplete (estimates are not available during July and August during which no DO drawdown events occurred) with a limited sample size; however, the available data indicate minimally-variable drawdown rates throughout the year (See supporting information, Figure 4.A.4). This is consistent with tropical, oligotrophic systems, where seasonal patterns in solar radiation weakly vary throughout the year, and therefore there is no strong pattern in biological oxygen demand. On the other hand, in tropical systems sediment oxygen demand can significantly differ in the wet and dry seasons (Grenz et al., 2010); in Bahía Almirante, precipitation patterns are distinct from other regions in the tropics, and there is significant precipitation throughout the year, even during the dry seasons (Adelson et al., 2022; Patton, 2023, Collin et al., submitted), suggesting that this estuary may not have the sediment oxygen demand seasonality described in other tropical systems.

If the net oxygen consumption is consistent throughout the year, then DO seasonality is likely attributable to annual patterns in the primary reoxygenation mechanism, here, deep water renewal. The deep water renewal timescale, τ_{DWR} depends on the variability of the offshore density and must be applied on timescales sufficiently long to sample the distribution of offshore density. The annual pattern in hypoxia indicates that one year is

an acceptable period, and we calculate the standard deviation of the density outside of the bay, σ_ρ (Section 4.4.5), over the full two-year time series. Over shorter time periods, the density history also plays a role in renewal ability. As we show through the deep water renewal framework (Figure 4.2), reoxygenation of the inner bay is strongly dependent on the along-estuary density difference, because the bottom velocity is most often inward. Because the inner bay density reduction is a slow process (Table 4.1), the density outside the bay is critically important to renewal.

In order to better understand the density variation outside of the bay over the course of the annual cycle and therefore the ability to reoxygenate the inner bay, we consider the monthly mean densities for the near-bottom (1 mab) at IB and near-surface density at OC (approximately 8 m; Figure 4.5 a), the latter of which we have shown to be correlated to the near-bottom density at BdD (Chapter 3) and the monthly mean near-bottom (1 mab) IB DO (Figure 4.5 b). The mean DO is hypoxic for all months except for February, March, and April during the time series, although there is evidence of reoxygenation events in October through January, consistent with mid-season intermittent renewal observed in Adelson et al. (2022).

While the density outside the bay ultimately sets the upper limit for IB bottom density, the monthly mean IB density exceeds OC's in all months besides January, February, and March, which are common times for reoxygenation. This indicates that the density outside the bay is sufficient for refreshment of the isolated bottom layer at IB. There are concurrent changes in DO, with the highest values occurring during the months when the IB density is comparable to or less than the offshore density (Figure 4.5), again consistent with refreshment at depth. When the error bars overlap, reoxygenation is more likely, which is is the case during the times when intermittent reoxygenation typically occurs (September and October) and when seasonal reoxygenation occurs (November - February; Adelson et al., 2022). This is consistent with the deep water renewal timescale; we consider shorter timescales when the mean densities must be considered in addition to

the variability so that we can elucidate the causes of the annual DO patterns. The relative density patterns at OC and IB drive the hypoxia seasonality at depth in Bahía Almirante.

The seasonal variation in the density outside the bay is linked to precipitation, which leads to decreased surface salinity and increased stratification (Adelson et al., 2022). Other offshore processes may modulate the density and stratification, on a seasonal timescale or causing interannual variation and warrant further investigation.

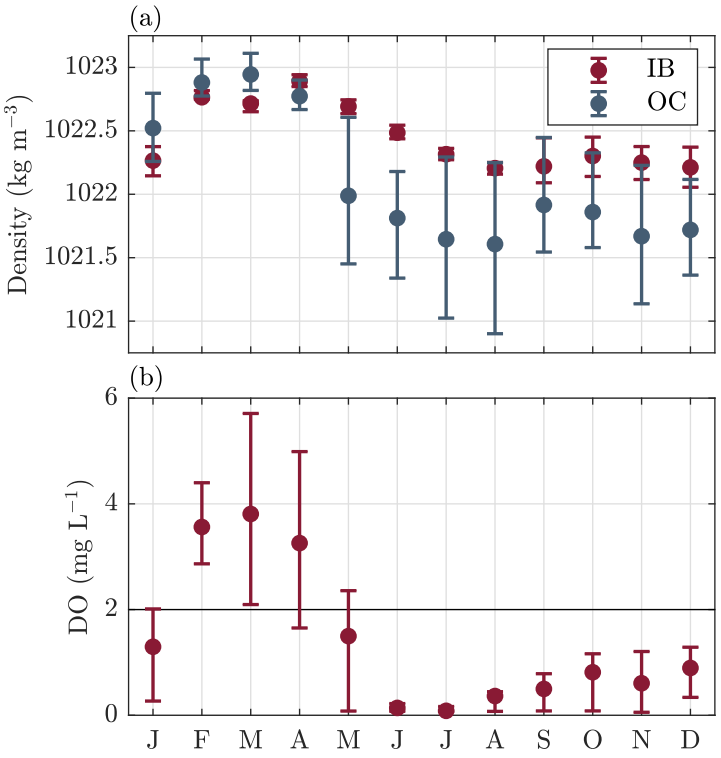

Figure 4.5. Monthly means of: (a) density (kg m^{-3}) at IB (1 mab) and OC (approximately 8 m). (b) DO (mg L^{-1}; 1 mab) at IB. 2 mg L^{-1} hypoxia threshold shown in black for reference. Error bars show second and third quartiles (25% to 75%).

As previously noted, the direction of the bottom layer along-channel velocity in the channels is also important to deep water renewal. Variations in bottom velocities likely contribute to interannual variability in hypoxia in Bahía Almirante. Chapter 3 shows that the net flow through the system is correlated to the along-coast flow, and Kastner et

al. (submitted) suggests that the net flow through Bahía Almirante is associated with mesoscale Caribbean Current eddy motions. There is no seasonality in the eddy occurrence, with a frequency of 116 days ± 31.5, and thus could play a role in the hypoxia onset by modifying the inflow during the time periods with sufficient density conditions.

4.5.5 Shoaling events

Bahía Almirante has experienced documented die offs due to hypoxia. In particular, Altieri et al. (2017) and Johnson et al. (2021) note massive bleaching events in shallow areas of Bahía Almirante in September 2010 and 2017, respectively. Previous work has shown that hypoxia develops at depth every year (Adelson et al., 2022) and in this analysis, we have identified annual variability in OC density as the driver of hypoxia seasonality. Nonetheless, bleaching events are not observed every year, despite regular monitoring.

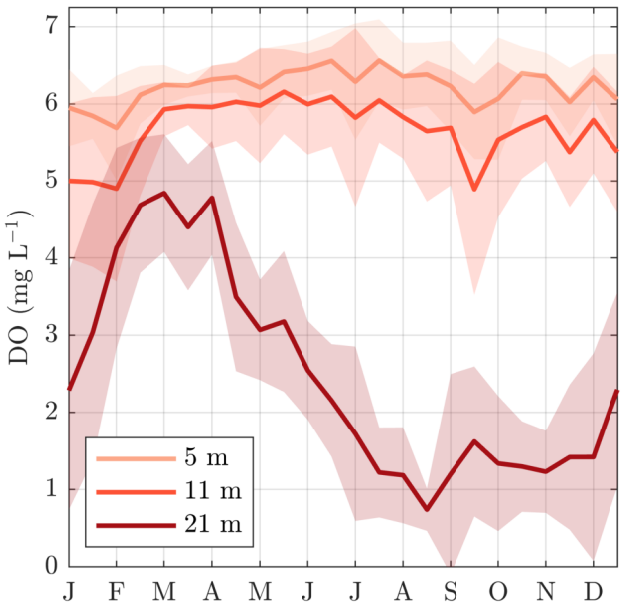

Figure 4.6. DO climatologies, averaged in half month intervals at three depths: 5 m, 11 m, and 21 m, using the STRI monitoring data in the inner bay. Patches indicate ±1 standard deviation.

Figure 4.6 shows the inner bay annual average DO for three depths of the STRI

weekly monitoring data. At the shallower depths (5 m and 11 m), DO tends to decrease during September, following a DO increase at depth. Adelson et al. (2022) shows a case study in which lateral advection leads to upward displacement of the hypoxic layer, which is consistent with the DO patterns in this climatological view. In the annual sense, DO at depth declines from April to September (Figure 4.6), and therefore it is likely that the hypoxic volume is largest in September, when these intermittent reoxygenation events can lead to upward displacement of the hypoxic layer. This provides strong evidence to support our hypothesis that the die off events (Altieri et al., 2017; Johnson et al., 2021) are connected to the seasonal hypoxia observed at depth through the hypoxic layer shoaling, consistent with the view suggested by Lucey et al. (2021). Further investigation, particularly data with higher resolution of DO with respect to time and depth, is needed in order provided conclusive support for this hypothesis.

4.6 Summary

In this paper, we attribute reoxygenation in Bahía Almirante to physical forcing, specifically lateral advection. We show that deep water renewal is the primary mechanism for bottom water reoxygenation in Bahía Almirante , sharing this dynamical similarity with fjords.

There are critical differences from high latitude regions that may play a role in deep water renewal in other shallow systems as well. Density reduction of the isolated water mass is a critical component of deep water renewal, and in fjords, typically occurs due to diapycnal mixing. We show that diapycnal mixing cannot account for the heating observed in the bottom layer, and that the magnitude of residual heating can be captured by radiative heating estimates. Furthermore, radiative heating significantly contributes to the density reduction of the isolated water mass. This allows for more frequent reoxygenation events, by decreasing the required density offshore for renewal to occur, relative to the

density reduction occurring solely due to diapycnal mixing.

We compare timescales to hypoxia and a timescale for deep water renewal. Over long timescales, the refreshment intermittency is a function of the IB bottom water density reduction and the offshore density variance, and over the full time series, we find a timescale of $\tau_{DWR} = 173.7$ days. We compare the timescale for renewal to the DO drawdown timescale, and see that $\tau_{hyp} = 11.4$ days, which is much shorter than the renewal timescale. In the bulk sense, Bahía Almirante tends towards hypoxia, which is consistent with the DO time series.

The hypoxia seasonality described in Adelson et al. (2022) can be attributed to deep water renewal conditions, particularly the annual pattern in density outside the bay and vertical stratification. Based on previous work and our estimates, there is not a strong seasonality in DO drawdown, and the DO state of the estuary depends on the refreshment capabilities of waters outside the bay. Intermittent deep water shoaling is a reasonable hypothesis that links this deep water DO seasonality to shallow hypoxic events given that prior shallow events have occurred during the season with the maximum deep water hypoxic volume.

4.7 Acknowledgements

We would like to thank Plinio Gondola and the environmental monitoring staff at STRI's Bocas del Toro Research Station and volunteers who have collected the long-term data set. We would also like to thank Steve Patton for the maintenance of the meteorological data. We would also like to thank the people who helped in the field, including Isabella Arzeno-Soltero, Ximena Boza, Viviana Bravo, Sebastian Castillo, Carolina Cesar, Antonia Helwig, Cynthia Pena, Max Rintoul, Duncan Wheeler, Jennifer Yin, and all the folks who keep the STRI Bocas station running.

All data has been collected under permits from MiAmbiente and ARAP. AEA was

supported by a Smithsonian Fellowship. This work was supported by a National Science Foundation grant, NSF OCE - 1924220 (RC), NSF OCE - 1924551 (GP), NSF OCE - 1924664 (KAD). No conflicts of interest.

Chapter 4, in part, is currently being prepared for submission for publication of the material. Adelson, A.E. Collin, R, Davis, K.A., Giddings, S.N., Kastner, S.E., and Pawlak, G., Deep water renewal episodes dictate hypoxic state of a shallow tropical estuary. The dissertation author was the primary investigator and author of this paper.

4.A Supporting information

The following is the supporting information for Chapter 4.

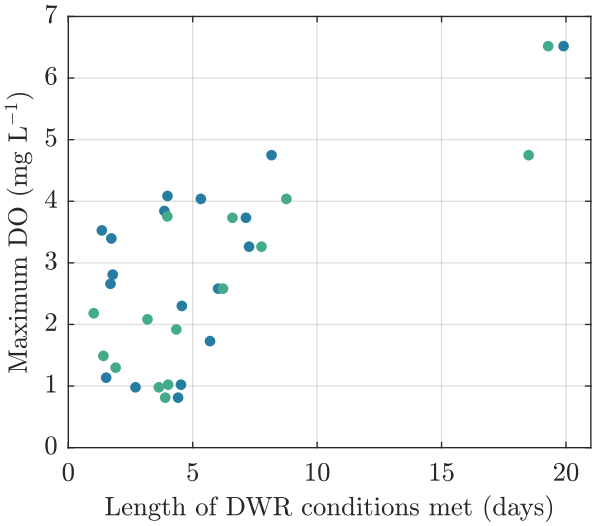

Figure 4.A.1. Maximum DO v. length of deep water renewal conditions met. Maximum DO is defined as the greatest DO measurement from deep water renewal conditions onset (as defined in Figure 4.2) to seven days after termination. Deep water renewal conditions must be met for at least one day to be considered.

Throughout the time series, the bottom water of the inner bay is not DO-saturated, with the exception of a period in March/April 2020 during normoxia (Figure 4.A.2). This suggests that the temperature effects on DO solubility are minimal, despite the concurrent warming at depth described in Adelson et al. (2022).

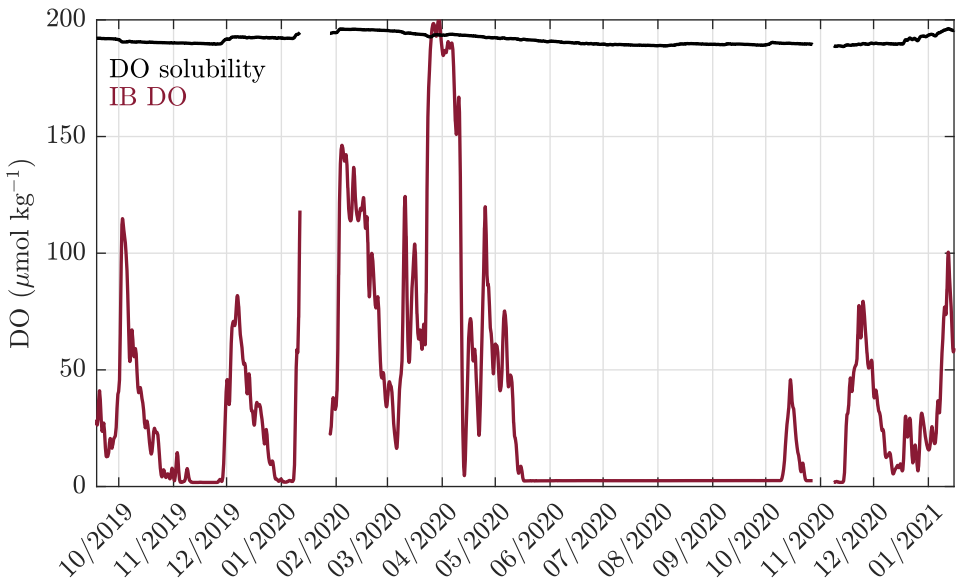

Figure 4.A.2. Time series of IB near-bottom DO (1 mab) in red and DO solubility based on water properties (Garcia and Gordon, 1992) in black.

The DO drawdown timescale does not exhibit strong seasonality, with values typically between 8-16 days (Figure 4.A.4). The mean DO drawdown timescale is much shorter than the deep water renewal timescale, suggesting that the system tends toward hypoxia as $\mathcal{T} < 1$. DO drawdown timescales are typically shorter than the isolation events, which indicates that hypoxia is likely to occur in the system. The deep water renewal timescale estimate falls within the range of observed event lengths, but it is much longer than most hypoxic events in Bahía Almirante.

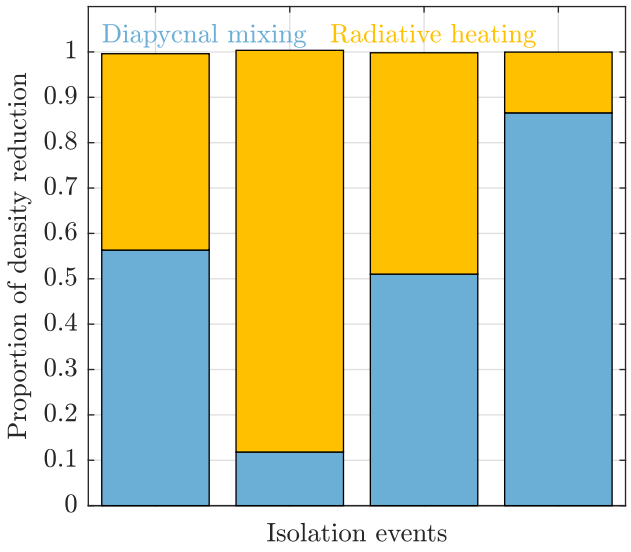

Figure 4.A.3. Diapycnal mixing (blue) and radiative heating (yellow) contributions to total density reduction for the four isolation events, with all $\partial\rho/\partial t$ values reported in Table 4.1.

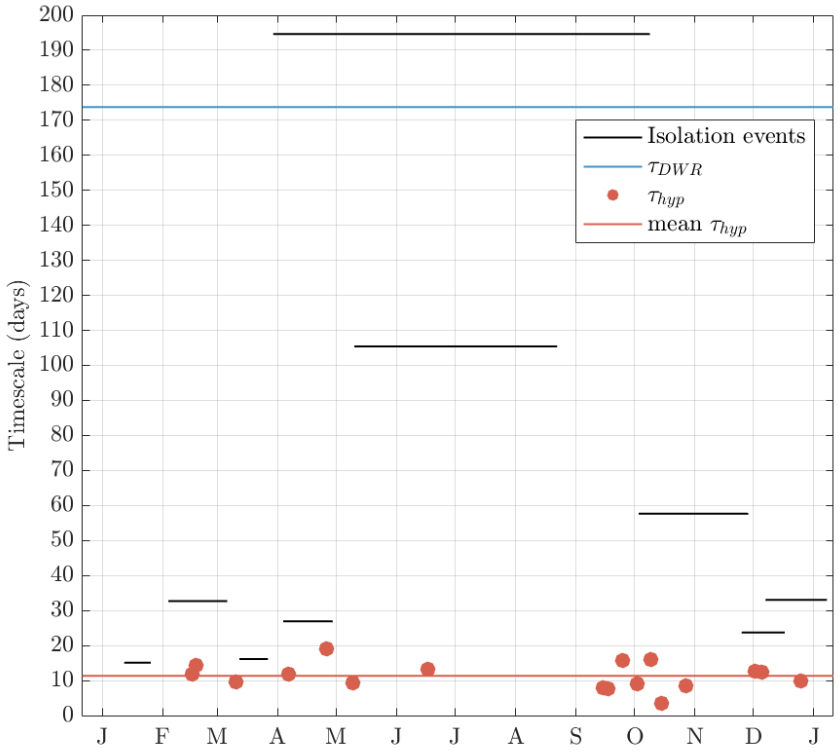

Figure 4.A.4. Timescale comparison of observed events, DO drawdown, and deep water renewal, with all timescales referenced to day of year. Individual events are shown in black lines, with the onset and termination shown as the termini; Deep water renewal timescale, τ_{DWR}, is shown in blue; DO drawdown timescales for each event shown in red dots, with mean shown in red line.

Chapter 5

Conclusions

Estuaries are situated at coastal boundaries and are therefore complex and dynamic systems. Because tropical estuaries are subject to different environmental controls than temperate and subtropical systems, it is important to understand their differences — and similarities — to their higher latitude counterparts.

The chapters presented in this dissertation provide insight into hypoxia and hydrodynamics of Bahía Almirante across a variety of timescales, from the course of a single event to the seasonal cycle. We aim to provide an understanding of the dynamical processes that influence hypoxic events and temperature inversions in Bahía Almirante, building the understanding of tropical estuaries such that the ideas explored here might be adapted to other tropical systems. Chapter 2 takes a seasonal view and describes the hydrography of the system and the factors that contribute to to hypoxia and temperature inversions. In Chapter 3, we describe the hydrodynamics of the bay, diagnose the relative importance of subtidal barotropic and baroclinic influences, and examine the processes that set the density properties within the estuary. Chapter 4 adapts the deep water renewal paradigm from fjordal systems and aims to show that while there are many meaningful differences between Bahía Almirante and a canonical fjord, the fundamentals of deep water renewal apply. We show that the timescale of this deep water renewal relative to DO drawdown determines the oxygen state of the bottom layer of the inner bay, and the seasonality is

driven by offshore density patterns.

Any analysis of estuarine observations must grapple with the ability to generalize to estuaries — or even tropical estuaries — more broadly. The research presented here is focuses on Bahía Almirante, which has distinguishing features, including multiple inlets and unusual precipitation patterns for tropical regions. There remain significant questions about the extent to which the findings of this dissertation might extrapolate to other tropical estuaries; however, in order to understand tropical estuaries generally, we need to study individual systems. This research is one small contribution to ameliorating the paucity of tropical estuarine observations. Ideally, we can apply the results to interdisciplinary research in other systems, just as we adapted fjordal deep water renewal to Bahía Almirante.

Eutrophication frequently contributes to coastal hypoxia (Howarth, 2008; Scully, 2013), and yet the role of nutrients in driving hypoxia in Bahía Almirante is not directly addressed in these chapters, leaving open questions about its importance. In this dissertation, we show that there are physical processes that can be conducive to hypoxia, including strong vertical stratification and long residence times, with or without excess nutrient inputs. Eutrophication can be expected to exacerbate hypoxia, and further work in Bahía Almirante should elucidate the role of nutrients delivered via terrestrial runoff or urban point sources in the system. Conversely, future studies of other tropical systems should consider the physics that promote hypoxia development and drive hypoxia termination.

Ultimately, resolving the hydrodynamics Bahía Almirante and how they may regulate the coincident stressors of low-DO and temperature inversions provides context needed to evaluate if these physical dynamics are present in other shallow, tropical estuaries. This dissertation is a step in addressing the knowledge gap in these systems and the fundamental connections between estuarine dynamics and biogeochemistry. However, more observations and improved modeling capabilities are needed for, and a worthwhile investment in, further scientific advancement.

Bibliography

Adelson, A. E., Altieri, A. H., Boza, X., Collin, R., Davis, K. A., Gaul, A., Giddings, S. N., Reed, V., and Pawlak, G. (2022). Seasonal hypoxia and temperature inversions in a tropical bay. *Limnology and Oceanography*, 67(10):2174–2189.

Altieri, A. H. and Gedan, K. B. (2015). Climate change and dead zones. *Global change biology*, 21(4):1395–1406.

Altieri, A. H., Harrison, S. B., Seemann, J., Collin, R., Diaz, R. J., and Knowlton, N. (2017). Tropical dead zones and mass mortalities on coral reefs. *Proceedings of the National Academy of Sciences*, 114(14):3660–3665.

Altieri, A. H., Johnson, M. D., Swaminathan, S. D., Nelson, H. R., and Gedan, K. B. (2021). Resilience of tropical ecosystems to ocean deoxygenation. *Trends in Ecology & Evolution*, 36(3):227–238.

Andrade, C. A. and Barton, E. D. (2000). Eddy development and motion in the caribbean sea. *Journal of Geophysical Research: Oceans*, 105(C11):26191–26201.

Armi, L. and Farmer, D. (1986). Maximal two-layer exchange through a contraction with barotropic net flow. *Journal of Fluid Mechanics*, 164:27–51.

Aure, J. and Stigebrandt, A. (1990). Quantitative estimates of the eutrophication effects of fish farming on fjords. *Aquaculture*, 90(2):135–156.

Avendaño-Alvarez, O., Salas-Monreal, D., Marin-Hernandez, M., Salas-de Leon, D. A., and Monreal-Gomez, M. A. (2017). Annual hydrological variation and hypoxic zone in a tropical coral reef system. *Regional Studies in Marine Science*, 9:145–155.

Bates, N. R. (2017). Twenty years of marine carbon cycle observations at devils hole bermuda provide insights into seasonal hypoxia, coral reef calcification, and ocean acidification. *Frontiers in Marine Science*, 4:36.

Beck, H. E., Zimmermann, N. E., McVicar, T. R., Vergopolan, N., Berg, A., and Wood, E. F. (2018). Present and future köppen-geiger climate classification maps at 1-km

resolution. *Scientific data*, 5(1):1–12.

Boesch, D. F. and Rabalais, N. N. (1991). Effects of hypoxia on continental shelf benthos: comparisons between the new york bight and the northern gulf of mexico. *Geological Society, London, Special Publications*, 58(1):27–34.

Borsuk, M., Stow, C., Luettich Jr, R., Paerl, H., and Pinckney, J. (2001). Modelling oxygen dynamics in an intermittently stratified estuary: estimation of process rates using field data. *Estuarine, Coastal and Shelf Science*, 52(1):33–49.

Breitburg, D., Levin, L. A., Oschlies, A., Grégoire, M., Chavez, F. P., Conley, D. J., Garçon, V., Gilbert, D., Gutiérrez, D., Isensee, K., et al. (2018). Declining oxygen in the global ocean and coastal waters. *Science*, 359(6371).

Buijsman, M. C. and Ridderinkhof, H. (2007). Water transport at subtidal frequencies in the marsdiep inlet. *Journal of Sea Research*, 58(4):255–268.

Centurioni, L. R. and Niiler, P. P. (2003). On the surface currents of the caribbean sea. *Geophysical Research Letters*, 30(6).

Chan, F., Barth, J., Lubchenco, J., Kirincich, A., Weeks, H., Peterson, W. T., and Menge, B. (2008). Emergence of anoxia in the california current large marine ecosystem. *Science*, 319(5865):920–920.

Chassignet, E. P., Hurlburt, H. E., Smedstad, O. M., Halliwell, G. R., Hogan, P. J., Wallcraft, A. J., Baraille, R., and Bleck, R. (2007). The hycom (hybrid coordinate ocean model) data assimilative system. *Journal of Marine Systems*, 65(1):60–83. Marine Environmental Monitoring and Prediction.

Chen, A. A. and Taylor, M. A. (2002). Investigating the link between early season caribbean rainfall and the el niño+ 1 year. *International Journal of Climatology: A Journal of the Royal Meteorological Society*, 22(1):87–106.

Clark, K. E., Bravo, V. D., Giddings, S. N., Davis, K. A., Pawlak, G., Torres, M. A., Adelson, A. E., César-Ávila, C. I., Boza, X., and Collin, R. (2022). Land use and land cover shape river water quality at a continental caribbean land-ocean interface. *Frontiers in Water*, 4:737920.

Collin, R. (2005). Ecological monitoring and biodiversity surveys at the smithsonian tropical research institute s bocas del toro research station. *Caribbean Journal of Science*.

Collin, R. and Chan, K. Y. K. (2016). The sea urchin lytechinus variegatus lives close to the upper thermal limit for early development in a tropical lagoon. *Ecology and*

Evolution, 6(16):5623–5634.

Collin, R., D'Croz, L., Gondola, P., and Del Rosario, J. B. (2009). Climate and hydrological factors affecting variation in chlorophyll concentration and water clarity in the bahia almirante, panama. In *Proceedings of the Smithsonian Marine Science Symposium*. Smithsonian Institution Scholarly Press.

Corredor, J. E., Howarth, R. W., Twilley, R. R., and Morell, J. M. (1999). Nitrogen cycling and anthropogenic impact in the tropical interamerican seas. In *New perspectives on nitrogen cycling in the temperate and tropical Americas*, pages 163–178. Springer.

Cramer, K. L. (2013). History of human occupation and environmental change in western and central caribbean panama. *Bulletin of Marine Science*, 89(4):955–982.

Darelius, E. (2020). On the effect of climate trends in coastal density on deep water renewal frequency in sill fjords—a statistical approach. *Estuarine, Coastal and Shelf Science*, 243:106904.

D'Croz, L., Rosario, J. B. d., and Gondola, P. (2005). The effect of fresh water runoff on the distribution of dissolved inorganic nutrients and plankton in the bocas del toro archipelago, caribbean panama. *Caribbean Journal of Science*.

Diaz, R. J. and Rosenberg, R. (2008). Spreading dead zones and consequences for marine ecosystems. *science*, 321(5891):926–929.

Durack, P. J., Gleckler, P. J., Purkey, S. G., Johnson, G. C., Lyman, J. M., and Boyer, T. P. (2018). Ocean warming: From the surface to the deep in observations and models. *Oceanography*, 31(2):41–51.

Duran-Matute, M., Gerkema, T., and Sassi, M. G. (2016). Quantifying the residual volume transport through a multiple-inlet system in response to wind forcing: The case of the western d utch w adden s ea. *Journal of geophysical research: Oceans*, 121(12):8888–8903.

Estadístico, I. (2021). Instituto nacional de estadística y censos.

Fabião, J. P. F., Rodrigues, M. F. G., Fortunato, A. B., Jacob, J. M. Q. d. B., and Cravo, A. M. F. (2016). Water exchanges between a multi-inlet lagoon and the ocean: the role of forcing mechanisms. *Ocean Dynamics*, 66:173–194.

Fairall, C. W., Bradley, E. F., Rogers, D. P., Edson, J. B., and Young, G. S. (1996). Bulk parameterization of air-sea fluxes for tropical ocean-global atmosphere coupled-ocean atmosphere response experiment. *Journal of Geophysical Research: Oceans*, 101(C2):3747–3764.

Farmer, D. M. and Freeland, H. J. (1983). The physical oceanography of fjords. *Progress in oceanography*, 12(2):147–219.

Fennel, K. and Testa, J. M. (2019). Biogeochemical controls on coastal hypoxia. *Annual review of marine science*, 11:105–130.

Fonseca, L. S., Lessa, G. C., Marta-Almeida, M., and Teixeira, C. E. P. (2024). Coastal upwelling and estuarine gravitational circulation: A feedback system in a tropical estuary in the south atlantic. *Estuaries and Coasts*, pages 1–16.

Gade, H. and Edwards, A. (1980). Deep water renewal in fjords. In *Fjord oceanography*, pages 453–489. Springer.

Gade, H. G. (1973). Deep water exchanges in a sill fjord: a stochastic process. *Journal of physical Oceanography*, 3(2):213–219.

Gallegos, A. (1996). *Descriptive Physical Oceanography of the Caribbean Sea*, chapter 3, pages 36–55. American Geophysical Union (AGU).

Garcia, H. E. and Gordon, L. I. (1992). Oxygen solubility in seawater: Better fitting equations. *Limnology and oceanography*, 37(6):1307–1312.

Gargett, A. (1984). Vertical eddy diffusivity in the ocean interior. *Journal of Marine Research*, 42(2):359–393.

Geyer (2010). Estuarine salinity structure and circulation. *Contemporary issues in estuarine physics*, 12:26.

Geyer, W. and Cannon, G. (1982). Sill processes related to deep water renewal in a fjord. *Journal of Geophysical Research: Oceans*, 87(C10):7985–7996.

Geyer, W. R. and MacCready, P. (2014). The estuarine circulation. *Annual review of fluid mechanics*, 46:175–197.

Gilbert, D., Rabalais, N., Diaz, R., and Zhang, J. (2010). Evidence for greater oxygen decline rates in the coastal ocean than in the open ocean. *Biogeosciences*, 7(7):2283–2296.

Gillibrand, P. A., Cromey, C. J., Black, K. D., Inall, M. E., and Gontarek, S. J. (2006). Identifying the risk of deoxygenation in scottish sea lochs with isolated deep water. In *Scottish Aquaculture Research Forum, SARF*, volume 7. Citeseer.

Glenn, E., Comarazamy, D., González, J. E., and Smith, T. (2015). Detection of recent regional sea surface temperature warming in the caribbean and surrounding region. *Geophysical Research Letters*, 42(16):6785–6792.

Godin, G. (1973). The analysis of tides. *The analysis of tides*.

Goreau, T. J. and Hayes, R. L. (1994). Coral bleaching and ocean" hot spots". *Ambio-Journal of Human Environment Research and Management*, 23(3):176–180.

Grenz, C., Denis, L., Pringault, O., and Fichez, R. (2010). Spatial and seasonal variability of sediment oxygen consumption and nutrient fluxes at the sediment water interface in a sub-tropical lagoon (new caledonia). *Marine Pollution Bulletin*, 61(7-12):399–412.

Guzman, H. M., Barnes, P. A., Lovelock, C. E., and Feller, I. C. (2005). A site description of the caricomp mangrove, seagrass and coral reef sites in bocas del toro, panama. *Caribbean Journal of Science*.

Guzman, H. M. and Guevara, C. A. (2001). Arrecifes coralinos de bocas del toro, panama: Iv. distribucion, estructura y estado de conservacion de los arrecifes continentales de peninsula valiente. *Revista de Biología Tropical*, 49(1):53–67.

Hansen, D. V. and Rattray Jr, M. (1966). Gravitational circulation in straits and estuaries.

Harrison, S. and Phizacklea, A. (1987). Vertical temperature gradients in muddy intertidal sediments in the forth estuary, scotland 1. *Limnology and Oceanography*, 32(4):954–963.

Howarth, R. W. (2008). Coastal nitrogen pollution: a review of sources and trends globally and regionally. *Harmful algae*, 8(1):14–20.

Hughes, D. J., Alderdice, R., Cooney, C., Kühl, M., Pernice, M., Voolstra, C. R., and Suggett, D. J. (2020). Coral reef survival under accelerating ocean deoxygenation. *Nature Climate Change*, 10(4):296–307.

Inall, M. and Gillibrand, P. (2010). The physics of mid-latitude fjords: a review. *Geological Society, London, Special Publications*, 344(1):17–33.

Johnson, M. D., Rodriguez, L. M., and Altieri, A. H. (2018). Shallow-water hypoxia and mass mortality on a caribbean coral reef. *Bulletin of Marine Science*, 94(1):143–144.

Johnson, M. D., Scott, J. J., Leray, M., Lucey, N., Bravo, L. M. R., Wied, W. L., and Altieri, A. H. (2021). Rapid ecosystem-scale consequences of acute deoxygenation on a caribbean coral reef. *Nature Communications*, 12(1):4522.

Kang, X., Xia, M., Pitula, J. S., and Chigbu, P. (2017). Dynamics of water and salt exchange at maryland coastal bays. *Estuarine, Coastal and Shelf Science*, 189:1–16.

Kaufmann, K. and Thompson, R. C. (2005). Water temperature variation and the meteorological and hydrographic environment of bocas del toro, panama. *Caribbean*

Journal of Science.

Kealoha, A. K., Doyle, S. M., Shamberger, K. E., Sylvan, J. B., Hetland, R. D., and DiMarco, S. F. (2020). Localized hypoxia may have caused coral reef mortality at the flower garden banks. *Coral Reefs*, 39(1):119–132.

Kelly, S., de Eyto, E., Dillane, M., Poole, R., Brett, G., and White, M. (2017). Hydrographic maintenance of deep anoxia in a tidally influenced saline lagoon. *Marine and Freshwater Research*, 69(3):432–445.

Kemp, W., Testa, J. M., Conley, D. J., Gilbert, D., and Hagy, J. D. (2009). Temporal responses of coastal hypoxia to nutrient loading and physical controls. *Biogeosciences*, 6(12):2985–3008.

Kurien, J. (1996). People and the sea. In *SEMINAR-NEW DELHI-*, pages 27–29. MALYIKA SINGH.

Le Moal, M., Gascuel-Odoux, C., Ménesguen, A., Souchon, Y., Étrillard, C., Levain, A., Moatar, F., Pannard, A., Souchu, P., Lefebvre, A., et al. (2019). Eutrophication: a new wine in an old bottle? *Science of the Total Environment*, 651:1–11.

Lemagie, E. P. and Lerczak, J. A. (2015). A comparison of bulk estuarine turnover timescales to particle tracking timescales using a model of the yaquina bay estuary. *Estuaries and coasts*, 38:1797–1814.

Levin, L. A. and Breitburg, D. L. (2015). Linking coasts and seas to address ocean deoxygenation. *Nature Climate Change*, 5(5):401–403.

Li, A. and Reidenbach, M. A. (2014). Forecasting decadal changes in sea surface temperatures and coral bleaching within a caribbean coral reef. *Coral Reefs*, 33(3):847–861.

Li, C. (2013). Subtidal water flux through a multiple-inlet system: Observations before and during a cold front event and numerical experiments. *Journal of Geophysical Research: Oceans*, 118(4):1877–1892.

Limburg, K. E., Breitburg, D., Swaney, D. P., and Jacinto, G. (2020). Ocean deoxygenation: A primer. *One Earth*, 2(1):24–29.

Lucey, N., Haskett, E., and Collin, R. (2020a). Multi-stressor extremes found on a tropical coral reef impair performance. *Frontiers in Marine Science*, 7:1079.

Lucey, N. M., Collins, M., and Collin, R. (2020b). Oxygen-mediated plasticity confers hypoxia tolerance in a corallivorous polychaete. *Ecology and evolution*, 10(3):1145–1157.

Lucey, N. M., Haskett, E., and Collin, R. (2021). Hypoxia from depth shocks shallow tropical reef animals. *Climate Change Ecology*, 2:100010.

MacDonald, D. G. and Geyer, W. R. (2004). Turbulent energy production and entrainment at a highly stratified estuarine front. *Journal of Geophysical Research: Oceans*, 109(C5).

Mao, M. and Xia, M. (2018). Wave–current dynamics and interactions near the two inlets of a shallow lagoon–inlet–coastal ocean system under hurricane conditions. *Ocean Modelling*, 129:124–144.

McDougall, T. J. and Barker, P. M. (2011). Getting started with teos-10 and the gibbs seawater (gsw) oceanographic toolbox. *SCOR/IAPSO WG*, 127:1–28.

Medeiros, C. and Kjerfve, B. (2005). Longitudinal salt and sediment fluxes in a tropical estuary: Itamaracá, brazil. *Journal of Coastal Research*, pages 751–758.

Menezes, M. O. B., Pontes, R. K. d. S., Galo, M., Carmo, A. M. C. D., Vinzon, S. B. V., Rosário, R. P., et al. (2009). Forcing and mixing processes in the amazon estuary: a study case.

Monsen, N. E., Cloern, J. E., Lucas, L. V., and Monismith, S. G. (2002). A comment on the use of flushing time, residence time, and age as transport time scales. *Limnology and oceanography*, 47(5):1545–1553.

Mooers, C. and Maul, G. A. (1998). Intra-americas sea circulation. *The sea*, 11:183–208.

Moser, G. A., Gianesella, S. M. F., Alba, J. J. B., Bérgamo, A. L., Saldanha-Corrêa, F. M., Miranda, L. B. d., and Harari, J. (2005). Instantaneous transport of salt, nutrients, suspended matter and chlorophyll-a in the tropical estuarine system of santos. *Brazilian journal of oceanography*, 53:115–127.

NASA/LARC/SD/ASDC (2015). Ceres regionally averaged toa fluxes, clouds and aerosols hourly terra edition4a.

Neal, B., Condit, C., Liu, G., dos Santos, S., Kahru, M., Mitchell, B., and Kline, D. (2014). When depth is no refuge: cumulative thermal stress increases with depth in bocas del toro, panama. *Coral Reefs*, 33(1):193–205.

Nelson, H. R. and Altieri, A. H. (2019). Oxygen: the universal currency on coral reefs. *Coral Reefs*, 38(2):177–198.

Nittrouer, C. A., Brunskill, G. J., and Figueiredo, A. G. (1995). Importance of tropical coastal environments. *Geo-Marine Letters*, 15(3-4):121–126.

Oczkowski, A. J., Santos, E. A., Martin, R. M., Gray, A. B., Hanson, A. R., Watson, E. B., Huertas, E., and Wigand, C. (2020). Unexpected nitrogen sources in a tropical urban estuary. *Journal of Geophysical Research: Biogeosciences*, 125(3):e2019JG005502.

Officer, C. B., Biggs, R. B., Taft, J. L., Cronin, L. E., Tyler, M. A., and Boynton, W. R. (1984). Chesapeake bay anoxia: origin, development, and significance. *Science*, 223(4631):22–27.

Orescanin, M., Raubenheimer, B., and Elgar, S. (2014). Observations of wave effects on inlet circulation. *Continental Shelf Research*, 82:37–42.

Patton, S. (2023). Data sets provided by the physical monitoring program of the smithsonian tropical research institute. (2).

Pawlak, G. and Armi, L. (1997). Hydraulics of two-layer arrested wedge flows. *Journal of Hydraulic Research*, 35(5):603–618.

Pawlowicz, R., Beardsley, B., Lentz, S., Dever, E., and Anis, A. (2001). Software simplifies air-sea data estimates.

Payne, R. E. (1972). Albedo of the sea surface. *Journal of Atmospheric Sciences*, 29(5):959–970.

Pezner, A. K., Courtney, T. A., Barkley, H. C., Chou, W.-C., Chu, H.-C., Clements, S. M., Cyronak, T., DeGrandpre, M. D., Kekuewa, S. A., Kline, D. I., et al. (2023). Increasing hypoxia on global coral reefs under ocean warming. *Nature Climate Change*, 13(4):403–409.

Pilgrim, D. (1987). Measurement and estimation of the extinction coefficient in turbid estuarine waters. *Continental Shelf Research*, 7(11-12):1425–1428.

Pomeroy, L. R. and Wiebe, W. J. (2001). Temperature and substrates as interactive limiting factors for marine heterotrophic bacteria. *Aquatic Microbial Ecology*, 23(2):187–204.

Rabalais, N., Diaz, R. J., Levin, L., Turner, R., Gilbert, D., and Zhang, J. (2010). Dynamics and distribution of natural and human-caused hypoxia. *Biogeosciences*, 7(2):585–619.

Reimers, C. E., Özkan-Haller, H. T., Berg, P., Devol, A., McCann-Grosvenor, K., and Sanders, R. D. (2012). Benthic oxygen consumption rates during hypoxic conditions on the oregon continental shelf: Evaluation of the eddy correlation method. *Journal of Geophysical Research: Oceans*, 117(C2).

Restrepo, J. C., Schrottke, K., Traini, C., Bartholomae, A., Ospino, S., Ortíz, J. C., Otero, L., and Orejarena, A. (2018). Estuarine and sediment dynamics in a microtidal tropical

estuary of high fluvial discharge: Magdalena river (colombia, south america). *Marine Geology*, 398:86–98.

Salamena, G. G., Whinney, J. C., Heron, S. F., and Ridd, P. V. (2021). Internal tidal waves and deep-water renewal in a tropical fjord: Lessons from ambon bay, eastern indonesia. *Estuarine, Coastal and Shelf Science*, 253:107291.

Sale, P. F., Agardy, T., Ainsworth, C. H., Feist, B. E., Bell, J. D., Christie, P., Hoegh-Guldberg, O., Mumby, P. J., Feary, D. A., Saunders, M. I., et al. (2014). Transforming management of tropical coastal seas to cope with challenges of the 21st century. *Marine Pollution Bulletin*, 85(1):8–23.

Saramul, S. and Ezer, T. (2014). On the dynamics of low latitude, wide and shallow coastal system: numerical simulations of the upper gulf of thailand. *Ocean Dynamics*, 64:557–571.

Schettini, C. A. F., Pereira, M. D., Siegle, E., de Miranda, L. B., and Silva, M. P. (2013). Residual fluxes of suspended sediment in a tidally dominated tropical estuary. *Continental Shelf Research*, 70:27–35.

Scranton, M. I., Taylor, G. T., Thunell, R., Benitez-Nelson, C. R., Muller-Karger, F., Fanning, K., Lorenzoni, L., Montes, E., Varela, R., and Astor, Y. (2014). Interannual and subdecadal variability in the nutrient geochemistry of the cariaco basin. *Oceanography*, 27(1):148–159.

Scully, M. E. (2010). The importance of climate variability to wind-driven modulation of hypoxia in chesapeake bay. *Journal of Physical Oceanography*, 40(6):1435–1440.

Scully, M. E. (2013). Physical controls on hypoxia in chesapeake bay: A numerical modeling study. *Journal of Geophysical Research: Oceans*, 118(3):1239–1256.

Sheng, Y., Peene, S., and Yassuda, E. (1996). Circulation and transport in sarasota bay, florida: The effect of tidal inlets on estuarine circulation and flushing quality. *Mixing in Estuaries and Coastal Seas*, 50:184–210.

Silva, N. and Vargas, C. A. (2014). Hypoxia in chilean patagonian fjords. *Progress in Oceanography*, 129:62–74.

Smith, R. (1976). Longitudinal dispersion of a buoyant contaminant in a shallow channel. *Journal of Fluid Mechanics*, 78(4):677–688.

Smith, S. V. and Hollibaugh, J. T. (2006). Water, salt, and nutrient exchanges in san francisco bay. *Limnology and Oceanography*, 51(1part2):504–517.

Spalding, A. K., Grorud-Colvert, K., Allison, E. H., Amon, D. J., Collin, R., de Vos, A., Friedlander, A. M., Johnson, S. M., Mayorga, J., Paris, C. B., et al. (2023). Engaging the tropical majority to make ocean governance and science more equitable and effective. *npj Ocean Sustainability*, 2(1):8.

Stanley, D. W. and Nixon, S. W. (1992). Stratification and bottom-water hypoxia in the pamlico river estuary. *Estuaries*, 15(3):270–281.

Stigebrandt, A. (2001). Physical oceanography of the baltic sea. In *A systems analysis of the Baltic Sea*, pages 19–74. Springer.

Stigebrandt, A. (2012). Hydrodynamics and circulation of fjords. *Encyclopedia of lakes and reservoirs*, 327:344.

Stigebrandt, A., Aure, J., and Molvjer, J. (1996). Oxygen budget methods to determine the vertical flux of particulate organic matter with application to the coastal waters off western scandinavia. *Deep Sea Research Part II: Topical Studies in Oceanography*, 43(1):7–21.

Stramma, L., Schmidtko, S., Levin, L. A., and Johnson, G. C. (2010). Ocean oxygen minima expansions and their biological impacts. *Deep Sea Research Part I: Oceanographic Research Papers*, 57(4):587–595.

Talley, L. D. (2011). *Descriptive physical oceanography: an introduction*. Academic press.

Tenorio-Fernandez, L., Valle-Levinson, A., and Gomez-Valdes, J. (2018). Subtidal hydrodynamics in a tropical lagoon: A dimensionless numbers approach. *Estuarine, Coastal and Shelf Science*, 200:449–459.

Thomson, R. E. and Emery, W. J. (2014). *Data analysis methods in physical oceanography*. Newnes.

Valle-Levinson, A. and Schettini, C. A. (2016). Fortnightly switching of residual flow drivers in a tropical semiarid estuary. *Estuarine, Coastal and Shelf Science*, 169:46–55.

Vaquer-Sunyer, R. and Duarte, C. M. (2008). Thresholds of hypoxia for marine biodiversity. *Proceedings of the National Academy of Sciences*, 105(40):15452–15457.

Vaquer-Sunyer, R. and Duarte, C. M. (2011). Temperature effects on oxygen thresholds for hypoxia in marine benthic organisms. *Global Change Biology*, 17(5):1788–1797.

Vieillard, A., Newell, S., and Thrush, S. (2020). Recovering from bias: A call for further study of underrepresented tropical and low-nutrient estuaries. *Journal of Geophysical Research: Biogeosciences*, 125(7):e2020JG005766.

Wang, C.-F., Hsu, M.-H., and Kuo, A. Y. (2004). Residence time of the danshuei river estuary, taiwan. *Estuarine, Coastal and Shelf Science*, 60(3):381–393.

Waterhouse, A. F., Valle-Levinson, A., and Winant, C. D. (2011). Tides in a system of connected estuaries. *Journal of physical oceanography*, 41(5):946–959.

Weinstock, J. B. and Collin, R. (2021). Hypoxia and warming are associated with reductions in larval bivalve abundance in a tropical lagoon. *Marine Ecology Progress Series*, 662:85–95.

Weinstock, J. B., Vargas, L., and Collin, R. (2022). Zooplankton abundance reflects oxygen concentration and dissolved organic matter in a seasonally hypoxic estuary. *Journal of Marine Science and Engineering*, 10(3):427.

Wells, J. R., Fram, J. P., and Pawlak, G. (2012). Solar warming of near-bottom water over a fringing reef. *Journal of Marine Research*, 70(4):641–660.

Wetz, M. S., Hales, B., Chase, Z., Wheeler, P. A., and Whitney, M. M. (2006). Riverine input of macronutrients, iron, and organic matter to the coastal ocean off oregon, usa, during the winter. *Limnology and Oceanography*, 51(5):2221–2231.

Wiseman, W. J., Rabalais, N., Turner, R., Dinnel, S., and MacNaughton, A. (1997). Seasonal and interannual variability within the louisiana coastal current: stratification and hypoxia. *Journal of Marine Systems*, 12(1-4):237–248.